

Conductivity gradient focusing by pervaporation- and osmosis- induced fluxes

Master thesis

Laurens van Oostveen

March 29th 2007

BIOS document 009/2007/BIOS

Committee:

Dr. J. C. T. Eijkel
Dr. ir. W. Olthuis
Prof. Dr. ir. A. van den Berg
Dr. Ir. R.B.M. Schasfoort

BIOS, Lab-on-a-Chip Group
Electrical Engineering
University of Twente

Summary

It is possible to perform conductivity gradient focusing (CGF) with a conductivity gradient caused by pervaporation- or osmosis-induced fluxes. This is concluded from results obtained from a theoretical exploration and the results from experiments with glass microchannels with a PDMS roof. A minimal concentration factor of 28.6 was observed at experiments that proved that pervaporation flux was created in the channels. The flow velocity that was reached was at least $5.4 \cdot 10^{-6} \text{ m s}^{-1}$. CGF experiments showed that concentrating of species with this CGF method is possible, however the created concentration peaks were instable and more study is necessary to improve the stability. Indications are found that separation with this CGF method is possible. This deserves more study. Finally it is recommended to do more study at absorption and adsorption of species in or at PDMS.

Preface

The research project described in this report is the final thesis of the master ‘Microsystems and Microelectronics’ of my study Electrical Engineering at the University of Twente. It was performed in the BIOS *Lab on a Chip* group. I would like to thank my first supervisor Jan Eijkel for the things he learned me and for his incredible faith in me. I would also like to thank my second supervisor Wouter Olthuis for his support. He has also been a great support as teacher and tutor during my study. The rest of the teachers who taught me during my study receive my thanks too for the theoretical and practical wisdoms they gave me. During my assignment I had great technical support from Johan Bomer, Daniël Wijnperlé and Jan van Nieuwkastele, for which I like to thank them. The rest of my colleagues from the BIOS group receive my thanks for their technical tips and sociability, especially my running mates. Special thanks go to my friends from the study, sports or my former band, who made it pleasant to live in Enschede and study at the University of Twente. Also special thanks go to my girlfriend Eva and my sister Caroline for supporting me. Last, but not least I would like to thank my parents, Arjan and Astrid, for giving me the opportunity to study at the University of Twente and supporting me during my youth and study time.

Laurens

Contents

Summary.....	3
Preface	5
Mathematical symbols.....	9
Constants.....	10
Abbreviations	10
Chapter 1 - Introduction	11
Chapter 2 - Theory	13
2.1 Flows and fluxes in the channel	13
2.2 System resolution.....	29
2.4 Fluorescence microscopy	29
2.5 PDMS absorption and adsorption of fluorescent species	31
2.6 Pre-priming.....	32
2.7 Electrode reactions	32
2.8 Temperature effects	33
Chapter 3 - Device design and fabrication	35
3.1 Device demands	35
3.2 Device outlook.....	35
3.3 Device materials.....	36
3.4 Device design.....	42
3.5 Device fabrication.....	52
3.6 Results and discussion	56
3.7 Summary device design and fabrication	63
Chapter 4 - Experimental.....	65
4.1 Measurement setup	65
4.2 Chemicals	68
4.3 Device priming	70
4.4 Experimental protocol	71
Chapter 5 - Results and discussion	73
5.1 Pervaporation.....	73

5.2 Molecular absorption and adsorption of PDMS.....	80
5.3 Conductivity gradient focusing by pervaporation	84
5.4 Conductivity gradient focusing by osmosis	94
5.5 Separation.....	101
Chapter 6 - Conclusions.....	105
Chapter 7 - Recommendations	107
References.....	109
Appendices.....	115
Appendix A. Process flow pervaporation channel glass wafer.....	115
Appendix B. Process flow PDMS	117

Mathematical symbols

<i>c</i>	Concentration	[mol m ⁻³]
<i>d</i>	Thickness	[m]
<i>h</i>	Height	[m]
<i>k</i>	Rate constant	[s ⁻¹]
<i>p</i>	Pressure	[Pa] or [N m ⁻²]
<i>q</i>	Species charge	[C]
<i>r</i>	Radius	[m]
<i>t</i>	Time	[s]
<i>n</i>	Valence	-
<i>v</i>	Velocity	[m s ⁻²]
	Reaction rate	[mol s ⁻¹]
<i>w</i>	Width	[m]

<i>A</i>	Area	[m ²]
	Frequency factor	[s ⁻¹]
<i>D</i>	Diffusion coefficient	[m ² s ⁻¹]
<i>E</i>	Electric field	[V m ⁻¹]
	Energy	[J]
	Activation energy	[J mol ⁻¹]
	Young's modulus	[N m ⁻²]
<i>H</i>	Heat generation	[W s ⁻¹]
<i>I</i>	Electrical current	[A]
<i>J</i>	Molar flux	[mol m ⁻² s ⁻¹]
	Mass flux	[kg m ⁻² s ⁻¹]
	Volume flux	[m ³ m ⁻² s ⁻¹]
<i>L</i>	Length	[m]
<i>N</i>	Plate number	-
	Amount of species	-
<i>P</i>	Permeability	[m ³ m ⁻¹ Pa ⁻¹ s ⁻¹] or [m ² s ⁻¹]
	Load	[N m ⁻²]
	Power	[W]
	Pressure	[Pa] or [N m ⁻²]
<i>R</i>	Resistance	[Ω]
	Resolution	-
<i>S</i>	Solubility coefficient	-
<i>T</i>	Temperature	[K]
<i>V</i>	Voltage	[V]
	Volume	[L] or [m ³]

<i>γ</i>	Surface tension	[N m ⁻¹]
<i>ε</i>	Permittivity	[F m ⁻¹]
<i>ξ</i>	Zeta-potential	[V]
<i>η</i>	Viscosity	[Pa s ⁻¹]
<i>θ</i>	Contact angle	[°]

λ	Wavelength	$[\text{m}^{-1}]$
μ	Mobility	$[\text{m}^2 \text{V}^{-1} \text{s}^{-1}]$
π	Osmotic pressure	$[\text{Pa}]$
ρ	Density	$[\text{kg m}^{-3}]$
	Resistivity	$[\Omega \text{m}^{-1}]$
σ	Conductivity	$[\Omega^{-1} \text{m}^{-1}]$
τ	Time	$[\text{s}]$

Constants

c	Velocity of light	$1.38 \cdot 10^8$	m s^{-1}
g	Gravity constant	9.81	m s^{-2}
h	Planck's constant	$6.626068 \cdot 10^{-34}$	J s
k	Boltzmann constant	$1.380 6505 \cdot 10^{-23}$	J K^{-1}
kT/q	Thermal voltage	$25 \cdot 10^{-3}$	V

F	Faraday constant	96,485.3383	C mol^{-1}
R	Gas constant	8.314472	$\text{J K}^{-1} \text{mol}^{-1}$

Abbreviations

AFM	atomic force microscopy
BIOS	biosensors group
BHF	buffered HF
BP	bandpass
CGF	conductivity gradient focusing
EOF	electroosmotic flow
EP	electrophoresis
FASS	fiels amplified sample stacking
HP	highpass
IBE	ion beam etching
PDF	pressure driven flow
PDMS	polydimethylsiloxane
PMT	photomultiplier tube
RF	radio frequency
RIE	reactive ion etching
Rpm	rounds per minute
SEM	scanning electron microscopy
TB buffer	TRIS boric acid buffer
TGF	temperature gradient focusing
TRIS	2-amino-2-(hydroxymethyl)propane-1,3-diol

Chapter 1 - Introduction

In the past 15 years microfluidics was developed from a simple concept to a basis of new biotechnology [1]. Where biotechnologists use labs on macro levels nowadays, microfluidics researchers developed technologies for labs on micro- or even nanolevel. This concept is called *Lab on a Chip*.



Figure 1.1. Lab on a chip: biomedical lab integrated on a chip

An example of an applied *Lab on a Chip* research project is a lithium analysis chip that monitors the lithium treatment of patient suffering from manic depression [2]. This chip will be commercially exploited soon by the company Medimate, a spin-off company from the University of Twente. One of the disciplines used for these applied microchips, microfluidics, is still point of interest in research for the BIOS group, or *Lab on a Chip* group, of the University of Twente. This project is only a foretaste of what to stand come in this field of science.

The project described in this report concerns the exploration of an existing microfluidic separation method; conductivity gradient focusing. It will be investigated whether the water permeability of a semi permeable membrane can be used to create a conductivity gradient of dissolved species inside a microchannel caused by a pervaporation or osmosis driven flux.

In this report the theoretical basics (chapter 2) and the experimental explorations will be described. Chapter 3 describes the design and fabrication of microfluidic devices that were used for experiments, which are described in chapter 4. Chapter 5 deals with the results and discussion of these experiments. Conclusions are drawn in chapter 6 and recommendations are given in chapter 7.

Chapter 2 - Theory

This chapter describes the theory that is necessary to be read for understanding ‘conductivity gradient focusing by pervaporation’ experiments. The flows and species fluxes in the channel are discussed in paragraph 2.1. Paragraph 2.2 discusses the resolution of the separation system. Paragraph 2.3 deals with fluorescence microscopy and paragraph 2.5 with the ab- and adsorption of fluorescent species in the PDMS. Paragraph 2.6 deals with the pre-priming of channels and 2.7 with the electrode reactions in the reservoirs. Finally paragraph 2.8 deals with the temperature effects that can occur in the microchannel as result from applied voltages.

2.1 Flows and fluxes in the channel

The ‘conductivity gradient focusing by pervaporation’ experiments are possible to perform, because liquid flow and species fluxes occur in the microchannel under the influence of several causes. The frequently used terms flux and flow are defined now in order to make clear the difference between them, which is helpful for understanding this report: Flux is the movement of dissolved species and flow is the bulk flow of a solution.

The total flux J_{total} in the microchannel can be described with the Nernst-Planck flux equation [3].

$$J_{total} = J_{diffusion} + J_{convection} + J_{migration} \quad (2.1)$$

Where J_{total} is the total molar flux, $J_{diffusion}$ the flux that result from diffusion, $J_{convection}$ the flux that results from all kinds of convection and $J_{migration}$ the flux that results from migration of dissolved species.

The species fluxes described in this paragraph can all be substituted in the Nernst-Planck flux equation. The flows and fluxes are described first.

2.1.1 Hydrostatic pressure induced flow

Capillary pressure and gravity induce hydrostatic pressure differences between reservoirs that induce flow in microchannels. Eijkel *et al.* described these pressures [4]. The capillary pressure P_{cap} [Pa] can be described by:

$$P_{cap} = \frac{2\gamma \cos \theta}{r_{reservoir}} \quad (2.2)$$

where γ [N m^{-1}] is the surface tension of water, θ [$^\circ$] the contact angle of water and $r_{\text{reservoir}}$ [m] the reservoir radius at the height of the meniscus. The pressure induced by gravity P_{grav} [Pa] can be described by:

$$P_{\text{grav}} = \rho g (h - h_0) \quad (2.3)$$

where ρ [kg m^{-3}] the water density, g [m s^{-2}] the acceleration constant, h [m] the height of the reservoir above sea level h_0 .

Figure 2.1 shows the situation that reservoir 1 has a lower water height than reservoir 2 and where reservoir 1 and 2 have water contact angles of 0° and 180° , respectively. The arrow shows the direction of the resulting hydrostatic pressure induced flow.

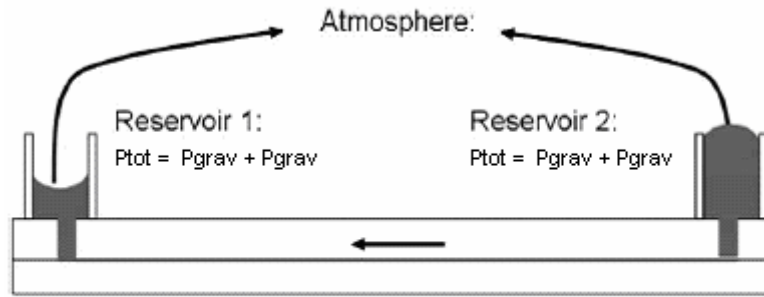


Figure 2.1 Channel with hydrostatic pressure induced flows [4]

The average velocity v_{PDF} [m s^{-1}] of the bulk liquid in a rectangular channel (width \gg height) induced by pressure differences between the reservoirs can be calculated by:

$$v_{PDF} = \frac{h^2}{12\eta} \frac{\Delta p}{L} \quad (2.4)$$

where h [m] is the height of the channel, L [m] the length of the channel, η [Pa s^{-1}] the viscosity of the fluid and Δp [Pa] the pressure difference. It can be seen that the velocity is constant along the channel. The species flux that results from the pressure driven flow, J_{PDF} [$\text{mol m}^2 \text{s}^{-1}$] is given by:

$$J_{PDF}(x) = v_{PDF}(x)c(x) \quad (2.5)$$

2.1.2 Flow and species flux induced by pervaporation

Pervaporation can be created by separating species in the liquid phase and the vapour phase by a membrane. The membrane acts as a selective barrier between the two phases: the liquid phase feed and the vapor phase permeate. It allows the desired species of the liquid feed to transfer through it by vaporization

Researches on pervaporation of water through polymers can be found in literature. Eijkel *et al.* described osmosis and pervaporation of water through the roof of all-polyimide channels [5]. They found flow velocities of up to $3 \cdot 10^{-6} \text{ ms}^{-1}$ for the pervaporation experiments and $70 \cdot 10^{-6} \text{ ms}^{-1}$ for the osmosis experiments in channels with a width of 2-30 μm , a length of 4 mm, a height of 500 nm and a polyimide thickness of $2.3 \cdot 10^{-6} \text{ m}$. Others describe pervaporation of water through PDMS structures [6][7][8]. The pervaporation through microchannels with PDMS roofs is described in this section.

Due to spaces between the flexible polymer chains in the PDMS, water is able to pervaporate. This is why PDMS can be seen as a membrane. The diffusion-solution model describes the volume flux through a membrane as [9]:

$$J_{\text{membrane}} = \frac{P(p_0 - p_l)}{d} \quad (2.6)$$

Where J_{membrane} [$\text{m}^3 \text{ m}^2 \text{ s}^{-1}$] is the flux through the membrane, P [$\text{m}^3 \text{ m}^{-1} \text{ Pa}^{-1} \text{ s}^{-1}$] is the permeability of the membrane, p_0 and p_l [Pa] the pressures at both sides of the membrane and d [m] the thickness of the membrane. The flux through the membrane is assumed to be constant along the channel in time, meaning that we neglect osmotic effects due to (changing) solute concentrations. The pervaporation flux in the channel can be influenced by adjusting the membrane thickness or the exterior water vapor pressure by adjusting the temperature or the humidity of the atmosphere. The permeability in [$\text{m}^2 \text{ s}^{-1}$] of the membrane is given by the product of the diffusion coefficient D [$\text{m}^2 \text{ s}^{-1}$] and the solubility coefficient S of the membrane [10]:

$$P = DS \quad (2.7)$$

The time constant τ [s] of the water to diffuse through the PDMS is given by:

$$\tau_D = \frac{d^2}{D} \quad (2.8)$$

In a microchannel with a PDMS roof and two reservoirs at the ends of the channel should, when it is filled with water, two opposite flows occur due to pervaporation of water through the PDMS roof. This is depicted in figure 2.2.

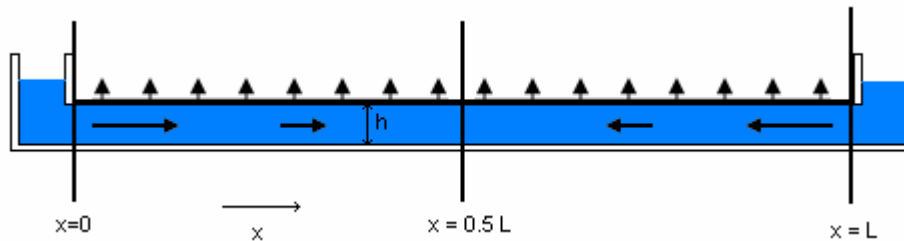


Figure 2.2 Channel with pervaporation

In the channel, the flow velocity v_{pervap} [$\text{m}^3 \text{m}^{-2} \text{s}^{-1}$] of the bulk at one half of the channel, generated by the volume flux of water through the roof, depends on the channel height h [m], the channel length L [m] and the position x in the channel:

$$v_{pervap} = -J_{membrane} \left(\frac{x - 0.5L}{h} \right) \quad (2.9)$$

Figure 2.3 shows the flow velocity that is induced by pervaporation along the channel.

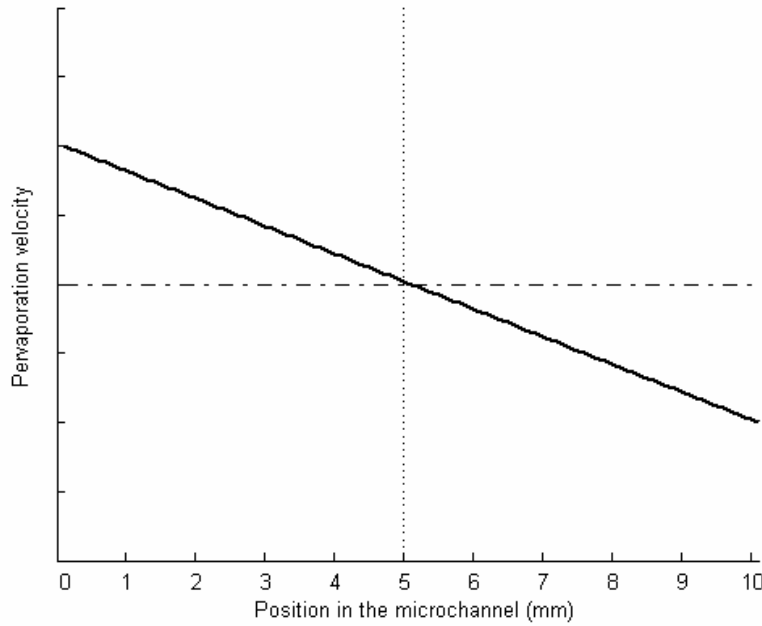


Figure 2.3. Flow velocity induced by pervaporation along the channel

It can be seen that the flow velocity is positive at the left side of the channel and negative at the right side of the channel and zero in the middle of the channel. This means that the solution flows to the middle of the channel, where accumulation of dissolved species will take place.

To calculate the molar pervaporation-induced flux J_{pervap} [$\text{mol m}^{-2} \text{s}^{-1}$] at position x , the pervaporation flux is multiplied by the concentration of the species at this position:

$$J_{pervap}(x) = v_{pervap}(x)c(x) = J_{membrane} \left(\frac{x - 0.5L}{h} \right) c(x) \quad (2.10)$$

A counteracting flux that causes the dissolved species to disperse is diffusion. Diffusion is the blending process of molecules, resulting from their random motion. The molar flux caused by diffusion J_{diff} [$\text{mol m}^{-2} \text{s}^{-1}$] can be expressed as the concentration gradient dc/dx

[mol m⁻³] multiplied by the diffusion coefficient D [m² s⁻¹], which is unique for all different matters. This is called the 1st diffusion law of Fick:

$$J_{diff} = -D \frac{dc}{dx} \quad (2.11)$$

When an equilibrium is reached, the total flux is zero:

$$J_{pervap} + J_{diff} = 0 \quad (2.12)$$

This means that:

$$J_{pervap} = -J_{diff} \quad (2.13)$$

When equation 2.10 and 2.11 are substituted in this equation, the following equation results:

$$-cJ_{membrane} \frac{(x - 0.5L)}{h} = D \frac{dc}{dx} \quad (2.14)$$

This can be written as:

$$\frac{dc}{c} = -\frac{J_{membrane}}{Dh} (x - 0.5L) dx \quad (2.15)$$

After integrating the left term over dc and the right term over dx , the equilibrium concentration at position x can be found by:

$$c(x) = c_0 \exp\left(-\frac{J_{membrane}x}{2Dh} (x - L)\right) \quad (2.16)$$

where c_0 is the solute concentration in the reservoirs.

Figure 2.4 shows the concentration plotted against the position in the channel for different D and certain values for $c_0 = 1 \cdot 10^{-7}$ M, $L = 5000$ μ m, $h = 1 \cdot 10^{-6}$ m and $J_{membrane} = 1 \cdot 10^{-20}$ m³ m⁻² s⁻¹. The amplitude was normalized to c_{max} .

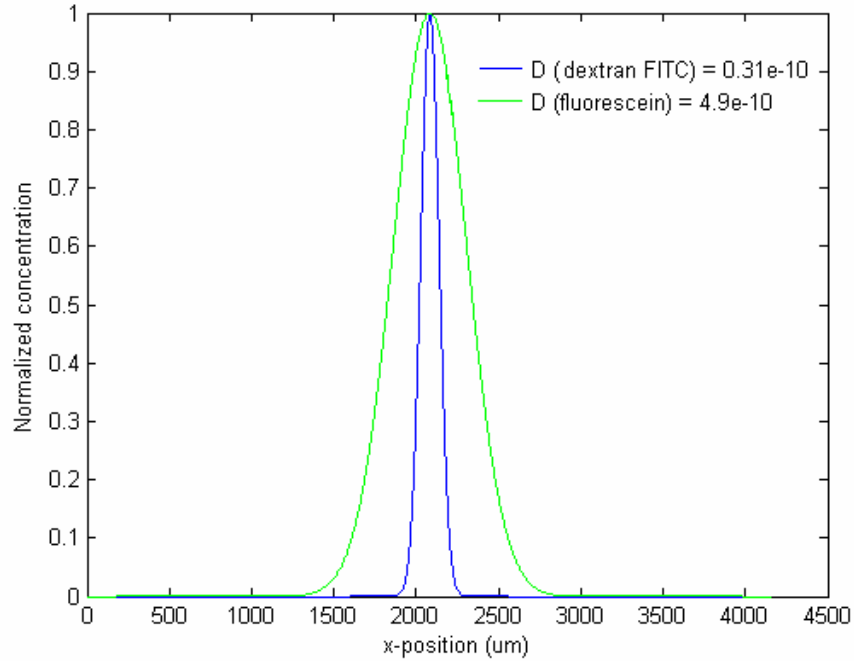


Figure 2.4 Normalized concentration profiles of the dissolved species in the channel at pervaporation when equilibrium is reached with diffusion. The diffusion coefficients of dextran FITC and fluorescein are used.

A sharp peak with a huge amplitude in the middle of the channel can be expected. The diffusion coefficient of fluorescein is 15.8 times higher than the diffusion coefficient of dextran FITC. The peak width at half height is factor 3.9 smaller.

2.1.3 Flow and species flux induced by osmosis

When the PDMS of the previous section is not covered by air, but by water with a lower solute concentration than the solute concentration in the channel, osmosis takes place. Osmosis is the movement of solvent molecules through a semi-permeable membrane. The hydrostatic pressure difference that it creates at equilibrium is called the osmotic pressure. Figure 2.5 shows the osmosis process.

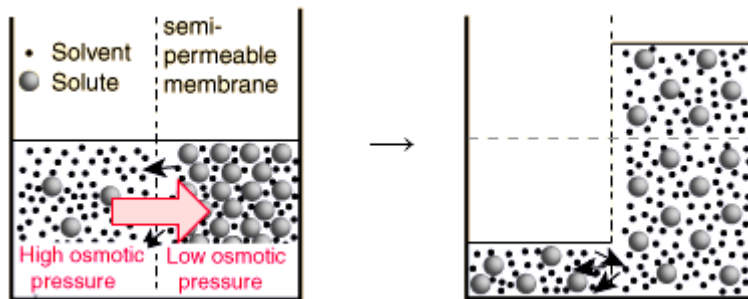


Figure 2.5 Osmotic pressure created by a difference in solute concentration

The osmotic pressure π (Pa) can be calculated with [4]:

$$\pi = cRT \quad (2.17)$$

With c is the concentration of the solution, T [K] the absolute temperature and R [$\text{J K}^{-1} \text{mol}^{-1}$] is the gas constant.

In a microchannel with a PDMS roof and two reservoirs at the ends of the channel should, when it is filled with water, two opposite flows occur due to osmosis of water through the PDMS roof. This is depicted in figure 2.6.

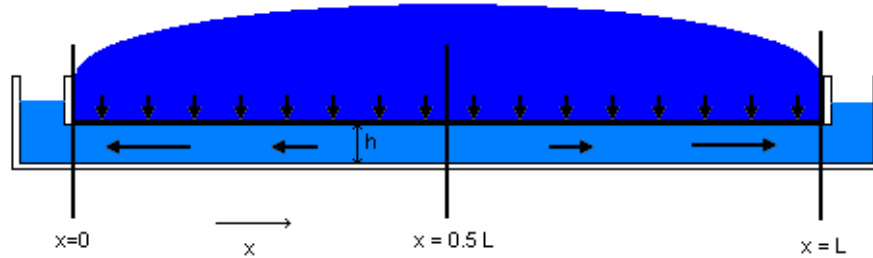


Figure 2.6 Channel with osmosis

The flow velocity that is induced by the osmotic pressure $v_{osmotic}$ can be calculated with equation 2.4, when the osmotic pressure is filled in as pressure difference. The flow velocity profile of the osmotic flow along the channel is the opposite of the flow velocity profile of the pervaporation-driven flow and is shown in figure 2.7.

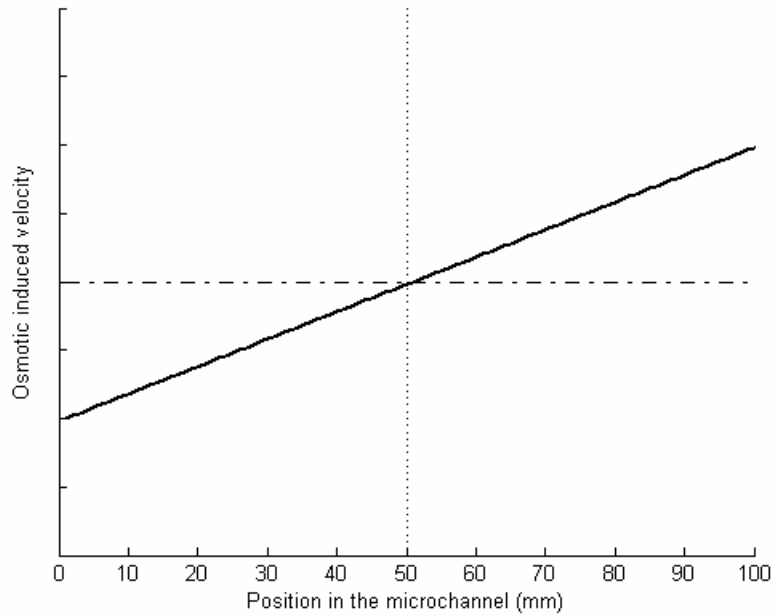


Figure 2.7. Flow velocity induced by osmosis along the channel

It can be seen that the flow velocity is negative at the left side of the channel, positive at the right side of the channel and zero in the middle of the channel. This means that the solution flows from the middle of the channel to the reservoirs causing dilution of dissolved species. To calculate the molar osmosis-induced flux $J_{osmosis}$ [mol m⁻² s⁻¹] at position x , the flow velocity is multiplied by the concentration of the dissolved species at this position:

$$J_{osmosis}(x) = v_{osmosis}(x)c(x) \quad (2.18)$$

The counteracting flux that causes the dissolved species to move back to the middle of the channel is diffusion. Diffusion is discussed in the previous section. Because in equilibrium the total flux is zero, the following equation can be derived in a similar way as equation 2.13.

$$J_{osmosis} = -J_{diff} \quad (2.19)$$

This results in:

$$cv_{osmosis}(x - 0.5L) = D \frac{dc}{dx} \quad (2.20)$$

The concentration at position x can be found by:

$$c(x) = c_0 \exp\left(\frac{v_{osmosis}x}{2D}(x - L)\right) \quad (2.21)$$

Figure 2.8 shows the concentration plotted against the position in the channel with osmosis for different D and certain values for $c_0 = 1 \cdot 10^{-7}$ M, $L = 5000$ μm , $h = 1 \cdot 10^{-6}$ m and $J_{membrane} = 1 \cdot 10^{-20}$ m³m⁻²s⁻¹.

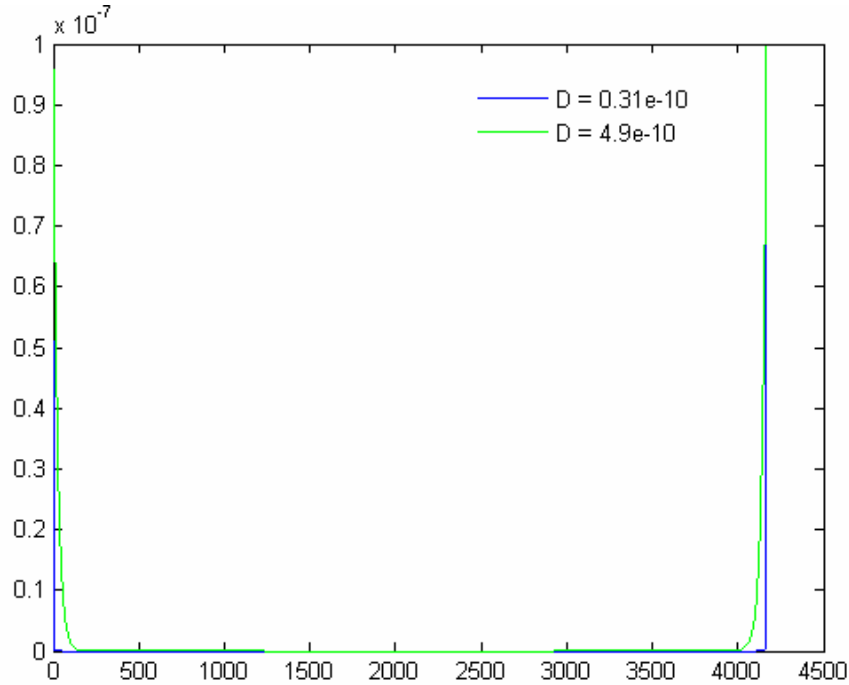


Figure 2.8 Concentration profile of the dissolved species in the microchannel after osmosis (in equilibrium with diffusion). The diffusion coefficients of dextran FITC and fluorescein are used.

It can be seen that in equilibrium large concentration gradients can be expected at the ends of the channel.

2.1.4 Flow and species flux induced by electroosmosis

Electrical Double layer

Electroosmotic flow (EOF) is the motion of a fluid through nano- or microchannels caused by an electrical field applied along the channel axis. The fluid in the channel contains ions. The microchannel wall of glass dissociates positive charges, and becomes locally negatively charged. Positive ions in the fluid are attracted to the wall and form a fixed layer, the Stern layer. Next to the Stern layer, there is accumulation of free moving positive ions in the diffuse double layer. The wall potential decreases linearly between the wall and Stern layer and it decreases exponentially in the diffuse double layer. The potential at the border of the Stern layer and the diffuse double layer (the ‘slip plane’) is called the zeta-potential. The electroosmotic mobility μ_{EOF} [$\text{m}^2 \text{V}^{-1} \text{s}^{-1}$] of a fluid depends on this zeta-potential:

$$\mu_{EOF} = \frac{\varepsilon \zeta}{\eta} \quad (2.22)$$

where ε [F m^{-1}] is the permittivity of the solution, η [Pa s^{-1}] the viscosity and ζ [V] the zeta-potential, which is determined by the nature and concentration of ions in the diffuse layer at the capillary/aqueous interface. Ren *et al.* showed that the electroosmotic

mobility of PDMS increases when PDMS is made hydrophilic [11]. The methods to make PDMS hydrophilic are described in section 3.4.3.

When a voltage is applied along the channel, and the wall is negatively charged (the most common case), the positive ions in the diffuse double layer will move towards the cathode. Due to friction, the rest of the fluid will be pulled along. The double layer and EOF direction are represented in figure 2.9.

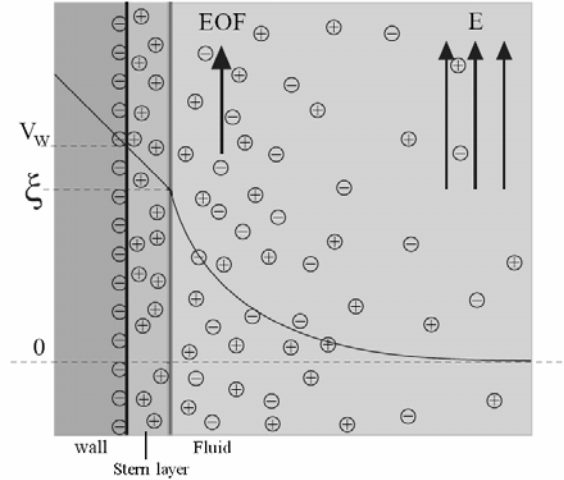


Figure 2.9 Electrical double layer with zeta-potential [16]

The electroosmotic velocity v_{EOF} [m s^{-1}] is given by the electroosmotic mobility multiplied by the electric field:

$$v_{EOF}(x) = \mu_{EOF} E(x) = \frac{\mu_{EOF} V}{L} \quad (2.23)$$

where V [V] is the voltage applied over the channel length and L [m] the length of the channel. The molar electroosmotic flow-induced flux J_{EOF} [$\text{mol m}^{-2} \text{s}^{-1}$] at position x can be calculated by multiplying the flow velocity with the concentration at position x .

$$J_{EOF} = v_{EOF} C(x) = \mu_{EOF} E(x) c(x) \quad (2.24)$$

Flow profile

The flow profile of EOF differs from the flow profile of pressure driven hydrodynamic flows. Pressure driven flows are subject to frictional forces which interact at the channel walls. This interaction results in a parabolic flow profile (see figure 2.10a). Because EOF occurs as a result of the electrical double layer movement, causing a virtual slip past the surface, the front of the flow profile is uniform (figure 2.10b).

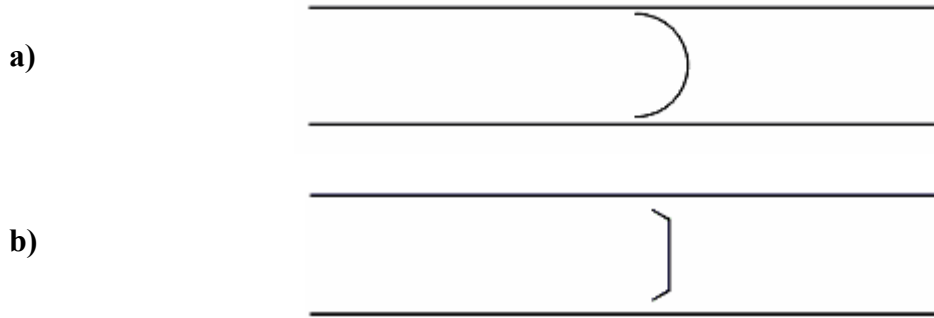


Figure 2.10 Flow profile of pressure driven flow (a) and EOF (b)

2.1.5 Species flux induced by electrophoresis

Electrophoresis is the motion (relative to the bulk liquid) of charged species or ions in a solution that results under the influence of an electrical field. The electrophoretic velocity is given by the product of the electrophoretic mobility μ_{EP} [$\text{m}^2 \text{V}^{-1} \text{s}^{-1}$] and the electric field E [V m^{-1}]:

$$v_{EP}(x) = \mu_{EP}E(x) \quad (2.25)$$

The electrophoretic mobility is related to the diffusion coefficient D [$\text{m}^2 \text{s}^{-1}$] by the Nernst-Einstein equation [12]:

$$\mu_{EP} = \frac{qD}{kT} \quad (2.26)$$

Where q [C] is the species charge, k [J K^{-1}] the Boltzmann constant and T [K] the absolute temperature of 293K. The electric field in the channel is given by:

$$E = \frac{I}{A\sigma} \text{ and } E = \frac{V_s}{L} \quad (2.27)$$

where I [A] is the electric current through the channel, A [m^2] the channel cross-sectional area, σ [$\Omega^{-1} \text{m}^{-1}$] the solution conductivity, V_s [V] the applied voltage and L [m] the length of the channel. The conductivity of a solution is determined by the concentration of ions and described by the following equation summing the contributions of all charged species [13]:

$$\sigma = F \sum_i |q_i| \mu_i c_i \quad (2.28)$$

where F [C mol^{-1}] is the Faraday constant, q_i the species charge, μ_i the mobility [$\text{m}^2 \text{V}^{-1} \text{s}^{-1}$] and c_i [mol m^{-3}] the concentration of the solute. When equation 2.25 and equation 2.28 are combined, the electrophoretic velocity for a negative ion and electric field shown in figure 2.11a can be derived from the concentration profile calculated with equation 2.16 and figure 2.11b from equation 2.21. The conductivity is proportional to the ion concentrations in the liquid and the electric field is inversely proportional to the conductivity, keeping in mind a constant current density.

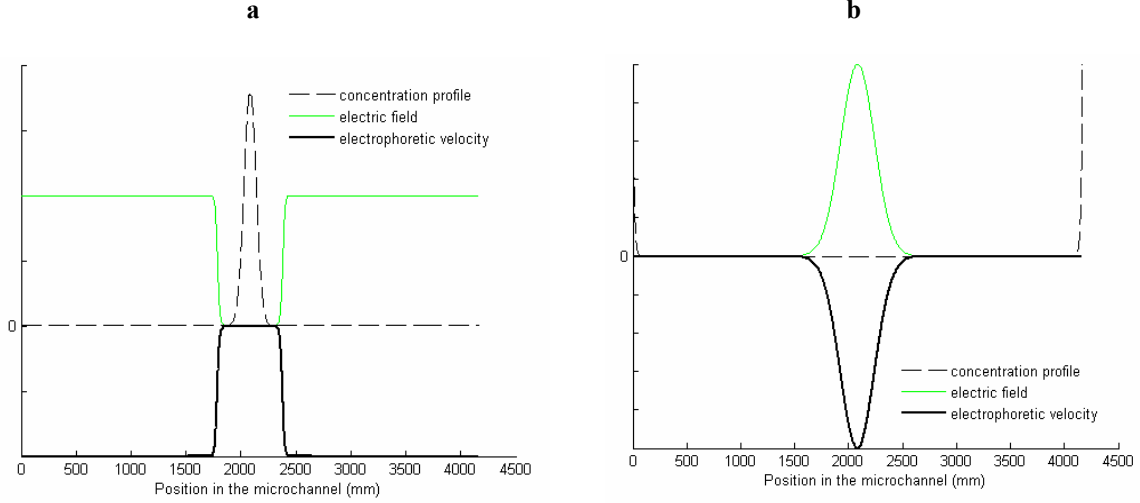


Figure 2.11 Profiles of the concentration, electric field and the electrophoretic velocity for a negative ion along the x-axis of the channel at pervaporation (a) or osmosis (b) after equilibrium is reached

The molar electrophoretic flux J_{EP} [$\text{mol m}^{-2} \text{s}^{-1}$] at position x can be calculated by multiplying the electrophoretic velocity with the concentration at position x .

$$J_{EP} = v_{EP}C(x) = \mu_{EP}E(x)c(x) \quad (2.29)$$

2.1.6 Total species flux in the channel

The total species flux in the channel is different with channels with uncovered PDMS roofs or PDMS roofs that are covered with liquid. In the first case pervaporation of the liquid takes place and in the second case osmosis takes place. In both cases the Nernst-Planck flux equation (equation 2.1) can be used:

$$J_{total} = J_{diffusion} + J_{convection} + J_{migration} \quad (2.30)$$

In both cases the diffusion term is the diffusion flux from equation 2.11 and the migration term is the electrophoretic flux:

$$J_{migration} = J_{electrophoretic} \quad (2.31)$$

Pervaporation

The convection term is for the pervaporation experiments:

$$J_{convection} = J_{PDF} + J_{pervap} + J_{EOF} \quad (2.32)$$

When this is substituted in the Nernst-Planck flux equation, J_{total} [$\text{mol m}^{-2} \text{s}^{-1}$] for the pervaporation experiments can be calculated with:

$$J_{total} = J_{PDF} + J_{diffusion} + J_{pervap} + J_{EOF} + J_{EP} \quad (2.33)$$

The total flow velocity J_{flow} can be calculated with:

$$v_{total} = v_{PDF} + v_{diffusion} + v_{pervap} + v_{EOF} + v_{EP} \quad (2.34)$$

When equilibrium has not reached $v_{diffusion}$ can be neglected. v_{PDF} and v_{EOF} are constant along the channel. v_{pervap} is also assumed to be negligible, as will be found in chapter 5. Figure 2.12 shows the electrophoretic flow of a negatively charged species and electroosmotic velocity in a channel with the concentration profile of a background analyte as calculated with equation 2.16 and 2.21. The sum of these velocities is also plotted (sum 1), just like the sum (sum 2) of the velocities with an absolute maximum electrophoretic velocity that is twice as high as with sum 1.

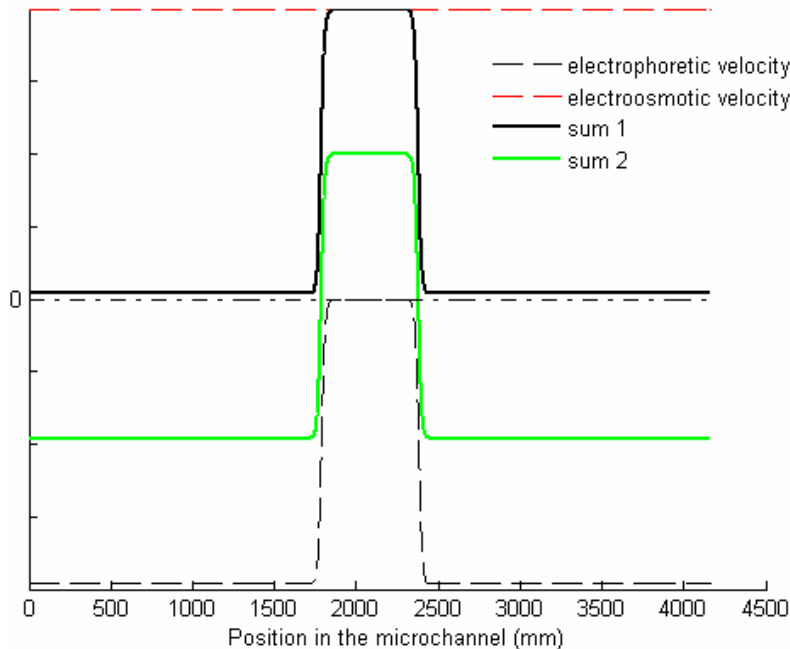


Figure 2.12 The sum of the electrophoretic velocity of a negatively charged species and the electroosmotic velocity in case of pervaporation. Sum 1 is with a small absolute maximum electrophoretic velocity and sum 2 is with an absolute maximum electrophoretic velocity that is twice as high as electroosmotic velocity.

The image shows two situations: v_{eof} is too high (sum 1) and v_{eof} is low, but not too low (sum 2).

When v_{eof} is too high, the total flux is directed from the anode (+) towards the cathode (-). Species move slow at the sides of the channel and are accelerated in the middle of the channel, because the electric field is low there. After they passed this zone they are decelerated. This causes species to accumulate at this position. Separation of species with an opposite charge can be performed in this situation, because the deceleration positions are mirrored at the middle of the channel for different charged species. Separation of species with the same charge sign and different mobilities can also be performed in this situation, because the deceleration position is shifted for different mobilities.

When v_{eof} is low, but not too low, the direction of the total flux is directed towards the anode at the sides of the channel. In the middle of the channel are two positions where the total velocity is zero (at the zero-crossings). At the zero-cross position that is situated nearest to the cathode, accumulation of species will take place, because species from the cathode reservoir and species that are already present between the zero-crossings of the total flux will be directed towards this position. At the zero-cross position that is situated nearest to the anode, no accumulation of species will take place, because species that are already present in the channel at the side of the anode will move towards the anode reservoir and the species that are already present between the zero-crossings of the total flux are directed to the other zero-cross position. The species that were present at this position before applying a voltage along the channel will stay at this zero-cross position. When two different species have opposite charge, they can be separated. They both accumulate at another zero-crossing. When two different species have the same charge sign, but have different electrophoretic mobilities, they can be separated as well in this situation, because the positions of the zero-crossings are different for different electrophoretic mobilities. However, when taking the total velocity profile into account, it is expected that separation with opposite charged species will have better separation results.

A situation that is not shown, but can be deduced from the image is when v_{eof} is too low. Then the total flux is directed from the cathode towards the anode. Species move slow at the sides of the channel and are accelerated in the middle of the channel, because the electric field is low there. After they passed this zone they are decelerated. This causes species to accumulate at this position. Here also separation can be done for the same reasons as in the high v_{eof} situation.

The accumulation of species is caused by the electroosmotic flux and the gradient in electrophoretic flux, which is caused by a gradient in conductivity by pervaporation induced flux. This means that it is possible to perform conductivity gradient focusing by pervaporation induced flux.

Osmosis

The convection term for the osmosis experiments is:

$$J_{convection} = J_{PDF} + J_{osmosis} + J_{EOF} \quad (2.35)$$

When this is substituted in the Nernst-Planck flux equation, J_{total} for the osmosis experiments can be calculated with:

$$J_{total} = J_{diffusion} + J_{osmosis} + J_{EOF} + J_{EP} \quad (2.36)$$

The total flow velocity J_{flow} can be calculated with:

$$v_{total} = v_{PDF} + v_{diffusion} + v_{osmosis} + v_{EOF} + v_{EP} \quad (2.37)$$

When equilibrium has not reached $v_{diffusion}$ can be neglected. v_{PDF} and v_{EOF} are constant along the channel. v_{PDF} and $v_{osmosis}$ are also assumed to be negligible. Figure 2.13 shows the electrophoretic- and electroosmotic velocity in a channel with the concentration profile of a background analyte as calculated with equation 2.21. The sum of these velocities is also plotted (sum 1), just like the sum (sum 2) of the velocities with an electrophoretic velocity that is twice as high as with sum 1.

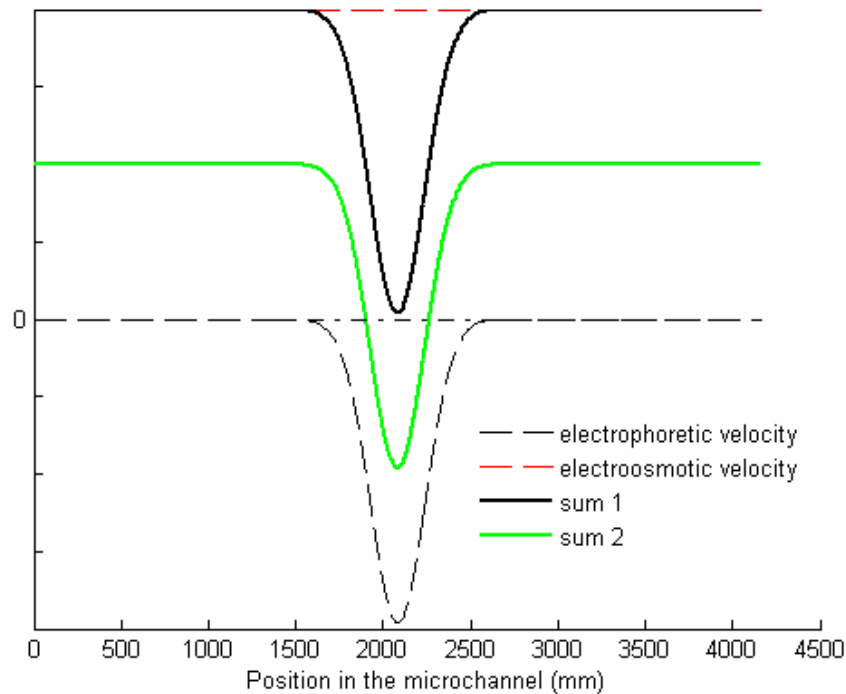


Figure 2.13 The sum of the electrophoretic velocity and the electroosmotic velocity in case of osmosis. Sum 1 is with a small absolute maximum electrophoretic velocity and sum 2 is with an absolute maximum electrophoretic velocity that is twice as high as electroosmotic velocity.

From this image also three situations can be deduced: v_{eof} is too high (sum 1), v_{eof} is low, but not too low (sum 2), and v_{eof} is too low.

When v_{eof} is too high, the total flux is directed from the anode towards the cathode. Species move fast at the sides of the channel and are decelerated in the middle of the channel, because the electric field is low there. This causes species to accumulate at this position. After they passed this zone they are accelerated. Separation of species with an opposite charge can be performed in this situation, because the deceleration positions are mirrored at the middle of the channel for different charged species. Separation of species with the same charge sign and different mobilities can also be performed in this situation, because the deceleration position is shifted for different mobilities.

When v_{eof} is low, but not too low, the direction of the total flux at the sides of the channel is high and directed towards the cathode. In the middle of the channel are two positions where the total velocity is zero (at the zero-crossings). At the zero-cross position that is situated nearest to the anode, accumulation of species will take place, because species from the anode reservoir and species that are already present between the zero-crossings of the total flux will be directed towards this position. At the zero-cross position that is situated nearest to the cathode, no accumulation of species will take place, because species that are already present in the channel at the side of the cathode will move towards the cathode reservoir and the species that are already present between the zero-crossings of the total flux are directed to the other zero-cross position. The species that were present at this position before applying a voltage along the channel will stay at this zero-cross position. When two different species have opposite charge, they can be separated. They both accumulate at another zero-crossing. When two different species have the same charge sign, but have different electrophoretic mobilities, they can be separated as well in this situation, because the positions of the zero-crossings are different for different electrophoretic mobilities. However, when taking the total velocity profile into account, it is expected that separation with opposite charged species will have better separation results.

A situation that is not shown, but can be deduced from the image is when v_{eof} is too low. Then the total flux is directed from the cathode towards the anode. Species move slow at the sides of the channel and are accelerated in the middle of the channel, because the electric field is low there. After they passed this zone they are decelerated. This causes species to accumulate at this position. Here also separation can be done for the same reasons as in the high v_{eof} situation.

The accumulation of species is caused by the electroosmotic flux and the gradient in electrophoretic flux, which is caused by a gradient in conductivity by osmosis induced flux. This means that it is possible to perform conductivity gradient focusing by osmosis induced flux.

2.2 System resolution

When separating with electrofocusing, the electroosmotic and electrophoretic velocity cause the species to concentrate at two different x-positions. Diffusion, however, causes the species to disperse. Figure 2.14 shows two Gaussian-like sample plugs.

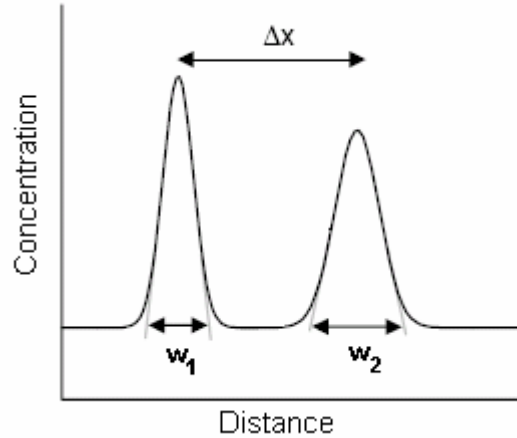


Figure 2.14 Two Gaussian-like sample plugs

The obtained resolution R_s can be described by the distance between centers of the plugs, Δx [m], and the plug widths, w_1 [m] and w_2 [m], and the ratio between the plug widths [14]:

$$R_s = \frac{\Delta x}{0.5w_1 + 0.5w_2} \quad (2.38)$$

The resolution can be improved by increasing Δx , or decreasing w_1 and w_2 . In the pervaporation or osmosis induced system the resolution can be improved by having a high pervaporation or osmosis induced flow which creates a high conductivity gradient.

2.4 Fluorescence microscopy

Illumination and observation by fluorescence microscopy is a common technique used for observation of fluid flows through micro- and nanochannels. Fluorescence microscopy is also used in cell biology, because of its specificity and selectivity. Fluorescence is a way of electron deexcitation. The electron deexcitation in the case of fluorescence is shown in figure 2.15

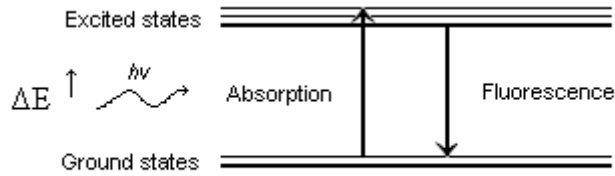


Figure 2.15 Energy level diagram of the absorption and fluorescence process [15]

When a molecule absorbs a photon of light, it is excited from the ground state to an excited state. The absorption takes about 10^{-15} s. The energy E [J] that is absorbed is given by:

$$E = hf = \frac{hc}{\lambda} \quad (2.39)$$

where h is Planck's constant, c [m s^{-1}] the velocity of light in a vacuum, λ [m] the wavelength of the incident light and f [s^{-1}] the frequency of the vibration of light. The molecule decays in about 10^{-12} s to the lowest level of the excited states while losing heat. The molecule stays in this excited state during a relative long time, usually 1-10 nanoseconds. This is called the fluorescence lifetime (τ). After the lifetime, the molecule is deexcited to the ground state, and a fluorescence photon with another wavelength than the excitation wavelength is emitted.

The wavelength of the excited and emitted light is specific for every species. This can be used to filter out the other wavelengths and thus increasing the signal over noise by using specific filters to filter out the other wavelengths.

The intensity of the illumination caused by fluorescence depends on the number of fluorescent molecules, the intensity of the incoming radiation and the efficiency of the fluorescence, expressed in the ratio of the number of photons emitted divided by the number of photons absorbed. The last one is also called the quantum yield.

Relation light intensity and concentration

The relation between the concentration of dissolved species and the light intensity is linear [16].

Photobleaching and self-quenching

Photobleaching and self-quenching are important phenomena that should be taken into account when using fluorescence microscopy. Photobleaching is the phenomenon that fluorescent molecules are irreparably damaged during excitation by a high intensity light source [17]. Self-quenching is the phenomena that fluorophores in high concentrations quench each other, due to the formation of stable non-fluorescent complexes [18]. It occurs at FITC concentrations above 10^{-3} M [19]. Figure 2.16 shows the effect of the fluorescent species concentration on the fluorescence [20].

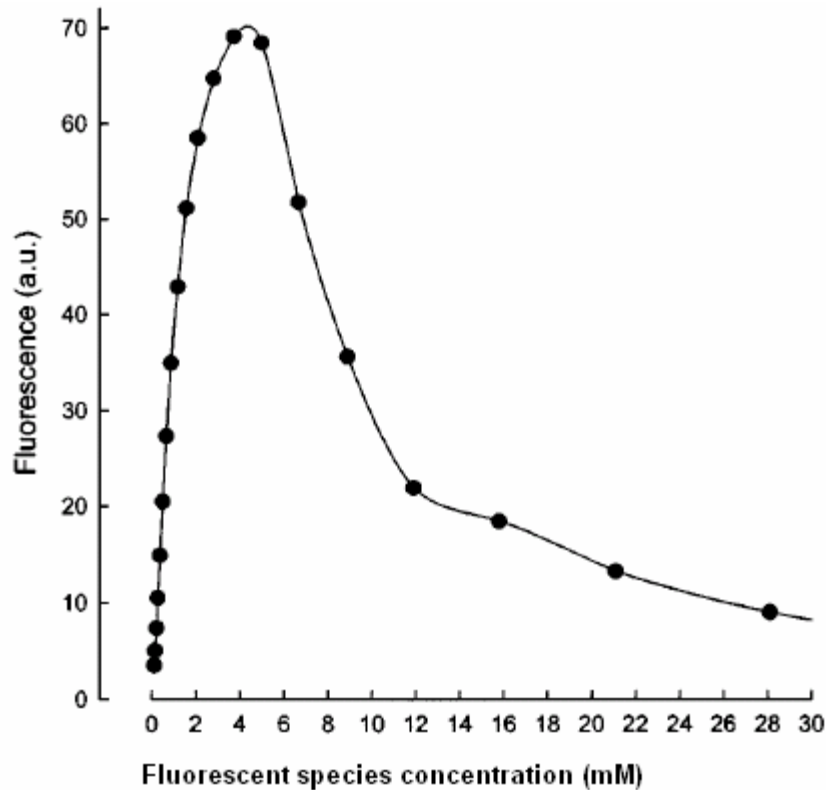


Figure 2.16 Effect of the fluorescent species concentration on the fluorescence. Calcein (fluorescein complex) was used for the measurements of this plot.

Both photobleaching and self-quenching phenomena cause a decrease in intensity of emission.

2.5 PDMS absorption and adsorption of fluorescent species

PDMS is able to absorb hydrophobic small species, like fluorescein which has a diameter of about 1 nm, that are dissolved in an aqueous solution [21]. The flexible polymer chains of the PDMS enable these species to diffuse into the bulk polymer. Because PDMS is hydrophobic in its natural state, the hydrophobic molecules prefer to diffuse into the PDMS instead of staying in the aqueous solution in the channel. This results in remaining species in the PDMS when a channel is flushed.

PDMS is also able to adsorb big hydrophilic species, like dextran FITC which has a typical diameter of several nanometers. These species are too big to diffuse into the PDMS and do not prefer to do this, because of their hydrophilicity. Species like dextran however, have hydrophobic FITC groups which prefer to adsorb on the PDMS surface, and adsorption of the entire molecule.

2.6 Pre-priming

Before using the devices in an experiment, they should be primed or even pre-primed. The priming in this research consists of filling the channel with water. Pre-priming consists of the proceedings that need to be executed in order to be able to fill the channels with water. Because PDMS is hydrophobic in its natural state (see chapter 3), pre-priming can be necessary.

Pre-priming with ethanol

Ethanol (C_2H_5OH) has a smaller contact angle with a PDMS surface than water. This means that the channel can be easier filled with ethanol than with water. When ethanol is placed in the channel first and the ethanol in the reservoirs is replaced by water then, the water diffuses into the channel through the ethanol.

Pressure driven filling

The second described method to let water enter a PDMS channel makes use of pressure. To counteract the capillary pressure, an external pressure can be applied. When the water is pumped into the channel, it will stay there when no external pressures are applied.

2.7 Electrode reactions

When an electrical current flows through a microchannel, oxidation and reduction of species takes place at the electrodes. This influences the pH which can affect the electrofocusing process and the fluorescence and charge of dissolved species, like fluorescence [16]. When platinum electrodes are used, the electrode reactions only concern the formation of the hydronium ion (H_3O^+) and the hydroxy ion (OH^-) in water. At the cathode the following reaction takes place:



and at the anode the following reaction takes place:



The electrolysis rate v_N [mol s^{-1}] can be calculated by:

$$v_N = \frac{I}{nF} \quad (2.42)$$

where I is the electrical current [A], n the valence of the electrolyzed species and F [C mol^{-1}] the Faraday constant. The amount of electrolyzed species N [mol] can be found by multiplying the electrolysis rate with the time t [s]:

$$N = v_N t \quad (2.43)$$

The concentration c_n [mol m⁻³] of the electrolyzed species can be calculated by:

$$c_n = c_0 - \frac{N}{V} \quad (2.44)$$

where c_0 is the initial concentration and V [L] the volume of the reservoir. The pH of a solution can be found by:

$$pH = -\log_{10}[H_3O^+] \quad (2.45)$$

where $[H_3O^+]$ is the concentration of hydronium ions in mol L⁻¹.

From the experiments described in chapter 5, the experiment with the dextran solution during osmosis was the most time taking experiment with the highest currents, namely 600 seconds with 12.4 μ A and 180 seconds with 15.5 μ A. This means that the total amount of electrolyzed species was $1 \cdot 10^{-7}$ mol. In the reservoir of 188 μ L, the concentration of H_3O^+ was increased with $5.3 \cdot 10^{-4}$ mol L⁻¹. This means that a buffer concentration of at least 0.53 mM should be in the reservoir with the cathode. This is the case in the experiments, because a TB-buffer with at least 10 mM was used. The pH of the TB buffer solution (pH 8.5) was almost the pKa of TRIS (8.3), and therefore the buffer was also convenient for buffering the reservoir with the anode.

Electrode reactions therefore had a negligible influence on the pH during the CGF experiments.

2.8 Temperature effects

Joule heating

Joule heating is the increase in temperature of a conductor as a result of resistance to an electrical current flowing through it. A microchannel can be seen as resistor. The power P [W] that is dissipated by a resistor is given by:

$$P = I^2 R = \frac{V^2}{R} \quad (2.46)$$

where I [A] is the electrical current, V [V] the voltage applied along the channel and R [Ω] the electrical resistance of the channel. The electrical resistance of the channel can be found with:

$$(2.47)$$

$$R = \rho \frac{L}{A}$$

where ρ [$\Omega \text{ m}^{-1}$] is the resistivity of the liquid in the channel, L [m] the length of the channel and A [m^2] the channel cross-sectional area. The total energy E [J] that is dissipated by the channel can be calculated by multiplying the power dissipation by a time of t [s] seconds.

$$E = Pt \tag{2.48}$$

The heat generation H [W m^{-1}] can be found by:

$$H = \frac{P}{L} \tag{2.49}$$

A rule of thumb is that heat generation should be below 1 Wm^{-1} will [16].

When equation 2.49 is substituted with the values for the voltages and current in the experiments of chapter 5, it can be found that heat generation caused by joule heating was maximal 0.07 Wm^{-1} and can be neglected in all experiments.

Temperature gradient focusing

Ross *et al.* created a field gradient by applying a temperature gradient along the channel. They proved that electrofocusing can be done with a temperature gradient. He called this method of field gradient focusing ‘temperature gradient focusing’ (TGF). [1] This proves that temperature differences along the channel will have influence on the electrofocusing measurements.

Chapter 3 - Device design and fabrication

This chapter describes the design and fabrication of the device that was used for the ‘conductivity gradient focusing by pervaporation’ experiments. The device demands are specified in paragraph 3.1. Then the outlook of the device is given in paragraph 3.2. Paragraph 3.3 describes why certain materials are chosen for the device. Paragraph 3.4 deals with the device design and paragraph 3.5 the device fabrication. Paragraph 3.6 describes the resulting device and its properties and at last a summary with a conclusion is given in paragraph 3.7.

3.1 Device demands

The purpose of the devices that have been fabricated is to assist the ‘conductivity gradient focusing by pervaporation’, which is described in chapter 2. The following device demands were specified in order to assist this concentration and separation method:

- The device should contain a microchannel, which is able to conduct water.
- In order to have flow by pervaporation in the channel, at least one of the channel walls should be porous for water.
- The channel should have two reservoirs at the ends of the channel. These should contain enough liquid to feed the channel during a pervaporation experiment of at least 2 hours.
- The channel should have a maximal peak capacity. Therefore a maximal flow rate is desirable.

3.2 Device outlook

In order to satisfy the device demands, the following device design was proposed:

The device consists of a substrate, which gives the device body and strength. The surface of the substrate contains an open microchannel. A water permeable layer is placed upon the substrate to form the channel roof. At the ends of the channel two reservoirs are placed. The cross-section of this channel is depicted in figure 3.1.

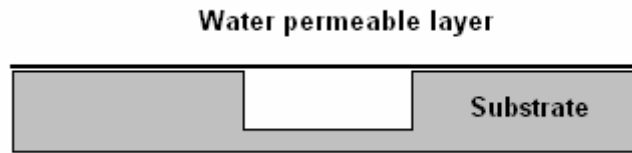


Figure 3.1 Cross-section of the proposed device with a water permeable layer on a substrate of which surface contains an open microchannel

3.3 Device materials

In microtechnology it is possible to choose from many materials to fabricate the substrate and the water permeable layer. A small selection of materials is discussed in this paragraph.

3.3.1 Substrate

The main demands of the substrate material are that the material:

- can be handled in the MESA+ cleanroom for microstructure assembly,
- is strong enough to carry the water permeable layer and the microchannel when it is filled with water,
- has a surface that is hydrophilic in its natural state or can be modified to make it hydrophilic. This property will be explained in section 3.3.2.

The materials silicon and glass satisfy these demands. Therefore these two materials are discussed in more detail.

Silicon

Silicon is widely used for the fabrication of electronic microchips, for it is a semiconductor. This is why a lot of knowledge is gained at MESA+ about the microfabrication of this material. It is also a strong material and has a surface that is naturally hydrophilic. A disadvantage of this material is that silicon conducts electrical current. This prevents electric fields to be formed in the channel. Another disadvantage of silicon is that the material is not transparent for visible light, which makes it difficult to see the separation which takes place inside the channel.

Glass

Devices that were made in the past show that a glass substrate is strong enough to carry microstructures filled with fluid [22]. It can also be handled in the MESA+ cleanroom. Figure 3.2 shows the chemical structure of glass.

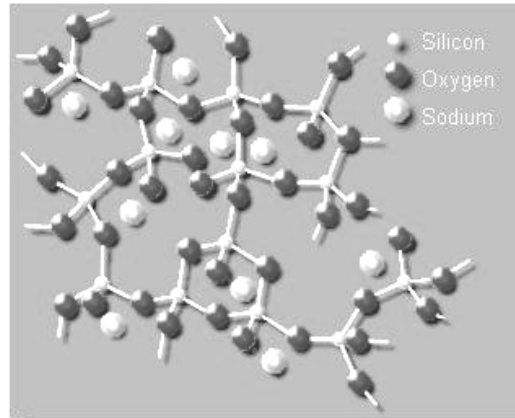


Figure 3.2 . Structure of glass

The glass that is commonly used for micromachining is borosilicate glass. Borosilicate glass is a particular type of glass, better known under the brand names Pyrex[®], Kimax[®] and Endural[®]. Pyrex[®] is mostly used in the MESA+ cleanroom. The chemical composition of Pyrex[®] is 80.6% SiO₂, 13% B₂O₃, 4% Na₂O and 2.3% Al₂O₃ [23]. It has a high durability, chemical and heat resistance and the thermal expansion of the material is low. These properties make the material very suitable for chemical laboratory equipment. A property that makes borosilicate glass suitable for the device is that it does not conduct electrical current, in contrary to silicon. Another positive property is that the surface of glass is hydrophilic. In contrary to silicon, glass is transparent for visible light. This makes the material more suitable for the device.

3.3.2 Water permeable layer

The main demands of the material of the water permeable layer are that the material:

- is water permeable and should have an as high as possible permeability coefficient,
- when it is used as roof, it is strong enough to not collapse due to capillary pressure (equation 2.2) and internal and external forces that work in the PDMS,
- makes an hydrophilic channel in combination with the other channel walls (equation 3.1),
- can be fabricated easily outside the cleanroom,
- is not autofluorescent.

When looking in the membrane science, it becomes clear that the best materials that can be used are polymers. Polymers are strong and are easy to fabricate in the BIOS laboratory. Polymers are used before in researches on pervaporation of water through membranes [5][24]. Commonly used polymers are polyimide and polydimethylsiloxane (PDMS).

Polyimide

Polyimide is a chain of imide monomers. An imide monomer is depicted in figure 3.3.

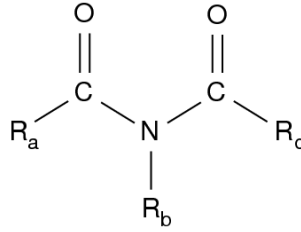


Figure 3.3 . The imide monomer [25]

Eijkel *et al.* used all-polyimide channels with a height of 500nm and a width of 30 μm on a silicon substrate in their pervaporation study. This shows that polyimide is strong enough to use as roof.

Polyimide is hydrophobic in its natural state, but with surface modifications it is possible to make it hydrophobic. These modifications will not be discussed for polyimide, but are similar to the surface modifications of PDMS, which are discussed in the section 3.4.3 about PDMS surface modifications.

Eijkel *et al.* also showed that fluids in polyimide channels flow through the channel due to pervaporation. This shows that polyimide is water permeable. The permeability of water through polyimide is determined by the diffusion coefficient and the water solubility (see equation 2.7). These respectively are $5.6 \cdot 10^{-13} \text{ m}^2 \text{ s}^{-1}$ and 3.3 wt% ($= 3.3 \cdot 10^{-2}$) [26]. Substituting these parameters in equation 2.7 gives a permeability of $1.8 \cdot 10^{-14} \text{ m}^2 \text{ s}^{-1} \text{ Pa}^{-1}$. The Young's modulus, the measure of the stiffness, of polyimide is about $2.5 \cdot 10^9 \text{ Pa}$ [27]. This a high value for the Young's modulus compared to the modulus of other polymers and this means that polyimide is a stiff polymer.

Another property of polyimide is that it is auto fluorescent. This makes polyimide not suitable for fluorescence microscopy.

Polydimethylsiloxane

Structure

Polydimethylsiloxane (PDMS) is formed by siloxane base oligomers. A cross-linking oligomer is necessary to polymerize the base oligomers. This is why commercial PDMS comes in two parts: a base and a curing agent. Figure 3.4 shows the chemical structures of the base oligomer and curing agent of PDMS.

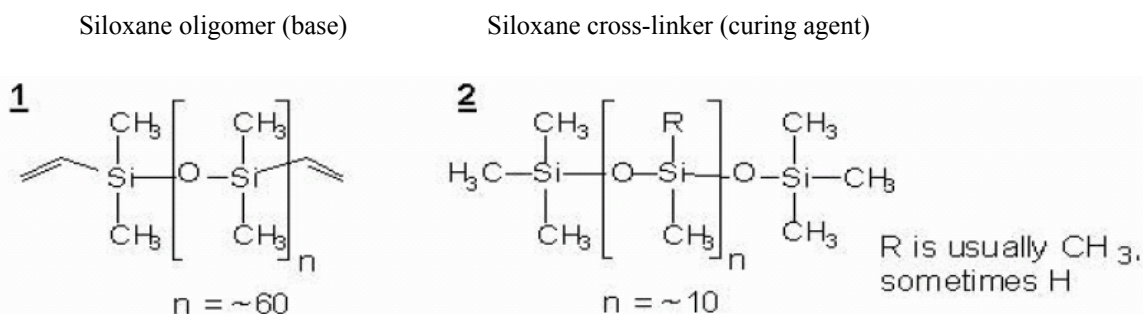


Figure 3.4 . The base and curing agent of PDMS [28]

PDMS is cured by a cross-slinking reaction. The siloxane base oligomers contain vinyl groups. The cross-linking oligomers contain at least 3 silicon hydride bonds each. The curing agent contains a platinum-based catalyst that catalyzes the addition of the SiH bond across the vinyl groups, forming Si-CH₂-CH₂-Si linkages. The multiple reaction sites on both the base and cross-linking oligomers allow for three-dimensional crosslinking. One advantage of this type of addition reaction is that no waste products, such as water, are generated [28]. Figure 3.5 shows the polymerization reaction of PDMS.

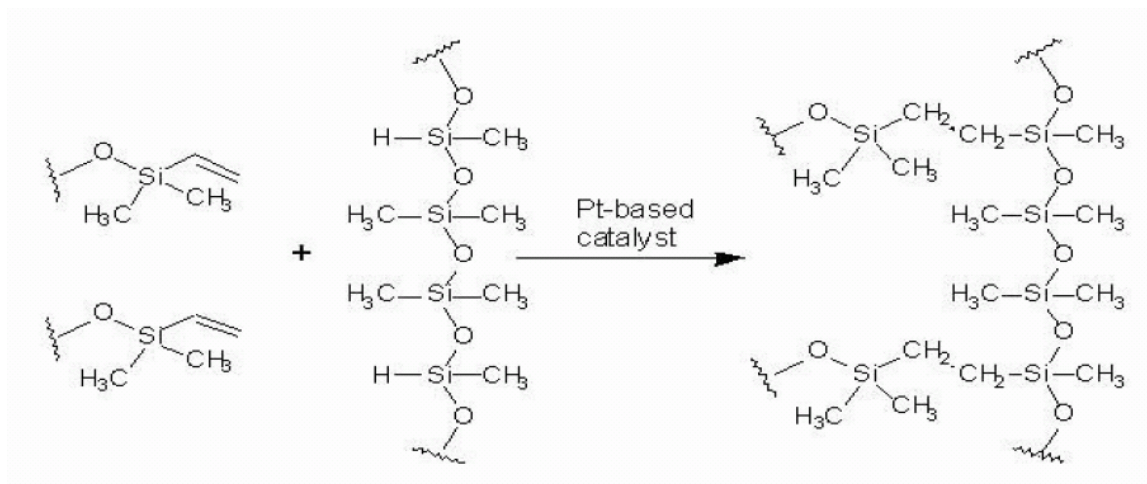


Figure 3.5. Polymerization reaction of PDMS [28]

Hydrophilicity

PDMS is hydrophobic in its natural state, but with surface modifications it is possible to make it hydrophobic. During the curing step the silicon and the oxygen atoms of the PDMS oligomers are bonded. A chain of these oligomers forms the PDMS polymer. Figure 3.6 shows the PDMS polymer at the surface of a PDMS slab.

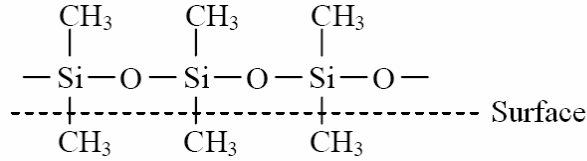


Figure 3.6 . PDMS surface [28]

It can be seen that CH₃ groups are present at the surface of the PDMS. These groups make the PDMS hydrophobic [29]. Hydrophobia is characterized by a large contact angle of water on a PDMS surface (more than 90°), the surface is non wetting. The initial water contact angle of cured PDMS is about 110° [30]. However, this is a variable value; it depends on the fabrication parameters of the PDMS. In general the initial water contact angle of PDMS is bigger than 90°.

The hydrophobicity has influence on the capillary pressure of water in the microchannel. Capillary pressure can prevent liquids to flow into the channel. The capillary pressure P_c [Pa] in a microchannel consisting of maximally four different materials can be calculated with equation 3.1 [31].

$$P_c = -\gamma \left(\frac{\cos \theta_b + \cos \theta_t}{h} + \frac{\cos \theta_l + \cos \theta_r}{w} \right) \quad (3.1)$$

Where γ [N m⁻¹] is the surface tension of the liquid, $\theta_{b,t,l,r}$ [°] are the contact angles of the liquid on the bottom, top, left and right walls, respectively, and h [m] and w [m] are the depth and the width of the microchannel, respectively. The flow velocity that can be created with the capillary pressure can be found by using equation 2.4.

It can be seen directly from equation 3.1 that the capillary pressure is high when all the channel walls have a large contact angle (>90°). This is the case with hydrophobia. PDMS for example has a water contact angle of about 110° and glass of about 45° [14][30]. For a glass channel with a height of 1µm and a width of 8µm, the capillary pressure is negative: -116,125 Pa (this is in the same order of magnitude like the atmospheric pressure of 101,325 Pa). This means that water will flow into the channel. The capillary pressure in the same channel now assembled with a PDMS roof is -39,548 Pa. This also results in that water will flow into the channel, but not as good as with the glass channel. The conclusion is that it is favourable to have small water contact angles. It was seen in experiments that the glass channels with PDMS roof did not fill with water, in contrary with the calculations made above. This can be due to irregularities of the material surfaces or larger contact angles.

When the contact angle of water on a surface is small, the surface is hydrophilic and it is wetting. When the PDMS can be made hydrophilic, the capillary pressure in a microchannel can be reduced.

Permeability

Research on permeability of water through PDMS is done in the past [7][8][10][22][24][32][33][34][58]. These show that PDMS is permeable for water. The permeability is not equal for all types of PDMS layers. It depends on factors like the quality and the roughness of the PDMS. This can be seen in the literature where different values for the diffusion coefficient are found [31][34]. Watson et al. give a diffusion coefficient of $2 \cdot 10^{-9} \text{ m}^2 \text{ s}^{-1}$ and a solubility coefficient of water in PDMS of 700 ppm ($=7.2 \cdot 10^{-4}$). When using equation 2.7 the permeability of water through PDMS can be calculated at $1.4 \cdot 10^{-12} \text{ m}^2 \text{ s}^{-1}$.

The Young's modulus of PDMS is about $7.5 \cdot 10^5 \text{ Pa}$ [35]. This means that PDMS is less stiff than polyimide. PDMS is not auto fluorescent. This makes PDMS very suitable for fluorescence microscopy.

Because the permeability of PDMS is about 75 times higher than the permeability of polyimide and PDMS is not auto fluorescent, PDMS is more suitable as material for the water permeable layer of the device.

3.3.3 Conclusion device materials

The substrate that acts like channel bottom and walls is made of glass, because this material can be handled in the MESA+ cleanroom, is strong to carry the water permeable layer and the microchannel when it is filled with water, has a surface that is hydrophilic in its natural and is transparent for visible light.

The water permeable layer that acts like channel roof is made of PDMS, because this material is water permeable with a high permeability coefficient, is strong enough, can be modified to make it hydrophilic and can be can be fabricated easily outside the cleanroom with the equipment available in the BIOS laboratory. Figure 3.7 shows the cross-sections of the device.

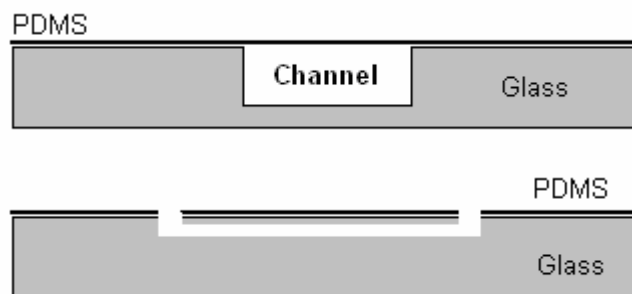


Figure 3.7 Cross-sections of the PDMS layer on the glass microchannel

3.4 Device design

The design of the device is also split in three parts: the design of the glass substrate, the design of the PDMS roof, the modification of the PDMS in order to get hydrophilic PDMS, and the design of the interface.

3.4.1 Glass substrate wafers design

Two glass wafers with different microchannel structures are used in this research. Both glass wafers are Pyrex[®] wafers. The design of the first glass wafer was carried out in the past by other researchers of the BIOS group and is a standard master wafer for microfluidics. Therefore the design of this wafer will not be described, but a short description of this ‘micropump wafer’ will be given. The results described in section 3.6.2 show that the channel width of the ‘micropump wafer’ was not suitable to carry the PDMS water permeable layer. Therefore a second design was made and wafers produced by a technician of the BIOS group especially for this research, after specifications formulated by the author. This wafer is called the ‘pervaporation channels wafer’ hereafter.

‘Micropump’ wafer design

The ‘micropump’ wafer contains microchannels with a length of about 12.5 mm and also contains longer microchannels. Only the 12.5 mm microchannels are used in this research. The height of the channels is 1 μm and the width 10, 20 or 30 μm . The wafer contains 26 channels with a width of 10 μm , 48 channels with a width of 20 μm and 34 channels with a width of 30 μm . Figure 3.8 shows the mask that was used for the fabrication of a single 10 μm wide channel.

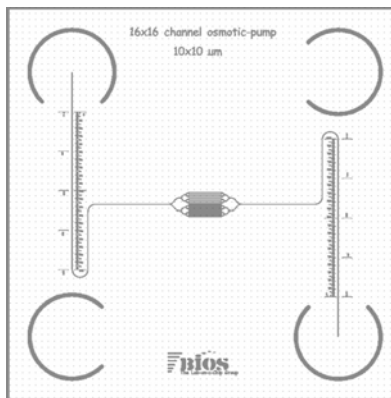


Figure 3.8 Mask of a microchannel with $w = 10 \mu\text{m}$ on the ‘micropump’ wafer

The pattern of the channel with a width of 10 μm was also used for the channels with a width of 20 μm and 30 μm .

3.5.2 ‘Pervaporation channels’ wafer design

The ‘pervaporation channels’ wafer contains an array of parallel microchannels of small width. Figure 3.9 depicts the cross-section of a microchannel with an array of 10 channels.



Figure 3.9 Cross-section of a microchannel with 10 parallel channels on the ‘pervaporation channels’ wafer

Figure 3.10 depicts the top-view of the same channel.



Figure 3.10 Top-view of a microchannel with 10 parallel channels on the ‘pervaporation channels’ wafer

The wafer contains different types of channels of different dimensions. Adjusted is the amount of parallel channels, the channel length and the channel width. The walls between the channels are 2 μm for each channel. The height is 1 μm . Table 3.1 shows the different channels and their properties. The channels have been fabricated with several methods. These are described in paragraph 3.5 ‘Device fabrication’.

Table 3.1 Channels on the ‘pervaporation channels’ wafer and their properties

Channel type	# channels (x)	Length (L) (mm)	Width (w) (μm)	Total channel width (w_t) (μm)	# channels
1 (base)	50	10	4	298	11
2	100	10	4	598	11
3	150	10	4	898	10
4	50	20	4	298	10
5	100	20	4	598	10
6	100	30	4	598	5
7	50	10	8	498	5
8	100	10	3	498	5
9	1	5	5	5	2
10	1	5	2	5	2
11	1	5	10	5	2

3.4.2 PDMS water permeable layer design

When taking equation 2.6 into account, it can be seen that it is necessary to create a glass channel structure with an as thin as possible PDMS roof in order to have an as big as possible pervaporation flow. In order to keep the channel open, it is necessary to create a PDMS roof that does not touch the bottom of the channel. This means that the maximal (centre) displacement of the PDMS should be smaller than the channel height. Figure 3.11 shows the PDMS film on the microchannel.

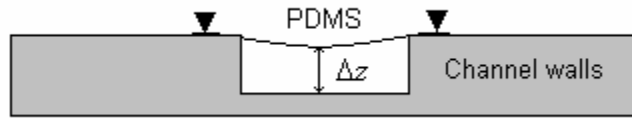


Figure 3.11 PDMS layer on the glass microchannel with the maximal displacement (Δz [m])

For a beam (in this case the PDMS roof) that is *clamped* on both sides, with channel width w [m], thickness d [m] and wall material with Young's modulus E [N/m²], the maximal (centre) displacement Δz [m] on application of a uniformly distributed load P [N/m²] is [36]:

$$\Delta z = \frac{Pw^4}{64Ed^3} \quad (3.2)$$

The beam length is the same as the channel width when the PDMS is applied on a microchannel. The Young's modulus is the modulus of elasticity and is a measure of the stiffness of a material. The uniform distributed load is determined by the capillary pressure (equation 2.2).

In order to have an as thin as possible PDMS layer and to have a maximal centre displacement that is larger than the channel height, other parameters can be adjusted. These are the channel width, the Young's modulus and the density of the PDMS. The design parameters are discussed below.

Thickness of the PDMS

The thickness of the PDMS layer is determined by the spinning rate and the spinning time. Figure 3.12 shows the thickness of the spin-coated PDMS as function of the spinning rate. The spinning time was fixed at 20 seconds.

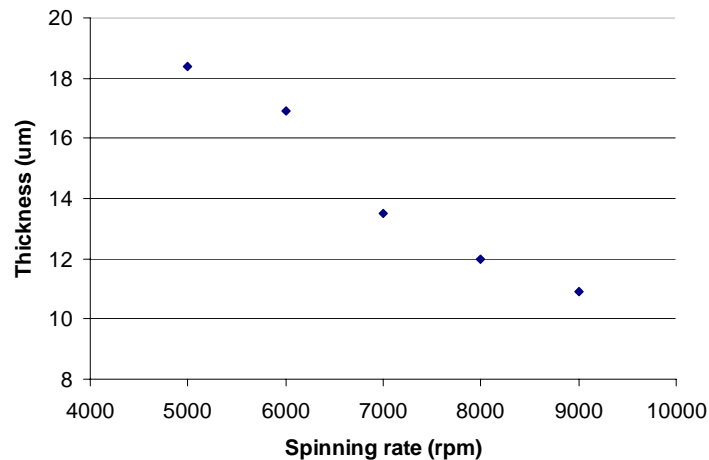


Figure 3.12 Thickness of spin-coated PDMS versus spinning rate [37]

It can be seen that the film thickness decreases when the spinning rate increases.

Channel width

The channel width is determined by the glass wafer design.

Young's modulus of the PDMS

The mixing ratio of the curing agent and base determine the degree of polymerization, and thereby the stiffness of the PDMS: the more curing agent is present, the more polymerization takes place and the stiffer the PDMS is. And stiff PDMS means a high Young's modulus. Figure 3.13 shows the Young's modulus of PDMS versus the mixing ratio.

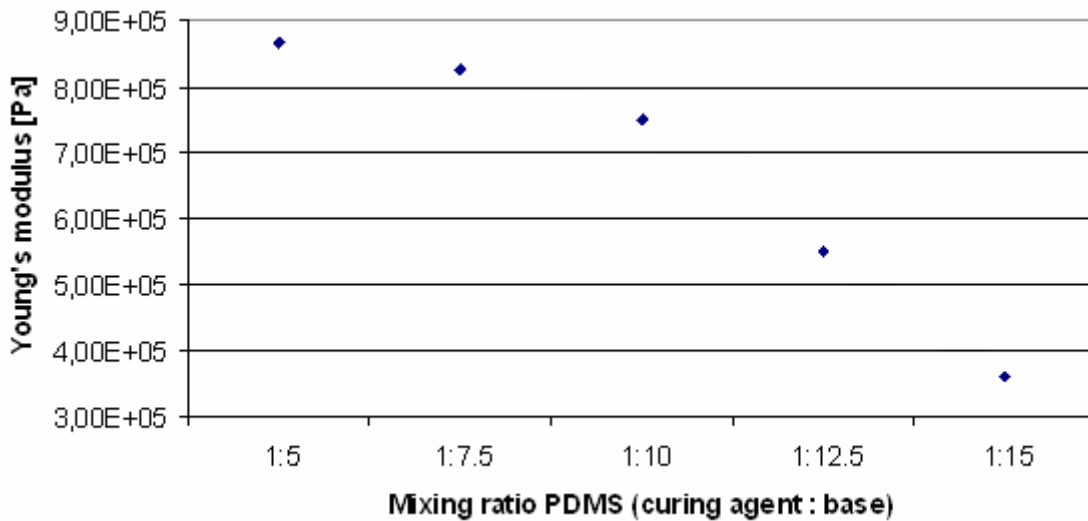


Figure 3.13 Young's modulus of PDMS versus the mixing ratio [35]

It can be seen that the Young's modulus (and the stiffness of the PDMS) decreases when the mixing ratio decreases.

The Young's modulus of PDMS is also determined by the curing time and curing temperature determining the reaction rate of polymerization. When the reaction rate is high, polymerization occurs fast and a high Young's modulus can be expected. When the reaction rate is low, polymerization occurs slowly. This can be that slow, that the PDMS is still reacting while the device is already finished. This can cause dimensional problems.

Just like many other reactions, PDMS polymerization follows the Arrhenius equation [38]:

$$k = Ae^{-E_a/RT} \quad (3.3)$$

Where k [s^{-1}] is the rate constant for the reaction, A [s^{-1}] the frequency factor, E_a [$kJ mol^{-1}$] the activation energy, R [$J K^{-1} mol^{-1}$] the gas constant and T [K] the temperature. The

frequency factor is a measure for the chance that a molecule hits another molecule in the right way in order to proceed the polymerization reaction. The activation energy, or threshold energy, is the minimal energy needed for a reaction to occur. Using equation 3.3 the reaction time τ [s] can be written as:

$$\tau = Ae^{E_a/RT} \quad (3.4)$$

It can be seen that the reaction time increases exponentially as a function of the inverse temperature. In other words: the higher the temperature, the faster the curing of the PDMS.

A decrease of the permeability of the PDMS is expected when the Young's modulus increases. This is based on the fact that more bonds are made when the Young's modulus increases.

Density of the PDMS

Figure 3.14 shows the density of PDMS versus the mixing ratio [35].

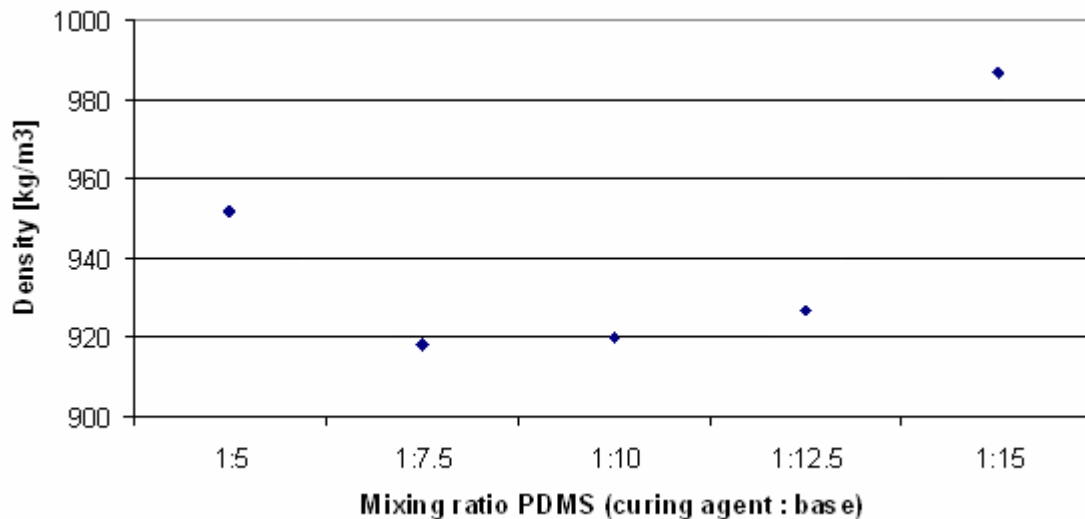


Figure 3.14 Density of PDMS versus the mixing ratio [35]

The density of PDMS is a function of the mixing ratio, but the difference in density is maximal 7% in the range used in figure 3.14. Differences are therefore negligible.

A decrease of the permeability of the PDMS is expected when the density increases. This is based on the fact that the space between PDMS polymers is smaller through which it is harder for the water molecules to pervaporate.

Bonding

The final PDMS fabrication step is to bond it on the glass wafer. When this is done with gluing, there is a risk that the channels will fill with glue and that the PDMS is not continuously bonded on the glass, which causes liquid to flow from the channel under the

PDMS layer. A more suitable method is to bond the PDMS covalently to the glass wafer. A plasma treatment step enables the PDMS slab to bind covalently to another slab, or in the case of this research on a glass surface that is also plasma treated. This is doubted by other researchers, but they agree that materials bond together after plasma treatment. Figure 3.15 shows a PDMS surface that is bonded to a silica surface after plasma treatment with a covalent binding.

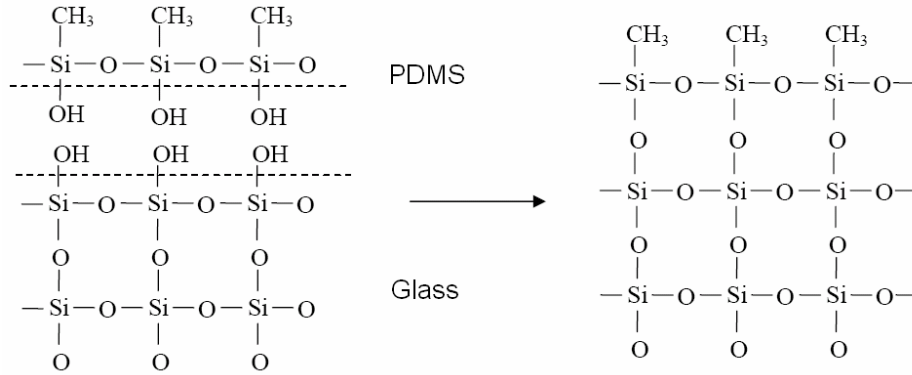


Figure 3.15 . PDMS bonded to glass [28]

The principle behind this is that oxygen plasma activates the surfaces of the materials, which causes the materials to bond covalently to each other. This activation means that the CH₃-groups of for example PDMS are eliminated and OH-groups comes into place at the surface. Section 3.4.3 shows other effects of the surface activation with oxygen plasma and describes the chemical reactions behind the principle in more detail.

Conclusion

In order to have a as thin as possible PDMS layer and to have a maximal centre displacement that is larger than the channel height, the channel width, the Young's modulus and the density of the PDMS can be adjusted. It is favourable to adjust the channel width for it is expected that it has no direct influence on the permeability of the PDMS.

3.4.3 Surface modifications of the PDMS

There are several methods to make the PDMS surface hydrophilic.

Plasma treatment

A method of making the PDMS surface hydrophilic (to increase the capillary filling pressure) is with plasma treatment [39][40]. After the curing step, the PDMS slab is loaded in a plasma cleaner with an oxygen plasma in it. During oxygen plasma treatment, the hydrophobic CH₃-groups on the PDMS surface are eliminated and hydrophilic OH-groups are formed, due to oxidation [41]. This is depicted in figure 3.16.

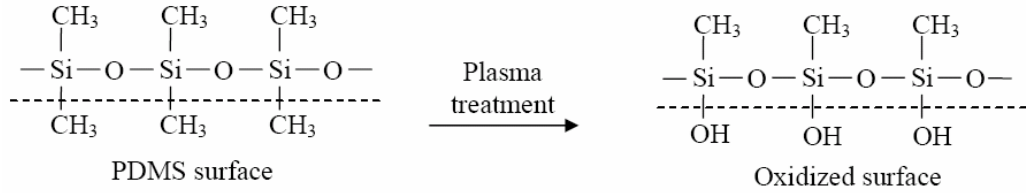


Figure 3.16. Plasma treatment of PDMS [28]

The OH-groups cause the PDMS surface to be hydrophilic. This however does not produce a long lasting effect. Bausch *et al.* treated PDMS for 5 minutes in RF plasma and then determined the water contact angle in time. This was done with PDMS samples that were stored in dry air at room temperature and samples that were stored in pure water. Figure 3.17 shows the recovery of the hydrophobic surface.

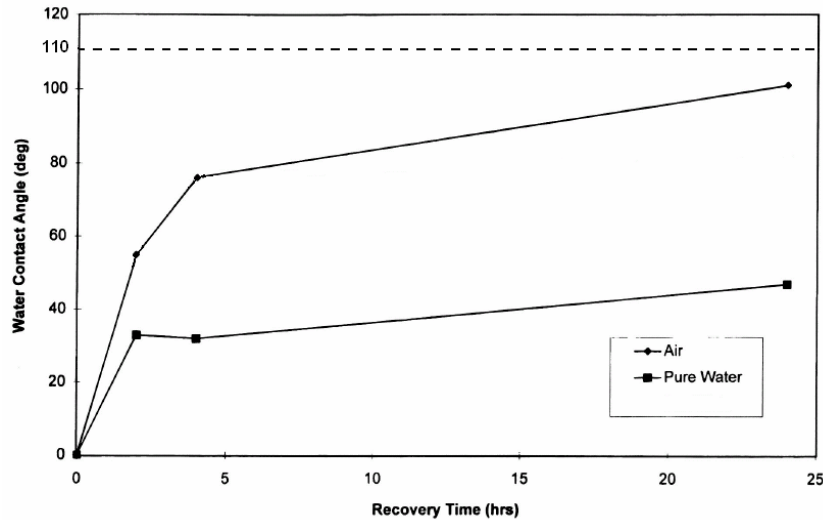


Figure 3.17 . The water contact angles of plasma treated PDMS samples stored in air or pure water measured in time. The initial water contact angle was 110° [30]

It can be seen that in the Bausch *et al.* research the PDMS returned almost to its old state after about 1 day when it was stored in air. Other groups measured recovery times from a few minutes to several days [29][41][42][43]. This means that the hydrophilicity of PDMS is unstable in air when treated with plasma. Owen's group gave a few possible causes of hydrophobicity recovery in air [42]. These differ from internal migration or diffusion of molecules to external contaminations which cover the PDMS.

Conclusion is that oxygen plasma treatment makes the PDMS surface hydrophilic, but the hydrophobia recovers within a few days when the PDMS is stored in air.

Two of the measures to resist the hydrophobic recovery are; storage of the PDMS in water, and extraction of unreacted oligomers. These are described below.

Plasma treatment and storage in water

Figure 3.17 also shows the contact angle of plasma treated PDMS that was stored in water. It can be seen that this PDMS is more stable for a longer time. This was also found in literature. Whitesides' group stated that PDMS definitely stays hydrophilic when it is stored in water [44][45]. Ren *et al.* measured the electroosmotic mobility of oxygen plasma treated PDMS channels that were stored in water and later exposed to air [43]. Figure 3.18 shows that oxygen plasma treated PDMS channels stored in water have a stable electroosmotic mobility. The electroosmotic mobility decreased, when the PDMS was exposed to air after the 4th day.

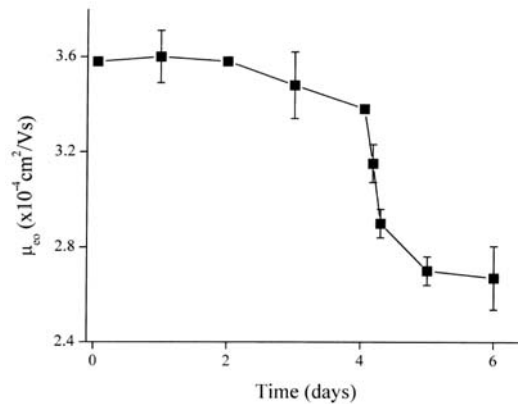


Figure 3.18. The electroosmotic mobility of oxygen plasma treated PDMS channels that were stored in water. After the 4th day the PDMS is exposed to air [43]

Plasma treatment and extraction of unreacted oligomers

A method to stabilize the hydrophilicity after plasma treatment was introduced by Vickers *et al.* In figure 3.4 it could be seen that the base oligomers contain 2 CH_3 -groups. Cured PDMS still contains unreacted base oligomers. The most likely explanation of the hydrophobic recovery is that unreacted oligomers diffuse to the PDMS surface and make the surface hydrophobic again, and hence it is favourable to eliminate these oligomers. Vickers *et al.* extracted unreacted oligomers after the curing step, by immersing the PDMS in triethylamine solution, ethyl acetate and acetone. Next, the oligomer-free PDMS was oxidized in an air plasma cleaner to generate a stable layer of SiO_2 . This layer was stable for at least 7 days in air [46].

Plasma treatment and polymer grafting

Another way to make PDMS longer hydrophilic after plasma treatment is grafting of polymers on the PDMS surface. This can be done with polymers like PEG, BSA and HEMA [47][48][49]. For example, Choi *et al.* showed that the water contact angle of PDMS grafted with HEMA remained smaller than PDMS without grafting (see figure 3.19).

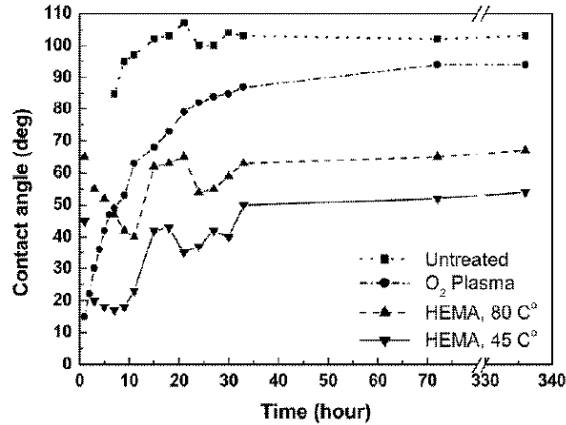


Figure 3.19 . Contact angles of PDMS surfaces after various treatments [47]

Cracks

Fritz *et al.* report that they found cracks in the PDMS when using plasma treatment for large exposure times and powers. This is due to silica forming on the PDMS at the surface. Figure 3.20 shows an image of a cracked PDMS surface.

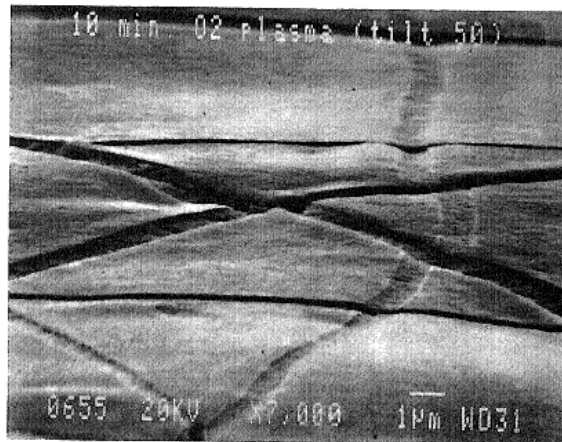


Figure 3.20 . Cracks in the PDMS after oxygen plasma treatment for 10 minutes at 70W [42]

Conclusion

It is theoretically possible to make and to keep PDMS hydrophilic with the described measures. It is not known what the measures do with the permeability of the PDMS.

3.4.4 Interface design

The interface consists of two reservoirs which can contain enough liquid to do pervaporation experiments of at least 2 hours. In paragraph 2.1 it was discovered that the flow velocity that is caused by pervaporation with polyimide channels can be $4 \cdot 10^{-6} \text{ ms}^{-1}$ [5]. When taking our channel dimensions in account (the pervaporation surface is 3 times

smaller the flow surface 1.88 times higher and the thickness of the roof 21.7 times higher) and the fact that the permeability of PDMS is 75 times higher than the permeability of polyimide, the expected flow velocity will be $8.64 \cdot 10^{-6} \text{ m s}^{-1}$. This means that per second $6.9 \cdot 10^{-17} \text{ m}^3$ or $6.9 \cdot 10^{-14} \text{ L}$ water moves into the reservoirs. For an experiment of 2 hours, each reservoir should contain at least $4.97 \cdot 10^{-10} \text{ L}$ or 49.7 nL of liquid.

One drop of water is about 50 μL , so it should be possible to eliminate the reservoirs from the design and use water drops for the supply of liquid. Water drops as reservoirs also have the problem that they are not electrically insulated enough. A film of water on the surface of the PDMS can electrically interconnect the reservoirs and causes part of the current to flow through this film instead of through the channel. This is not desirable when an electric field is applied in order to do electroosmosis and electrophoresis. This is why it is chosen to apply reservoirs on the channel ends.

The first action that has to be taken is to open the microchannels at the channel ends where the interconnections between the channel and the reservoirs are. This can be done with cutting or stamping.

Figure 3.21 shows two possible designs for the reservoirs.

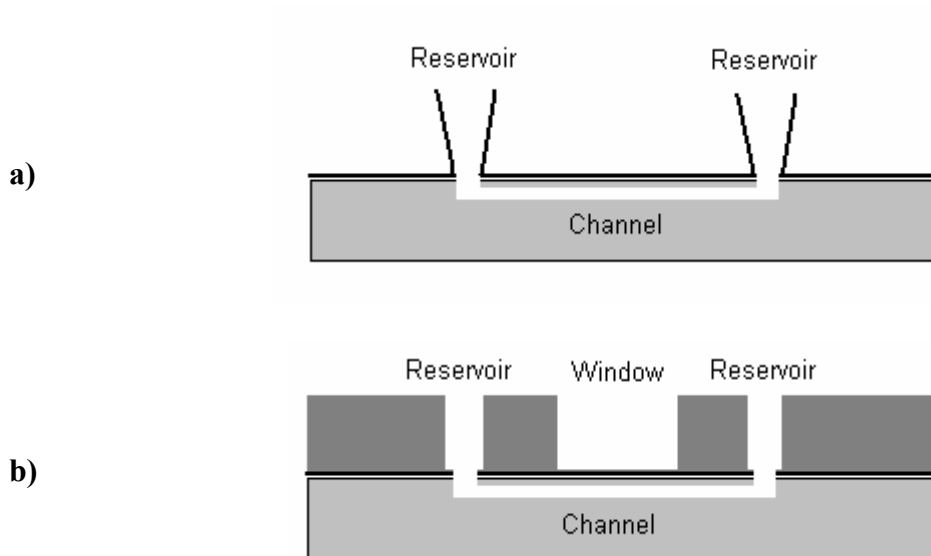


Figure 3.21. Two possible designs for reservoirs on the device

The first design (a) is the existing channel structure, including the glass substrate and the PDMS layer, with two separate reservoirs which are mounted above the channel ends. The material of the reservoirs can be plastic, glass or PDMS. The last ones can be surface activated and covalently bonded. This means that it is not necessary to use glue. The materials were both eliminated as candidates: The glass because it is expected that the

glass reservoir should have a smooth surface to keep the water in the reservoir. These reservoirs are hard to fabricate. The PDMS is expected to have too little bonding area around the channel ends to bond properly.

The second design (b) is the existing channel structure with one slab of material placed upon it. In this slab three holes are cut; two reservoir holes and one window hole, where the PDMS channel roof comes into contact with the atmosphere. The slab can be of different materials. A good material will be PDMS, because PDMS is easy to fabricate, transparent for light and can be bonded covalently to the PDMS layer.

It is desirable to close the reservoirs to prevent evaporation of liquid from the reservoirs

3.5 Device fabrication

This paragraph describes the fabrication of the devices, supported by the information that was gained in paragraph 3.4 about the design of the device. First the fabrication of the glass wafers is described. Then the fabrication of the PDMS roof and its modification will be described.

3.5.1 Glass substrate wafer fabrication

All wafers are fabricated in the MESA+ cleanroom by Johan Bomer, a technician of the BIOS-group.

‘Micropump’ wafer fabrication

Because this wafer was already fabricated before this project started and only used to tweak the process parameters of the PDMS roof, the fabrication of this wafer will not be described.

‘Pervaporation channels’ wafer fabrication

For the fabrication of the ‘pervaporation channels’ wafers a mask was created by Johan Bomer and the author. Figure 3.22 shows a channel of type 1.

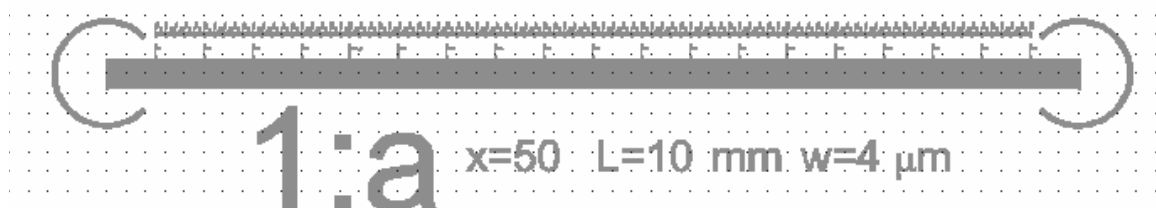


Figure 3.22 Mask of a microchannel of channel type 1 on the ‘pervaporation channel’ wafer

The complete ‘pervaporation channels’ mask is depicted in figure 3.23.

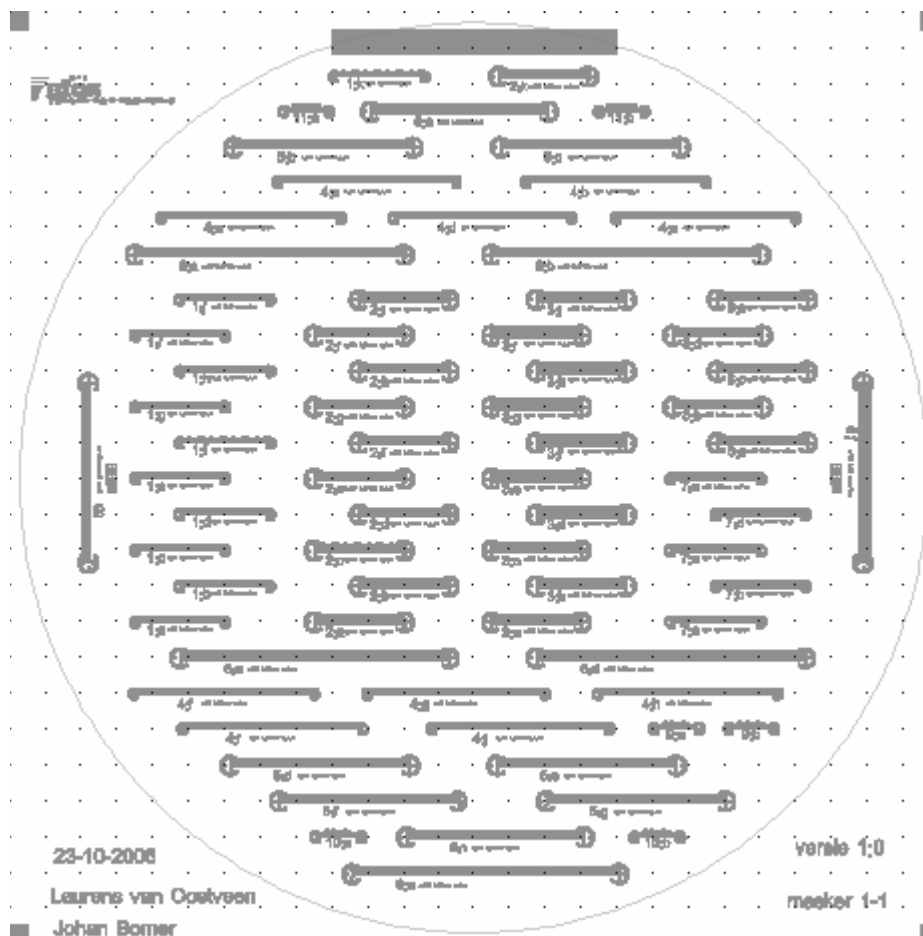


Figure 3.23 Mask of the 'pervaporation channels' wafer

Appendix A shows the process flows of the processing of the pervaporation channel wafer. Two etching methods are used for etching away the Pyrex (glass) at the channels: Reactive Ion Etching (RIE) and BHF etching. The first method is a dry etching method. It creates channels with straight walls (see the figures at method A in Appendix A). The second method is a wet etching method. It creates channels with bowl shaped walls (see the figures at method B in Appendix A). The chromium and gold are used as mask for the wet etching.

3.5.2 PDMS water permeable layer fabrication

After the glass wafer fabrication, the PDMS layers of both structures were created. Since the channels are etched in glass, direct spin-coating of the PDMS on the glass wafer was not possible, because the channels would be filled with PDMS. This is why a dummy wafer was used to spin-coat the PDMS on. The used PDMS was 2-component SYLGARD 184 of Dow Corning. To remove volatile pollutants, like air or water, the PDMS was degassed in a vacuum chamber.

On the dummy wafer (diameter = 100 mm) a transfer foil (3M CG3720) with a diameter of 108 mm was tightened with 3M adhesive tape at the backside of the silicon wafer and the overhanging foil. On the foil the PDMS layer was spin-coated. Then the PDMS was cured in an oven. After the curing step the transfer foil with PDMS layer was cut loose from the dummy wafer. The PDMS on foil was, together with the glass wafer, held in RF oxygen plasma for 5 minutes to activate the surfaces. The used equipment was Harrick plasma cleaner/sterilizer at pressure 400mTorr and with RF level 'Hi'. After the plasma step the PDMS was transferred from the foil to the glass surface by manually rolling the foil on the glass surface. The process flow of the PDMS production is described in Appendix B and depicted in figure 3.24.

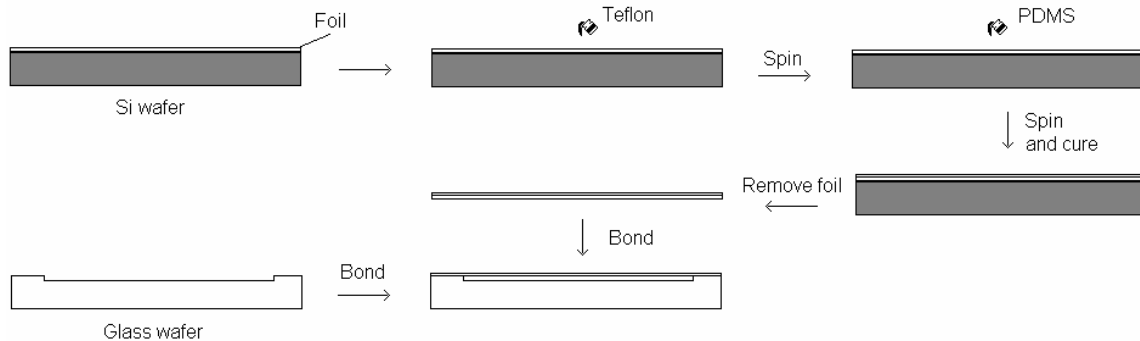


Figure 3.24 Process flow of the PDMS on the glass channel

As stated in the previous paragraph, the goal of the PDMS fabrication is to make a PDMS layer that is as thin as possible in order to create an as big as possible pervaporation flow. Therefore the following fabrication parameters were adjusted first for different PDMS layers: spinning rate, mixing ratio, curing time and curing temperature. These different PDMS layers were transferred on the 'micropump' wafer. The parameters that were adjusted are:

Spinning rate

The PDMS was spun on the transfer foil with several spinning rates; 2000 rpm, 4000 rpm and 9000 rpm, resulting in thicknesses of respectively 50, 20 and 15 μ m. The other parameters were kept constant; mixing ratio 1:10, curing time 60 minutes and curing temperature 60°C.

Mixing ratio

The mixing ratio was chosen as 1:5 and 1:10. The other parameters were kept constant; spinning rate 4000 rpm, curing time 60 minutes and curing temperature 60°C.

Curing time

Several curing times were used; 60 minutes and 17 hours. The other parameters were kept constant; spinning rate 4000 rpm, mixing ratio 1:10 and curing temperature 60°C.

Curing temperature

Several curing temperatures were used: 60°C and 80°C. The other parameters were kept constant; spinning rate 4000 rpm, the mixing ratio 1:10 and the curing time 60 minutes.

Channel width

The channel widths on the micropump wafer are 10, 20 or 30µm. Later the 'pervaporation channel' wafer was used. The channel widths on this wafer were 3, 4 or 8 µm (and 2, 5 and 10µm, including the test channels 9, 10 and 11). The other process parameters were chosen as follows: mixing ratio 1:10, spinning rate 6000 rpm (this should create a thickness of 17µm), curing temperature 80°C and curing time 60 minutes.

3.5.3 Surface modifications of the PDMS

A few methods to make the PDMS hydrophilic are used. All these methods make use of oxygen plasma treatment. This treatment was already executed in the PDMS fabrication step to let the PDMS covalently bond to the glass wafer and can be combined with the surface modification step. As described before, the PDMS on foil was held in RF oxygen plasma for 5 minutes. The used equipment was Harrick plasma cleaner/sterilizer at pressure 400mTorr and with RF level 'Hi'.

First it was investigated if water flows into the channel by diffusion via ethanol and by hydrodynamic pressure. Next it was investigated if the oxygen plasma created a hydrophilic PDMS surface. Then the stability of a PDMS layer was investigated for when it was stored in air or in water after the plasma treatment. Finally a PDMS sheet was treated with triethylamine, ethylacetate and acetone to extract the unreacted oligomers, as described in paragraph 3.4.3. Table 3.2 shows the steps which are followed in this treatment.

Table 3.2 Steps of extracting unreacted oligomers

Step	Duration	Activity
1	2 hours	PDMS slab was immersed in 200 ml triethylamine at 25°C
2	2 hours	PDMS slab was immersed in 200 ml ethylacetate at 25°C
3	2 hours	PDMS slab was immersed in 200 ml acetone at 25°C
4	2 hours	PDMS slab was dried in the oven at 80°C

3.5.4 Interface fabrication

To cut holes in the PDMS layer for the interconnections between the reservoirs and the channel both a scalpel and a stamp were used. The stamp was fabricated from a hollow pipe with an inner diameter of 0.5mm and an outer diameter of 1mm.

The two designs that were proposed in section 3.4.4 were used both to make reservoirs. The design with the two separate reservoirs (design A) was fabricated with plastic pipet-tips. First pipet-tips of 20 µL (for shorter experiments) were used. The outer diameter of the bottom was 2mm and the inner diameter 2mm. Second pipet-tips of 188 µL were

used. The outer diameter of the bottom was 4mm and the inner diameter 3mm. The tips were glued with Loctite Hysol epoxy, Araldyte rapid epoxy or Dow Corning 734.

3.6 Results and discussion

3.6.1 Glass substrate wafer results and discussion

Five ‘pervaporation channels’ wafers were created: two wafers with RIE and three with wet etching. Two wafers of method B were overetched. This resulted in elimination of the walls between the parallel channels. Figure 3.25 shows the shape of the channels created with RIE and wet etching and also shows the effects of overetching and underetching with wet etching.

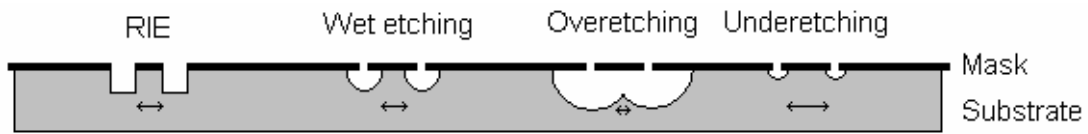


Figure 3.25. The cross-section of etching profiles of two parallel channels when RIE or wet etching is used. The etching profiles of wet etching in case of over- and underetching show that the channels respectively become wider and overlap, and become smaller with a wider separation.

3.6.2 PDMS water permeable layer results and discussion

As described in paragraph 3.4, four parameters of the PDMS processing for the ‘micropump wafer’ were changed: the spinning rate, the mixing ratio of the curing agent and base, the curing time and the curing temperature.

The parameters of the first PDMS layer were: mixing ratio 1:10, spinning rate 9000 rpm (this should create a thickness of 10 μ m), curing temperature 60°C and curing time 60 minutes. Figure 3.26 shows some of the resulting channels.

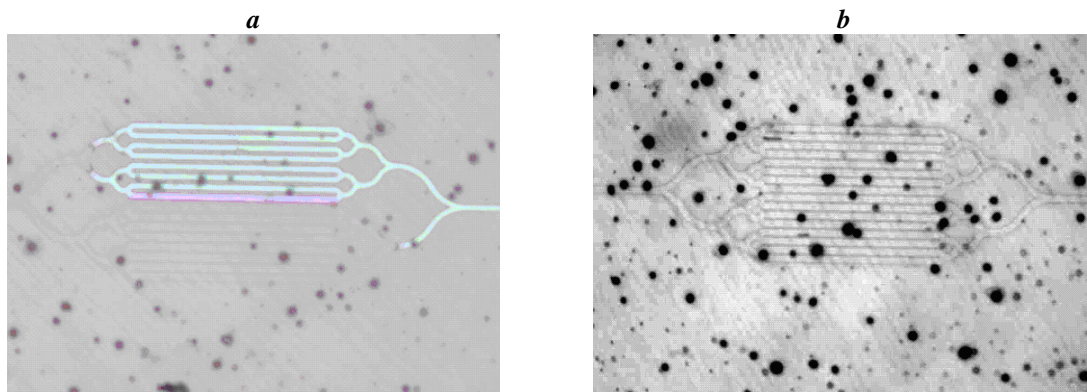


Figure 2.26 Microchannels, (a) is partly closed and (b) is completely closed. The dots in the images are bubbles in the PDMS

It can be seen that the channels are collapsed or partly collapsed, because the collapsed parts of the channel are dark gray and the not collapsed parts of are light gray. Expected is that this is due to the fact that the PDMS roof was not stiff enough and therefore bended so far that it stick to the bottom of the glass channel.

Other PDMS layers were processed. The process parameters of these layers were separately adjusted in order to create a stiffer PDMS roof.

Spinning rate

A spinning rate of 4000 rpm and a spinning rate of 2000 rpm were used to create a PDMS layer of respectively 50 μm and 20 μm thick. The result of both changes was that more 10 μm channels were not collapsed than with the first PDMS layer, indicating that the layer became stiffer. The difference between the results of the spinning rate of 2000 rpm and 4000 rpm was negligible. Because a thin PDMS layer is desirable in order to have a large pervaporation flow, the next parameters were adjusted at a constant spinning rate of 4000 rpm.

Mixing ratio

A PDMS layer with a mixing ratio of 1:5 was processed. The result was that most of the 10 μm channels were collapsed. This means that increasing the mixing ratio does not result in a better performance of the PDMS layer.

Curing time

The curing time was raised from 1 hour to 17 hours. The result was that the PDMS was stiffer: more 10 μm channels were not collapsed. This means that the increasing the curing time has a positive influence on the stiffness of the PDMS layer.

Curing temperature

The curing temperature was increased from 60 $^{\circ}\text{C}$ to 80 $^{\circ}\text{C}$. This was done for more PDMS layers. The stiffness of the PDMS layer did not increase

Finally, the PDMS on the micropump wafer was processed with the following parameters: mixing ratio 1:10, spinning rate 4000 rpm (this should create a thickness of 20 μm), curing temperature 60 $^{\circ}\text{C}$ and curing time 17 hours. Figure 3.27a shows the result of this processing.

During processing the PDMS it was discovered that, despise of the degassing step, many encapsulations were present in the PDMS (the spots in figure 3.27a). These are introduced with the spin-coating step. To solve this problem an extra degassing step was introduced after the spin-coating. The result was that less encapsulations were present in the PDMS. Figure 3.27b shows a microchannel with a PDMS roof that did not undergo an extra degassing step and a microchannel that did undergo an extra degassing step.

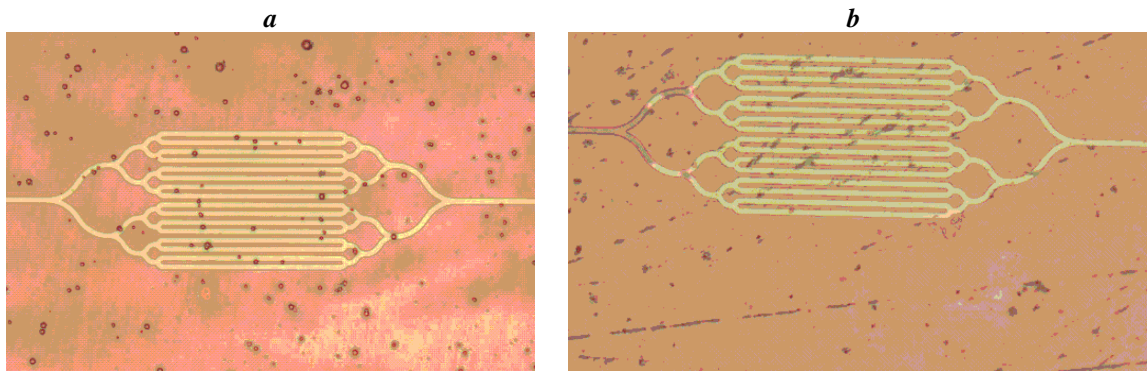


Figure 3.27. Fabricated 10µm microchannels without extra degassing (a), and with extra degassing (b). The cuts in (b) can be ignored, for it is caused by a processing failure

The transferring of the PDMS layer to the glass wafer sometimes gave problems. The adhesion of the PDMS layer to the glass layer was not good enough in some cases and the adhesion of the PDMS layer to the transfer foil was too good in other cases. The result was in both cases that spots on the glass wafer were not covered by PDMS or had an air bubble in between the glass wafer and the PDMS.

Conclusion is that the ‘micropump wafer’ is not suitable for carrying thin PDMS layers, despite the adjustments of the PDMS processing. One parameter that could not be adjusted, is the ‘channel width’, while mid-channel deflection depends on its 4th power. Therefore the ‘pervaporation channels’ wafer was used to adjust this parameter.

Channel width

The channels on the ‘pervaporation channels wafer’ have widths of 2, 3, 4, 5 or 10 µm. The channels with a width of 10 µm were completely or partly collapsed. The channels with a width of 5 µm or smaller were open in general. This means that the following PDMS process parameters can be used to create a 17 µm thin PDMS layer on a glass substrate: mixing ratio 1:10, spinning rate 6000 rpm, curing temperature 60°C and curing time 60 minutes. Figure 3.28a shows open parallel channels of a type 3 channel with a channel width of 4 µm and figure 3.28b the open parallel channels of a type 7 channel with a channel width of 8 µm.

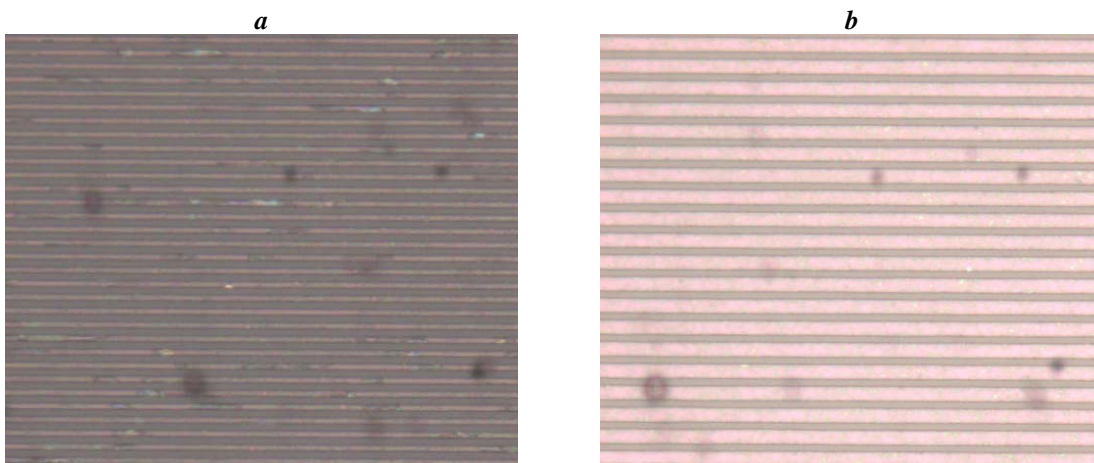


Figure 3.28. Open microchannels from the pervaporation channel with a) type 3 and b) type7

During the transfer of the PDMS layer from the foil to the glass wafer, air bubbles were captured under the PDMS, causing defects in the channels. At some spots the PDMS was folded, which also resulted in channel defects. For these imperfections most of the channels on the wafer could not be used in experiments, described in the next chapter. At most about 10 out of the 73 channels were faultless.

In a large series of experiments it was tried to optimize PDMS bonding in the wide microchannel devices, but without success. The PDMS cleaning procedure is given below.

PDMS removal

Advantage of the used method of transferring a PDMS layer to a glass wafer is that it was quite easy to fabricate devices with different PDMS roofs, because it was easy to remove the PDMS and transfer new PDMS on the same glass chip, without expensive and time consuming cleanroom steps.

The quick removal of PDMS was first performed with concentrated sulphuric acid (H_2SO_4). With a clean solution it took about 3 days to clean the glass wafer. But when the solution was polluted (due to exposure to air and preceding cleanings), the cleaning process took more time. With pure Polygone 500 of RPM Technology the cleaning time took one night. With polluted Polygone 500 it took a few days. The cleaning time decreased when the glass wafer was vibrated occasionally in an ultrasonic cleaner with isopropanol.

Because species like fluorescein and rhodamine have a low solubility in Polygone 500, it is important that the glass wafer is cleaned with acetone and water in order to remove all the remaining species from the microchannels.

3.6.3 Surface modifications of the PDMS results and discussion

Oxygen plasma treatment

When the PDMS came out of the plasma cleaner it was hydrophilic. This was tested by placing a drop of water on the surface. The water contact angle was smaller than 45° . After about two days it was not hydrophilic anymore, because the water contact angle was about 110° . This was expected, because literature supports this observation.

Extracting unreacted oligomers

The PDMS was hydrophilic when it came out the plasma cleaner. After two days it was not hydrophilic anymore, when stored in air. This is in contradiction with the literature about this method that is described in paragraph 3.4.

Water storage

All the PDMS layers which were not stored in water became hydrophobic after two days. The PDMS layers stored in water stayed hydrophilic for a longer time, which was not exactly measured. Channels that were filled with water after the reservoir fabrication, which is described in the next session, also were hydrophilic for at least 7 days. This was expected, because literature supports this observation.

Conclusion

PDMS is hydrophilic after an oxygen plasma treatment. Its hydrophobicity recovers after a two days. This decay of hydrophilicity can be stopped by storing the PDMS in water.

3.6.4 Interface results and discussion

The interface exists of a hole at the channel ends and reservoirs placed upon these holes.

Holes

The cutting of the holes with a scalpel gave the result depicted in figure 3.29a. The stamping gave the result depicted in figure 3.29b.

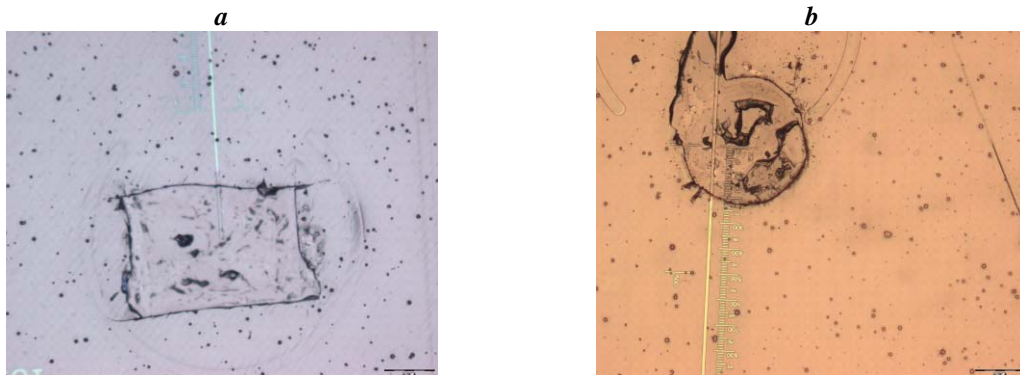


Figure 3.29 Holes in the PDMS at the ends of the open microchannels (green) performed with, (a) a scalpel and (b) a stamp

A problem is that with both techniques the PDMS roofs of the microchannels of the 'micropumps' wafer collapsed due to pressure exerted by the scalpel or stamp. This can be seen in the figure: the channel, which was open (green coloured) first, has collapsed at the edge of the hole, and now has the same colour as the surrounding PDMS. It was tried to solve this problem by fabricating a stronger PDMS layer. The fabrication was described in paragraph 3.5. The result was not satisfactory. The channels of the 'pervaporation channels' glass wafer on the other hand, did not collapse when a hole was cut at the channel ends. The PDMS was stiff enough to resist the pressure. This is depicted in figure 3.30.

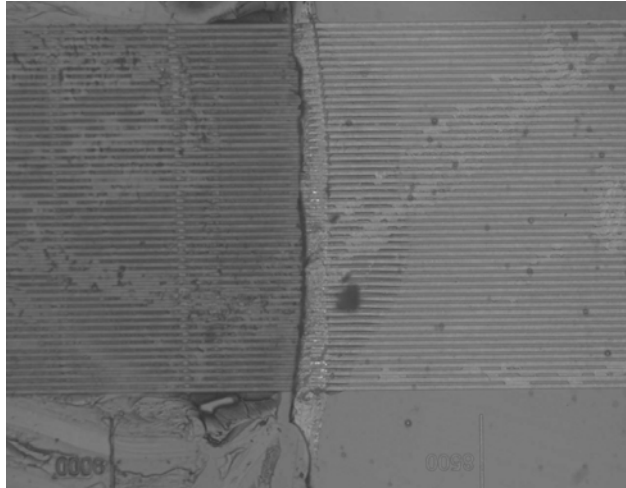


Figure 3.30 A cut at the end of a channel array from the 'pervaporation channels wafer'. The PDMS covers the channel array at the right side of the image. The PDMS was cut away from the glass wafer at the left side of the image

It can be seen that the channel did not collapse by the pressure of the scalpel.

Reservoirs

The first method with the separate reservoirs was carried out with plastic pipet tips. First small tips were used, but the inner diameter of these tips was that small that it was hard to place them over a hole. Also the glue that was rubbed under the tips ended up in the holes. For this reason, big reservoirs were used. The problems that were experienced with the small reservoirs did not occur anymore.

After gluing with Loctite Hysol epoxy and the Araldyte epoxy it was found that the channels were blocked at the glue spots. This problem did not occur when Dow Corning 734 was used. Disadvantage of this glue is that it stays fluid for a long time before it hardens and will end up in the holes when it is not hard enough. Another problem of this glue is that it is not strong enough to resist small pressures when it only is applied between the pipet tip and the PDMS slab, in contrary to Araldyte and Hysol. This was solved by applying more glue around the reservoir when the bottom glue was hardened.

To prevent the liquids in the reservoirs from evaporating, small caps to place upon the reservoir were fabricated. A resulting channel with reservoirs is depicted in figure 3.31a.

The channel is situated between the two reservoirs. These reservoirs have the caps. Other channels can be found on the wafer as well, but have no reservoirs in this image. Figure 3.31b shows the top view of the bottom of a reservoir. The edges of the hole and the channel end can be seen inside the black circle, which is the pipet tip. Because the tip and the glue around the tip take space on the device, the effective length (L_e) of the channels was the initial length (L) subtracted with about 0.5 mm. The pipet tips were also that large that they covered other microchannels when glued on the wafer.



Figure 3.31. a) Microchannels on a wafer, one microchannel has two reservoirs at the channel ends. b) top view of the bottom of a reservoir.

The second method to create reservoirs was making a PDMS slab of 1mm thickness and placing this on the PDMS layer by hand. In this slab three holes are made: two reservoir holes with a section of 1mm and a window of 1mm by 4mm that uncovers the microchannel. The slab was created in a mould. Figure 3.32 shows the microchannel with the slab upon it.

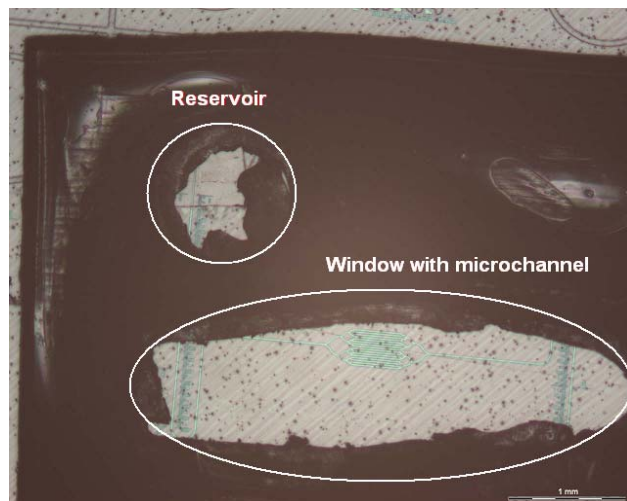


Figure 3.32. The PDMS slab with one reservoir and the window around the channel.

The reservoir was almost watertight and the reservoirs were still open after processing. Problem was that the reservoirs released after using them a few times. This is why reservoirs made of the large pipet tips were used as reservoirs, finally.

3.7 Summary device design and fabrication

A glass wafer with several microchannel structures (devices) and a PDMS roof was fabricated. First a glass wafer with too wide microchannels was used. The PDMS collapsed in these channels and stucked to the bottom, what resulted in closed channels. Next a glass wafer with smaller microchannels was designed and fabricated. The process parameters of the PDMS were adjusted to fabricate an as thin as possible PDMS layer in order to have an as big as possible pervaporation flow. The surface of the PDMS was modified with an oxygen plasma cleaner step in order to create hydrophilic channels. Reservoirs were mounted at the ends of the channels. The pipet tips were that large that they covered other microchannels when glued on the wafer.

Chapter 4 - Experimental

This chapter describes the preparations and the experimental conditions. Paragraph 4.1 describes the measurement setup and paragraph 4.2 the used chemicals. Paragraph 4.3 deals with the priming of the device and paragraph 4.4 finally describes the protocol that was followed during the measurements.

4.1 Measurement setup

The wafer with the devices was placed on top of an inverted microscope. The specific channel array on the wafer that was used for an experiment was prepared with platinum electrode wires in the reservoirs. These electrodes were connected to a voltage source. The device was filled with water or solution. This was exposed to light from a halogen lamp or a mercury lamp that was directed via a dichroic mirror below the wafer. The light was captured by an objective and was directed to the eye piece or video camera via a filter. The video camera was connected to a laptop which was prepared with image analysis software. The microscope, the device and the camera were placed inside a microscope tent. Figure 4.1 shows an overview of the measurement setup.

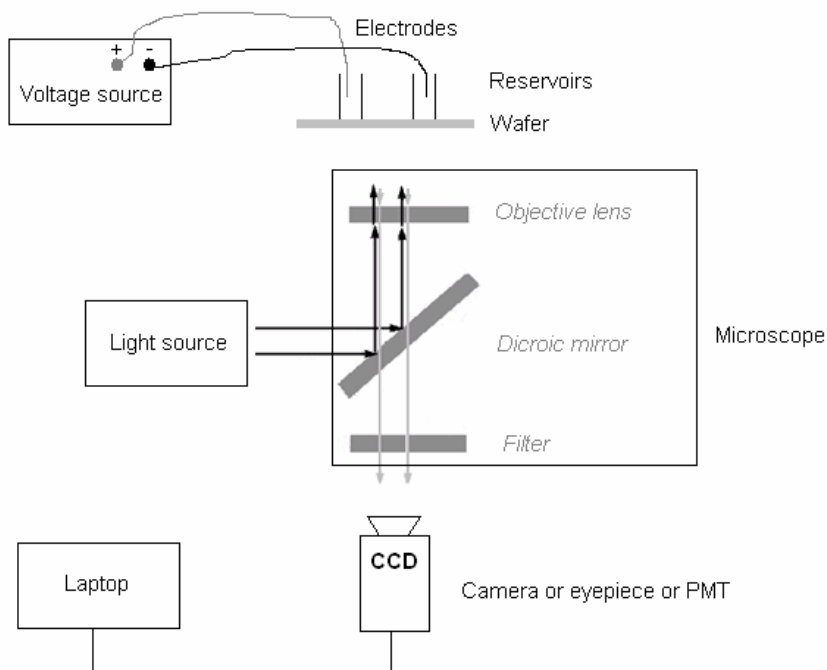


Figure 4.1 The measurement setup

The individual parts of the measurement setup are described below:

Device

The devices are described in chapter 3.

Power supply

The power supply that was used is the Keithley high-voltage SourceMeter 2410, which can source and measure voltages from $\pm 5 \mu\text{V}$ (source) and $\pm 1 \mu\text{V}$ (measure) to $\pm 1100 \text{ V}$ and current from $\pm 10 \text{ pA}$ to $\pm 1 \text{ A}$ [50].

Electrodes

Platinum wire with a diameter of 0.20 mm. The platinum wires were immersed for about 5 mm in the liquid in the reservoirs.

Microscope

The microscope that was used is the inverted microscope Leica DM-IRM. It was prepared with a mercury lamp and a halogen lamp. The used filterblocks on the microscope were a BF, L5 (excitation: BP 460-500 nm, suppresses: BP 512-542 nm, emission: HP 505 nm) and I3 (excitation: BP 450-490 nm, emission: HP 510 nm) filter. Figure 4.2 shows the spectrum of the L5 filter block [51].

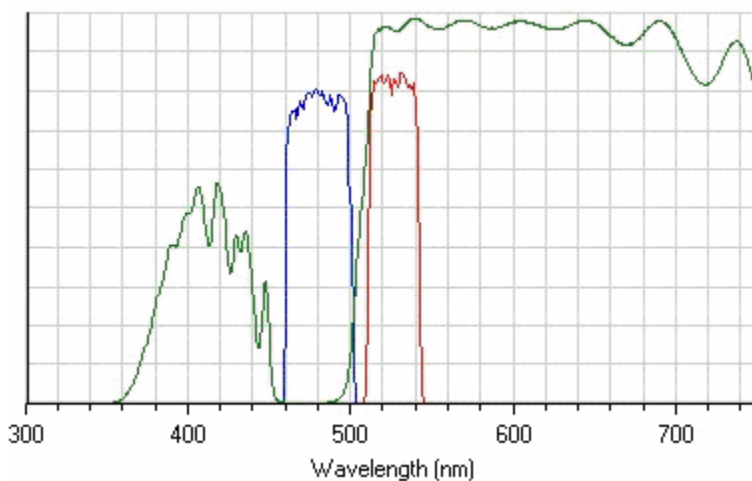


Figure 4.2 Spectrum of the L5 filter block (blue = excitation BP filter, green = emission HP filter and red = excitation BP suppressing).

Video camera

The used video camera is the Olympus CC-12. It has a resolution of 1376 x 1032 pixels and a dynamic range of 3 x 12 bits [52]. The camera has automatic gain.

Software

The image analysis software is Analysis Five of Olympus.

PMT

A H7422-02 PMT was used. The maximum output current is $100\mu\text{A}$. Therefore a Hamamatsu C7913 pre-amplifier was used was able to perform current to voltage conversions with amplifications of 10^5 , 10^6 or 10^7VA^{-1} .

Microscope tent

For the fluorescence microscopy a dark room is necessary, because otherwise background light introduces noise. Because a dark room was not available, a tent was fabricated. This tent was designed to contain the microscope with a PMT (which was not used in this research) and the camera on top, the mercury lamp at the back and some free space at both sides. It was also designed to fit in the workspace that was assigned for the setup.

The frame of the tent was made of wooden beams, connected together with glue and nails. The frame consists of horizontal and vertical pillars and is strengthened by crosses. The canvas was made of light absorbing cloth, nearly surrounding the complete frame as can be seen in figure 4.3.a. The front of the tent can be opened, because of the usage of Velcro. The back of the tent is prepared with cardboard wrapped in aluminium foil, preventing the hot mercury lamp from igniting the tent canvas. Figure 4.3.b shows a working person inside the microscope tent.

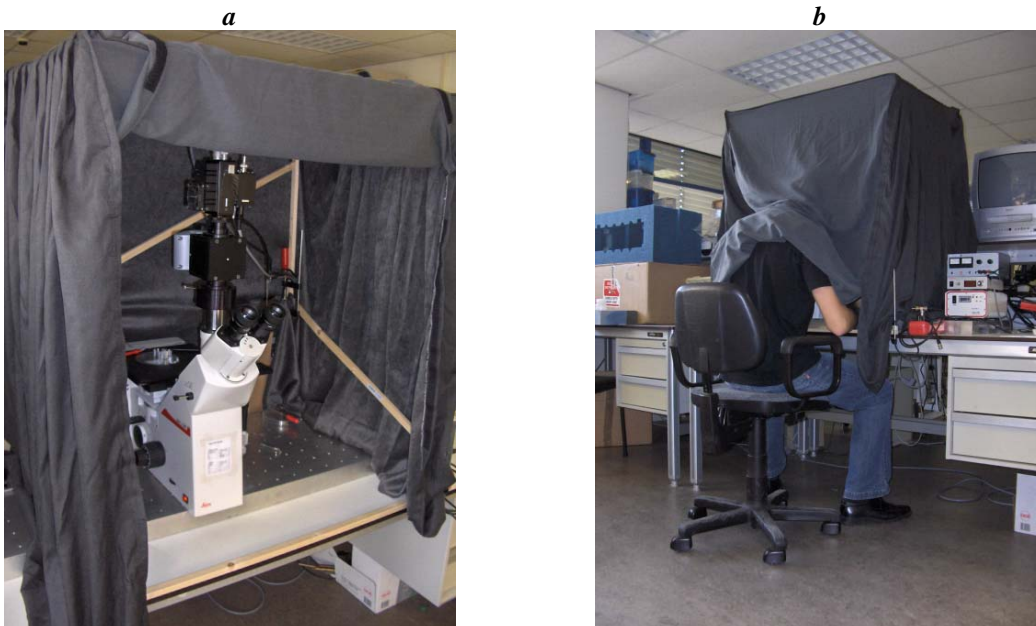


Figure 4.3. The microscope inside the microscope tent (a) and a person working inside the microscope tent (b)

Black plates

Except for the noise introduced by the background, also the reservoirs introduce noise when they are filled with fluorescent solutions and are excited by a mercury lamp. Figure 4.4 shows the light emission of reservoirs filled with fluorescent solutions.

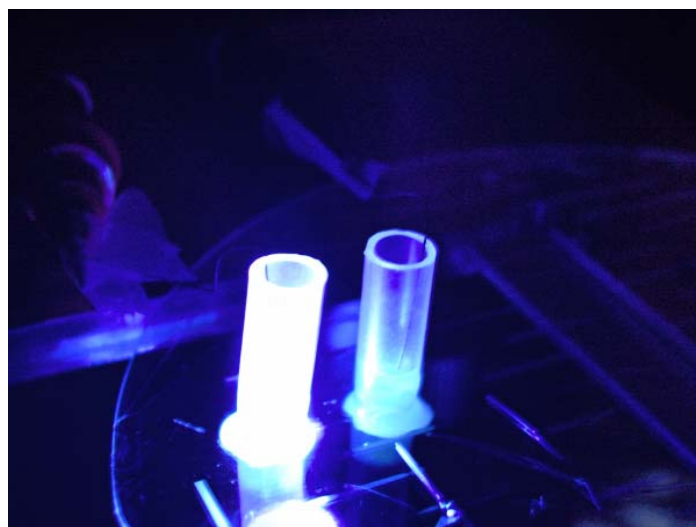


Figure 4.4 Light emission of the reservoir when filled with a fluorescent solution excited by a mercury lamp

To prevent this kind of background noise two black plates are placed between the mercury lamp and the two reservoirs. The channel it self was left uncovered.

4.2 Chemicals

4.2.1 Properties of the used chemicals

When the source is not mentioned, the properties are found at the website of Sigma Aldrich [53].

pH-buffer

A TB buffer with a pH of 8.5 (measured with a Radiometer PHM 83) was used as pH-buffer. This buffer consist of the chemicals TRIS (2-amino-2-(hydroxymethyl)propane-1,3-diol), or $C_4H_{11}NO_3$ in solution, and boric acid dissolved in water.

TRIS has a molecular weight of 121.14 gmol^{-1} and a pK_a of 8.30 at 20°C . The Brønsted equilibrium of TRIS is:



The solubility in water is 4M.

Boric acid, $B(OH)_3$, has a molecular weight of 61.83 gmol^{-1} and a pK_a of 9.24. The dissociation equilibrium for boric acid is:



$B(OH)_2O^-$ is called the borate ion. The solubility in water is 0.92 M.

Background analyte

Potassium chloride (KCL) was used as background analyte. The molecular weight of KCL is 74.55 gmol^{-1} . The diffusion coefficient of KCL is $1.65 \cdot 10^{-9} \text{ m}^2\text{s}^{-1}$ [54]. Its solubility in water is 4.6 M. At higher concentration it crystallizes.

Fluophores

The four different fluorophores that were used are listed below.

Fluorescein

Fluorescein ($C_{20}H_{10}Na_2O_5$) has a molar weight of 332.32 gmol^{-1} . Its diffusion coefficient is $4.9 \cdot 10^{-10}$ [Rani05]. The diameter of a fluorescein ion is about 1 nm. Its solubility in water is 1.6M. The ion is hydrophobic. Figure 4.5 shows the excitation and emission spectra of fluorescein.

Rhodamine 6G

Rhodamine 6G ($C_{28}H_{31}N_2O_3Cl$) has a molar weight of 479.02 gmol^{-1} . Its diffusion coefficient is $3.6 \cdot 10^{-10}$ [55]. Its solubility is about 0.1 M. Figure 4.5 shows the excitation and emission spectra of rhodamine 6G.

Rhodamine B

Rhodamine B ($C_{28}H_{31}N_2O_3Cl$) also has a molar weight of 479.02 gmol^{-1} . Its structure differs from the structure of rhodamine 6G. Its solubility is about 0.1 M. Figure 4.5 shows the excitation and emission spectra of rhodamine B.

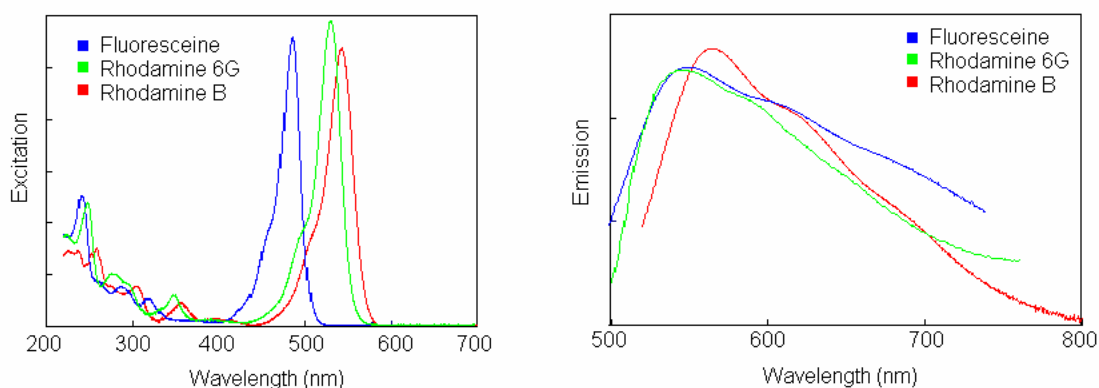


Figure 4.5 Excitation and emission wavelengths of fluorescein, rhodamine 6G and rhodamine B [56]

Dextran FITC 500,000 conjugate

Dextran FITC 500,000 conjugate has an average molar weight of 500,000 gmol^{-1} . The ratio between FITC and glucose is 1:100. This means that 1 mol of dextran FITC 500,000 conjugate has the fluorescence properties of 27.3 mol fluorescein.

The diffusion coefficient of dextran FITC 500,000 conjugate is $0.31 \cdot 10^{-10}$ [57]. The diameter of this molecule is about 14.7 nm. The solubility in water is about $6.25 \cdot 10^{-3}$ M.

At higher concentrations it becomes gel-like before it crystallizes. The molecule is hydrophilic. The excitation and emission spectra FITC are the same as for fluorescein. The fluorescence increases with pH and is optimal at pH 8 and above.

4.2.2 Solutions

Pervaporation experiments

In the pervaporation experiments a TB-buffer of 0.1x (0.01M) was used. The KCL concentration was 0.025M and the concentration of dextran FITC 500,000 conjugate and fluorescein were respectively 10^{-7} M and 10^{-5} M.

Osmosis experiments

In the osmosis experiments generally a TB-buffer of 10x (1M) was used. The KCL concentration was 1M and the concentration of dextran FITC 500,000 conjugate and fluorescein were respectively 10^{-7} M and 10^{-3} M.

Separation experiments

In the osmosis experiments generally a TB-buffer of 5x (0.5 M) was used. The KCL concentration was 1M and the concentration of fluorescein and rhodamine 6G were 10^{-3} M or 10^{-5} M.

4.3 Device priming

Because the PDMS channel walls are hydrophobic in their natural state it is necessary to pre-prime them in order to fill them with water (see chapter 3). After several attempts it became clear that the channels could be filled with water within half an hour after the oxygen plasma step. When water was added to the reservoirs during storage periods, the channels stayed filled with water. Therefore the pre-priming step was integrated in the first priming step.

At the start of the measurements, the microchannels were filled with water and remained so during a sequence of experiments.

4.4 Experimental protocol

All experiments followed approximately the same, following, protocol.

Light

The experiments took place inside the microscope tent, which was closed as much as possible during experiments. The lights in the room were switched off in order to prevent light incidence through openings in the microscope tent.

Lamps

The halogen and mercury lamps were switched on at least half an hour before the experiment started, in order to warm up.

Position

The wafer was positioned in such a way that the middle of the microchannel array which was to be used for the experiment was positioned in the middle of the field of view. The position of the wafer on the microscope was determined by using the halogen lamp and the BF filter. After determining the position, the black plates were placed under the reservoirs. The position of the wafer and black plates was secured by placing a heavy piece of metal on top of the wafer at a spot where no microchannels were present. Because the camera had another focal point than the eye pieces of the microscope, the focus was adjusted with help of the image analysis software. This resulted in a sharp image of the middle of the channel that was captured by the image analysis software.

Fluorescence

After the positioning of the wafer and the adjustment of the focusing, the mercury lamp was focused on the wafer and the BF filter was replaced by the I3 filter. The water in the reservoirs was replaced by the solution of the buffer, background analyte and fluorophore. The volume of the solution always was 100 μ L in both reservoirs. The difference between the experiments with pervaporation and the experiments with osmosis is that with the osmosis experiments a drop of deionized water is placed on the PDMS roof of the microchannel. In both types of experiments, directly after the replacement of water two platinum electrodes were placed in the separate reservoirs. It was checked afterwards if the wafer was not moved from its position.

Measuring

The experiment started when the water in the reservoirs was replaced by the solution. From this moment a timer was set on.

The shutter time of the camera was adjusted in order to receive enough light to create an image with the software. The software supports automatic gain which can be used for getting qualitative results, but cannot be used for getting accurate quantitative results, because it is not possible to discover the gain rate from the camera while measuring. *Unfortunately only automatic gain was available!!!*

The software was able to capture a movie or make images. For quantitative measurements it is important that the mercury lamp is only used to illuminate the chip, when a photograph is taken, in order to prevent photobleaching.

Applying voltage

Voltages were applied on the platinum electrodes after a period of about 15 minutes of pervaporation or osmosis. During the experiments the voltage was varied and the current through the microchannel arrays was measured with the Sourcemeeter.

Chapter 5 - Results and discussion

This chapter discusses the experimental results that were obtained. Experiments with pervaporation, conductivity gradient focusing and osmosis were done. Paragraph 5.1 deals with the pervaporation of water through the PDMS roof and paragraph 5.2 with the fluorescent species that remain in the channel after pervaporation. Paragraph 5.3 discusses the results obtained with conductivity gradient focusing by pervaporation experiments and paragraph 5.4 discusses the results obtained with conductivity gradient focusing by osmosis experiments. Finally paragraph 5.5 deals with separation experiments that were done in the microchannels.

5.1 Pervaporation

To investigate whether the PDMS roof is water permeable a set of experiments, including two similar pervaporation experiments with different fluorophore solutions, were done. The experiments were repeated 11 times, 9 times with dextran FITC 500,000 conjugate and 2 times with fluorescein. The results of the experiments described in this paragraph are typical results for the pervaporation experiments.

5.1.1 Experiments

The solution that was injected in the reservoirs for the first experiment consisted of a TB buffer of 0.01 M, a 25 mM KCL background analyte and 10^{-7} M fluorophore dextran FITC 500,000 conjugate (hereafter called dextran FITC). An array of 50 parallel microchannels, with $d = 20 \mu\text{m}$, $w = 8 \mu\text{m}$, $h = 1 \mu\text{m}$ and $L_e = 5 \text{ mm}$, was used for the experiment. An image of the array was captured 15 minutes after the start of the experiment. Figure 5.1 shows this image. The colors in this image were inverted in order to create a clear image. The black traces are fluorescent species. The width of the image is $884 \mu\text{m}$ while the effective length of the channel is about 5mm. Because the absolute x-position was not measured the relative x-position is plotted in the image.

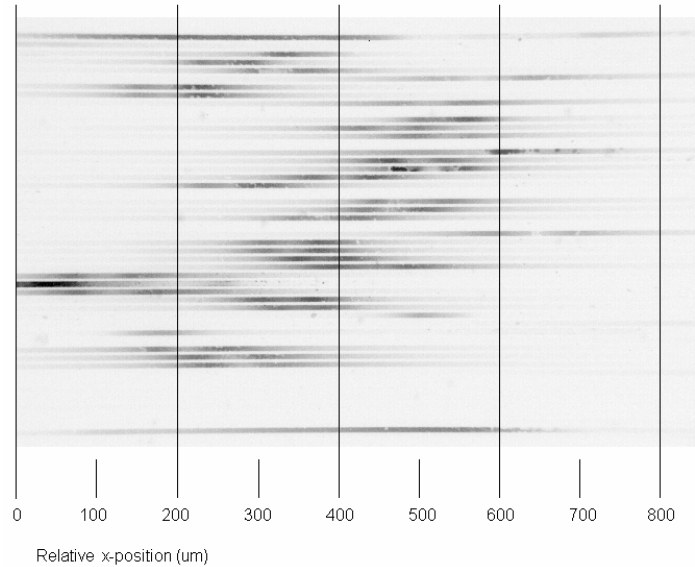


Figure 5.1. The inverted image of the concentration peaks in an array of channels with dextran FITC after 15 minutes of pervaporation

From this image different observations can be made, namely:

1. there is accumulation of fluorescence at certain positions in the microchannels,
2. not all channels have a concentration peak,
3. the position of the concentration peaks differs for the separate channels, but the peaks are relatively close since the channel has a length of 5 mm and the concentration peaks are situated maximally about 500 μm from each other,
4. the intensity of the peaks differs,
5. some channels do have spots with high intensity.

Similar concentration peaks were observed with most of the 9 experiments.

When the pervaporation was allowed to continue for a longer period than about 15 minutes, chunk-like phenomena were observed in the channels. Figure 5.2 depicts another channel array that contains such chunk-like phenomena. The relative x-position is also plotted.

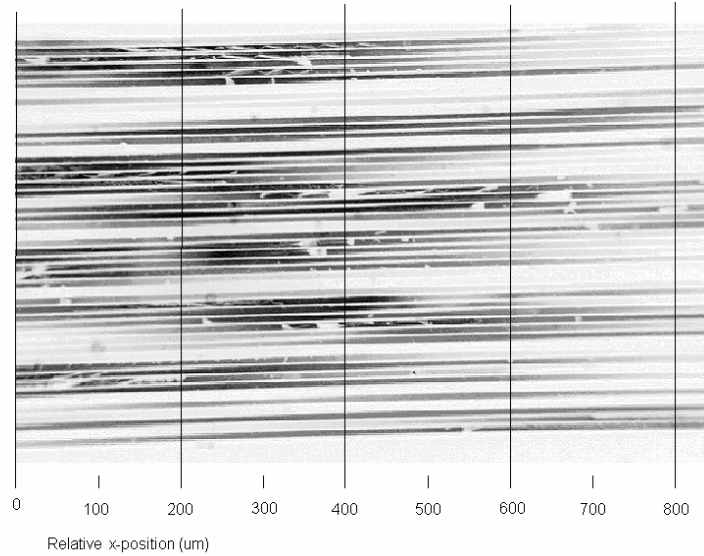


Figure 5.2 Inverted image of chunk-like phenomena in a channel with dextran FITC after pervaporation

When the pervaporation was allowed to continue for hours, the concentration profile did not change anymore.

Fluorescein

A similar experiment was done again, but now the dextran FITC was replaced by 10^{-5} M fluorescein. Figure 5.3 shows the resulting inverted fluorescence image taken after 15 minutes. The relative x-position is also plotted.

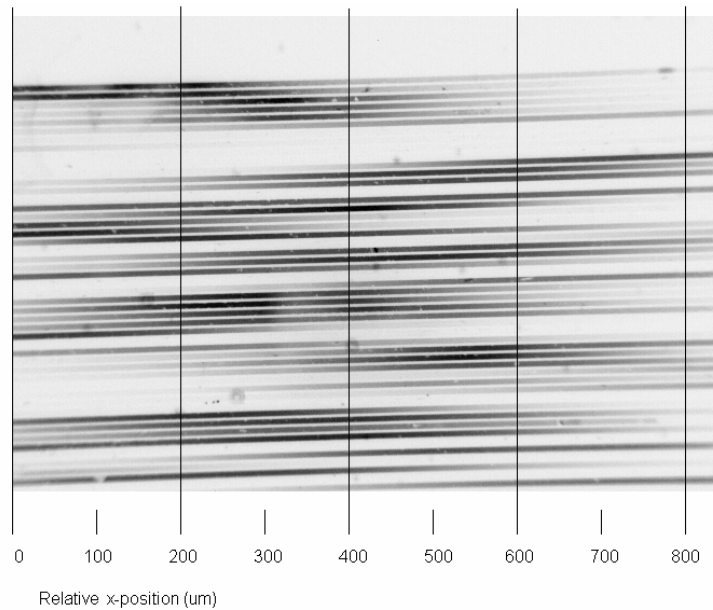


Figure 5.3 Inverted image of the concentration profiles of a channel with fluorescein after 15 minutes of pervaporation

The observations made with the same experiment with dextran FITC can also be made here. Additionally it can be seen that the fluorescent peaks have a larger width than the fluorescent peaks of the channels filled with dextran FITC. This observation will be quantified in the discussion section.

Similar concentration peaks were observed with all 2 experiments. Also with these experiments chunk-like phenomena were observed in the channels when the pervaporation was continued longer than about 15 minutes.

5.1.2 Discussion

Origin of observed profiles

The most important observation that was made is that in both experiments in different channels accumulation of fluorophore, centered around a certain location, takes place. This was expected. The accumulation can only be caused by a force that drives dissolved species from the reservoirs to this central location. The fluorophore fluxes that can be present in the microchannel are by pressure driven flow, by diffusion and by pervaporation.

The accumulation cannot be caused by pressure driven flow, which is described in paragraph 2.1, because this flow does not concentrate species at a certain position in the channel, but transports them from one reservoir to the other reservoir. From equations 2.2 and 2.3 the difference in pressure at the two reservoirs appears to be about 50 Pa maximum, taking the water height in reservoir 1 2 mm and in reservoir 2 3 mm and taken that the water contact angle of the fluid in reservoir 1 is 0° and in reservoir 2 is 180° . When using equation 2.4 it can be calculated that the velocity of the fluid induced by this pressure difference is maximal $4.68 \cdot 10^{-7}$ m/s. Therefore the pressure driven flow can also be assumed to be even more negligible.

The accumulation of fluorescence can also not be caused by diffusion. According to Fick's law in equation 2.11 the diffusion flux is always directed from positions in the solution with the highest dissolved species concentrations to positions with lower dissolved species concentrations. Immediately after the moment that the reservoirs are filled the dissolved species concentration is about 0 M inside the microchannel and the dextran concentration in the reservoirs is 10^{-7} M. This causes according to equation 2.11 a diffusion-driven flux of $6.2 \cdot 10^{-16}$ mol m^{-2} s^{-1} which is directed to the centre of the microchannel. When the dissolved species concentration is equal in the center of the channel and in the reservoirs after a certain period, no flux caused by diffusion will exist if no flux induced by pervaporation is present. This period would be after about 9 days, according to equation 2.8, if pervaporation was absent.

Because no other fluxes than the above discussed fluxes were created in the channel, the accumulation of the dextran FITC molecules had to be caused by pervaporation of water through the PDMS roof.

Peak shape and position for dextran FITC

Figure 5.4 shows intensity cross-sections in the x-direction of three channels filled with dextran FITC solution after 15 minutes of pervaporation.

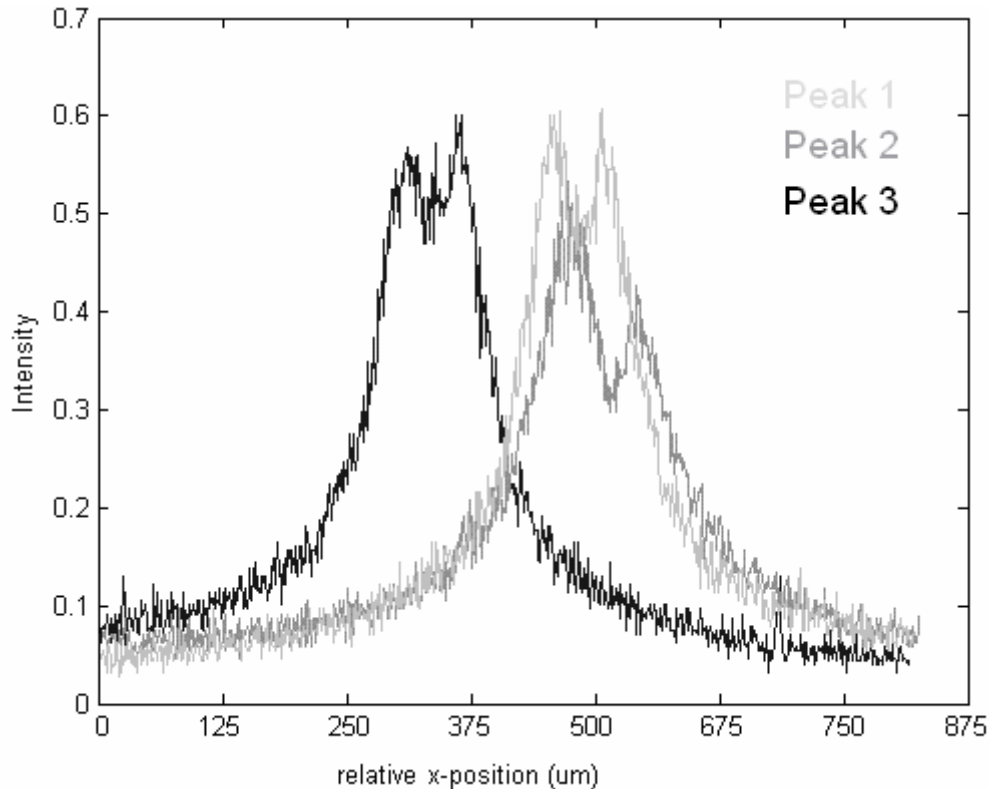


Figure 5.4. Normalized intensity cross-section of concentration peaks in the different channels from figure 5.1 (dextran FITC) after 15 minutes of pervaporation.

The concentration factor and pervaporation induced flux can be determined by the peak heights. However, because of the auto-gain function of the camera, absolute values for the peak heights could not be derived exactly. It was tried to fit equation 2.16 with the profiles in order to determine the pervaporation induced flux by the concentration gradients. This failed, because this equation counts for equilibrium between the diffusion flux and pervaporation induced flux, and that is probably not the case for the concentration peaks of figure 5.4. A minimal gain can be derived from figure 5.1 and 5.4. The normalized background signal was determined at 0.055. The initial fluorescence intensity was lower than this value. The highest peak has a normalized value of 1. The minimum gain is $1/0.055 = 18$. When the surface under the peak, that had a width of about $654 \mu\text{m}$, was determined, it was found that the minimum flow velocity was minimal about $3.27 \cdot 10^{-6} \text{ m s}^{-1}$ in both sides of the channel. The molar flux (J_{pervap}) is $3.27 \cdot 10^{-13} \text{ mol m}^{-2} \text{ s}^{-1}$, according to equation 2.10 when the reservoirs are filled with $1 \cdot 10^{-7} \text{ M}$.

An intensity decrease can be observed at the top of the peak for the separate profiles. These decreases can be caused by irregularities in the PDMS or the fact that concentrating caused the dextran solution to become more viscous. The intensity decrease

can not be caused by self-quenching, because in that case peak 3 can not have a lower maximum intensity than peak 1 and 2.

The peaks in figure 5.1 differ about 500 μm in x-position. This is a slight difference, when taking into account that the effective channel length is about 5000 μm . It was observed that peaks of neighbouring parallel channels are positioned at almost the same x-position. Also the peak intensity slightly differs. The difference between the groups and separate channels can possibly be explained with help of the channels depicted in figure 3.28. It can be seen that encapsulations cause the PDMS to have cavities. These irregularities can have influence on the pervaporation velocity and concentration profiles when they are positioned above a channel. Also pieces of PDMS that were cut loose during the cutting step and air bubbles in the channel can block a channel and influence the pervaporation speed. Both explanations for the fact that some channels do not contain a concentration peak at all can be applied; when no bulk flow can occur, no pervaporation flow can be created.

The widths of the peaks at 0.5h have an average of 147 μm for the three dextran FITC peaks depicted in figure 5.4.

Peak shape and position for fluorescein

Figure 5.5 shows the intensity cross-sections in x-direction of three channels filled with fluorescein solution after 15 minutes of pervaporation.

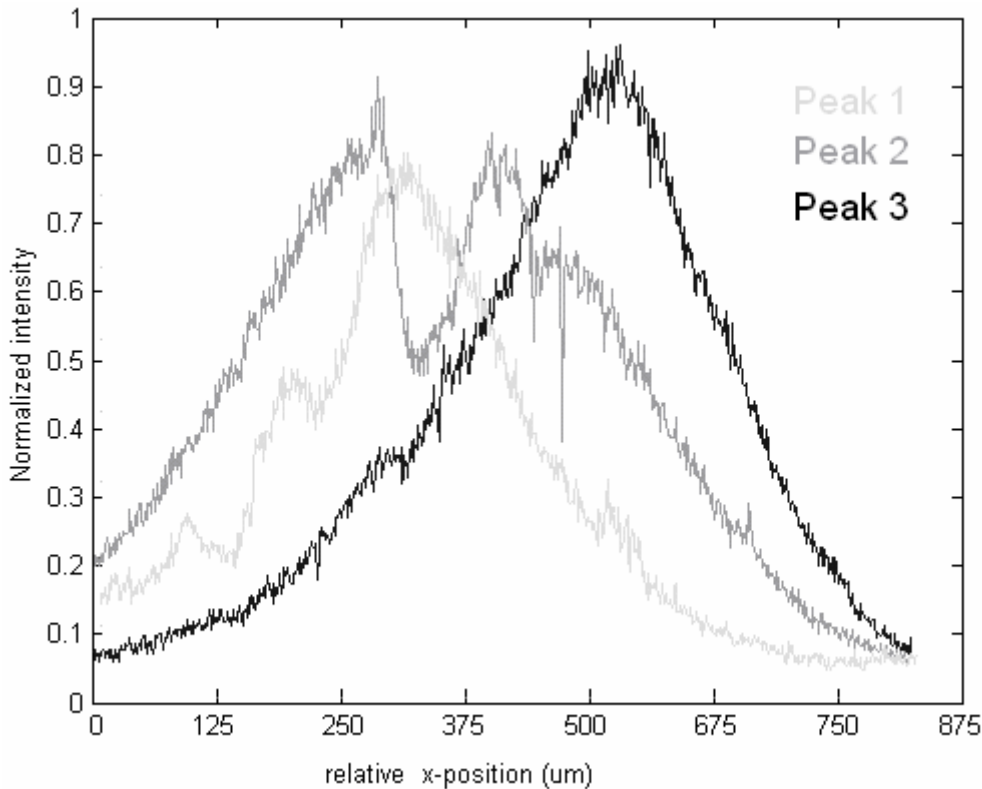


Figure 5.5. Normalized intensity cross-section of concentration peaks in the different channels from figure 5.3 (fluorescein) after 15 minutes of pervaporation.

It can be seen that the three peaks are positioned at nearly the same x-position in the channel, but not exactly. The peaks have different normalized maximum intensity and contain one or more maximums.

A minimal gain can be derived from figure 5.3. The normalized background signal was determined at 0.035. The initial fluorescence intensity was lower than this value. The highest peak has a normalized value of 1. The minimum gain is $1/0.035 = 28.6$. When the surface under the peak, that had a width of about $681 \mu\text{m}$, was determined, it was found that the minimum flow velocity was minimal about $5.4 \cdot 10^{-6} \text{ m s}^{-1}$ in both sides of the channel. In section 3.4.4 it was derived from literature that the flow velocity should be $8.64 \cdot 10^{-6} \text{ m s}^{-1}$. This is in the same order of magnitude. The molar flux in the channels is $5.4 \cdot 10^{-11} \text{ mol m}^{-2} \text{ s}^{-1}$, according to equation 2.10.

The theory predicts that when the concentration of the dissolved species in the centre of the channel increases as a result from the pervaporation flow, the diffusion flux will increase as well. At a certain moment the velocity of the pervaporation flow and the counteracting diffusion flow will be equal, and equilibrium is reached. From this moment the concentration peaks do not change in shape and amplitude anymore. Expected is that it takes minimal several hours to reach the equilibrium. This was found by substituting the parameters of equation 2.16.

The widths of the peaks at $0.5h$ have an average of $345 \mu\text{m}$ for the three fluorescein peaks depicted in figure 5.5. This is a factor 2.35 higher than the average peak width of dextran FITC. Paragraph 2.1 showed that in equilibrium the peak width of fluorescein is 3.9 times wider than the peak width of dextran FITC. The experiment however is not in equilibrium, but the fact that the fluorescein peak is wider corresponds to the theory.

The fluorescein peaks in general do not have an intensity decrease at the top, but at different x-positions of the concentration profile. Figure 5.3 shows that the intensity decreases of some separate parallel channels in the middle of the image are positioned in line. This can be caused by irregularities in the PDMS.

Chunks

When taking the solubility coefficients mentioned in paragraph 4.2 into account it can be calculated that KCL can be concentrated 184 and boric acid 92 times before they crystallize. TRIS, fluorescein and dextran FITC can be concentrated respectively 400, 160,000 and 500 times before they become crystallize or gel-like. The best explanation for the chunks is therefore that they are caused by crystallized boric acid and KCL.

Crystallization of the KCL and boric acid can be prevented by decreasing the pervaporation induced flow. This can be best established by increasing the PDMS thickness.

5.1.3 Conclusion

Arrays of microchannels filled with a solution consisting of a pH buffer, a background analyte and fluorescent species were observed by fluorescence microscopy. Fluorescent peaks appeared in the channels, which can only be caused by a pervaporation flow through the channel causing the local concentration to increase. When pervaporation continues for a longer period, chunk-like phenomena were observed. This indicates that the pervaporation flow led to too high concentrations in the fabricated microchannels and hence crystallization.

5.2 Molecular absorption and adsorption of PDMS

Between the experiments, the channels had to be flushed. When flushing the microchannels after experiments with fluorescein or dextran FITC, it was noticed that a part of the fluorescein or dextran FITC species stayed behind in the channel and that the concentration profiles were partly preserved. There also are some crystal-like spots in the concentration profiles. Figure 5.6 shows a fluorescence image of a residue fluorescein that was stored for 1 day.

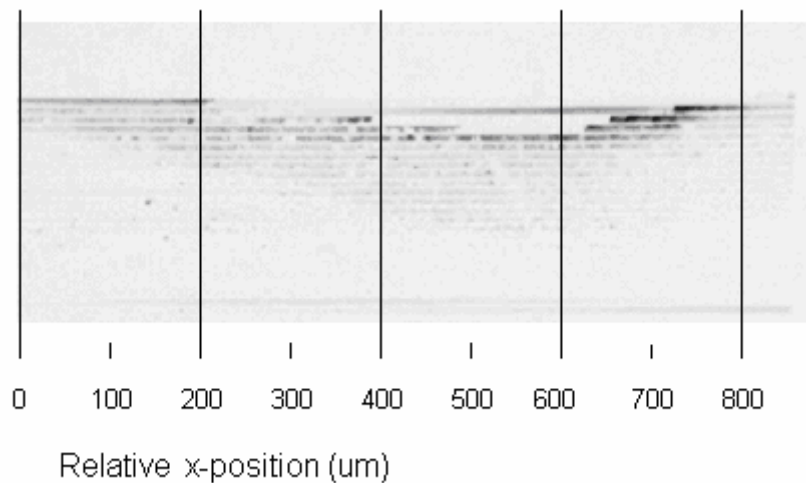


Figure 5.6. Inverted fluorescence image of a channel with fluorescein residue

There are several possible explanations for the remaining fluorescence in the microchannels. One possible explanation is that the species in case of the dextran FITC are adsorbed by the PDMS, and in case of the fluorescein are absorbed by the PDMS, resulting in remaining species at or in the PDMS. This is described in paragraph 2.5. Another possible explanation of the remained fluorescence is that cracking of the PDMS, which is described in section 3.3.4, has occurred during the plasma treatment step, forming cracks that allow fluidic transport from the channel to the upper side of the PDMS. Pinholes through the PDMS also would cause this fluidic transport. Figure 5.7 shows the possibilities.

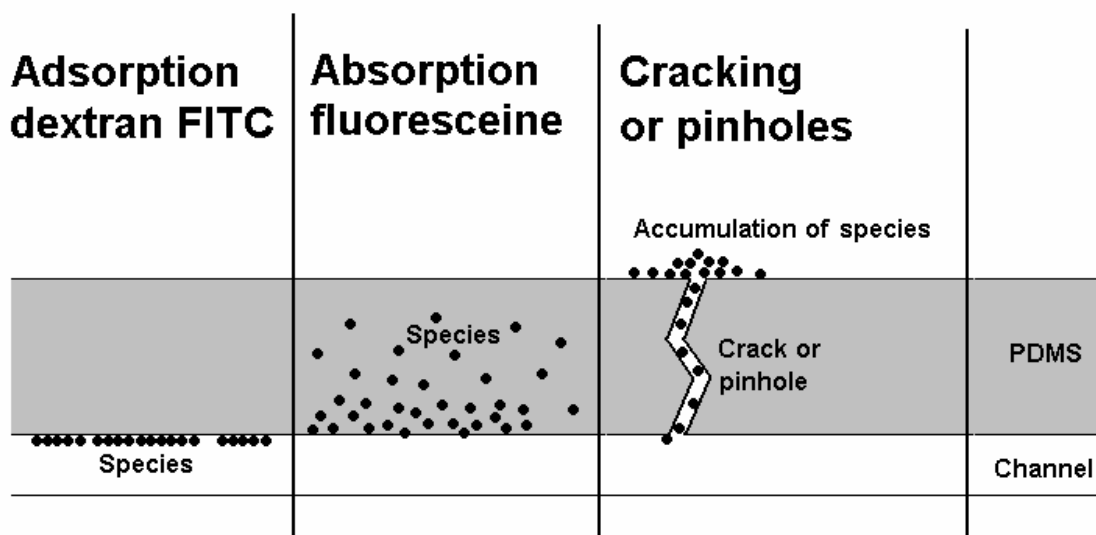


Figure 5.7. Cracking, adsorption of dextran FITC and absorption of fluorescein.

Absorption of fluorescein

First it was investigated if the remaining fluorescein species were in the channel or absorbed by the PDMS by first flushing the microchannel by electroosmosis, caused by an applied voltage of 200V along the channel. When no species travelled through the channel anymore a drop of water was placed on top of the microchannel and a voltage was applied across the PDMS roof, with the negative electrode on the channel side by placing the positive electrode in the drop of water and the negative electrode in a reservoir. The current through the PDMS was $0.07 \mu\text{A}$ with a voltage of 200 V. Probably due to electrophoresis through the PDMS some of the fluorescent species migrated back into the channel. These species could be flushed out of the channel with a voltage of 200 V ($0.8 \mu\text{A}$). The crystal-like spots remained unspoiled. The result can be seen in figure 5.8 a and b. It can be seen that a part of the fluorescent species that was absorbed by the PDMS migrated back into the channel, and a part of the fluorescent species that was stuck in the channel likely because of crystallization of the KCL salt. Further observations should be made with a confocal microscope to quantify ab- or adsorption.

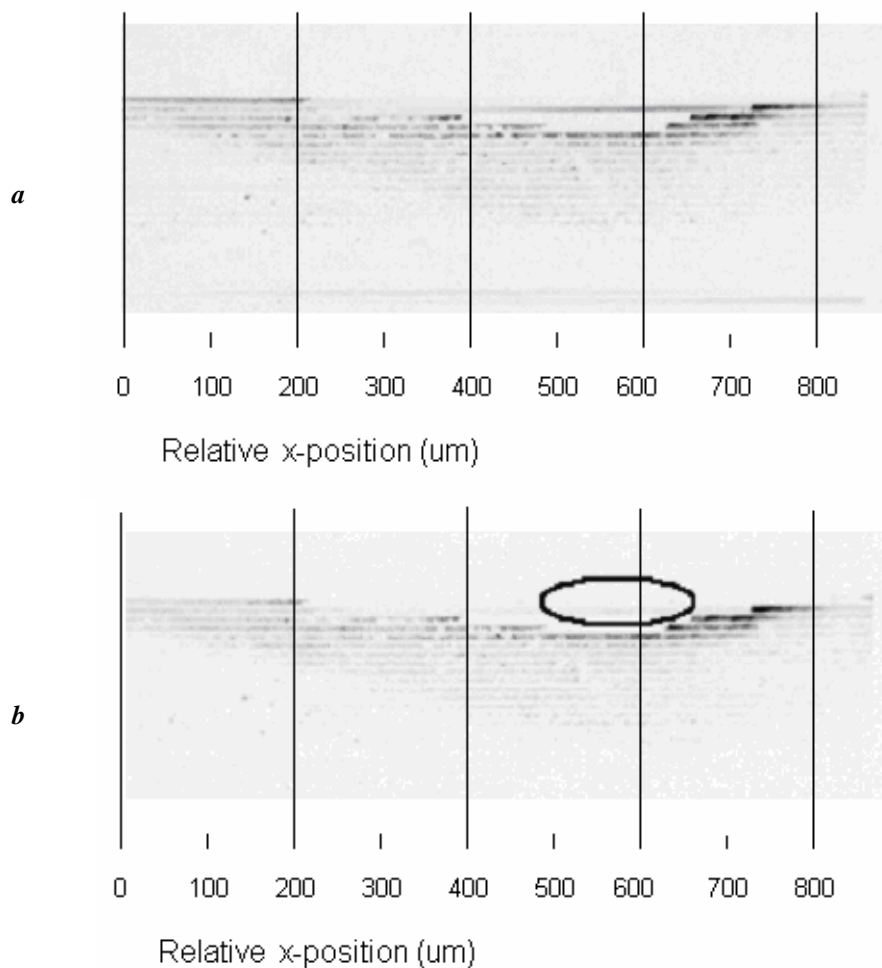


Figure 5.8. Inverted fluorescence image of a channel with fluorescein residue before (a) and after (b) flushing with EOF

Adsorption of dextran FITC

A similar experiment as described above was done with a channel with dextran FITC remains. The result was similar; a part of the fluorescent species could be migrated away from the PDMS wall and a part remained in the channel.

Cracking and pinholes

Some SEM and AFM surface images were taken from a plasma treated and an untreated PDMS slab to discover whether the PDMS has cracked. Figure 5.9 shows the AFM surface image of a piece of a treated and a piece of an untreated PDMS slab. The slabs were manufactured with the same process parameters as the PDMS roofs. To simulate the transfer of the PDMS from the foil to the glass wafer, the slabs were transferred from the foil to a piece of glass by rolling. Afterwards the treated slab was flipped in order to have the treated side upside.

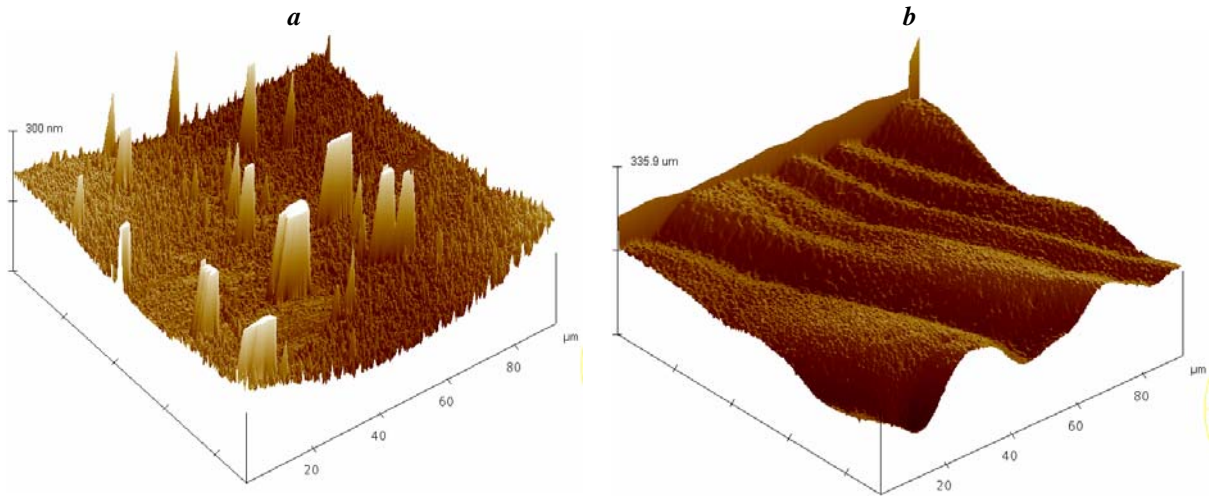


Figure 5.9. AFM surface images of a plasma treated (a) and a untreated (b) PDMS slab

The sharp peaks in the images are caused by faults in the AFM measurement process. It can be seen that the PDMS slabs in both AFM surface images do not have cracks or (pin)holes. Figure 5.10 shows SEM images of the treated PDMS slab. The object in the right upper corner of the right image is a dust particle.

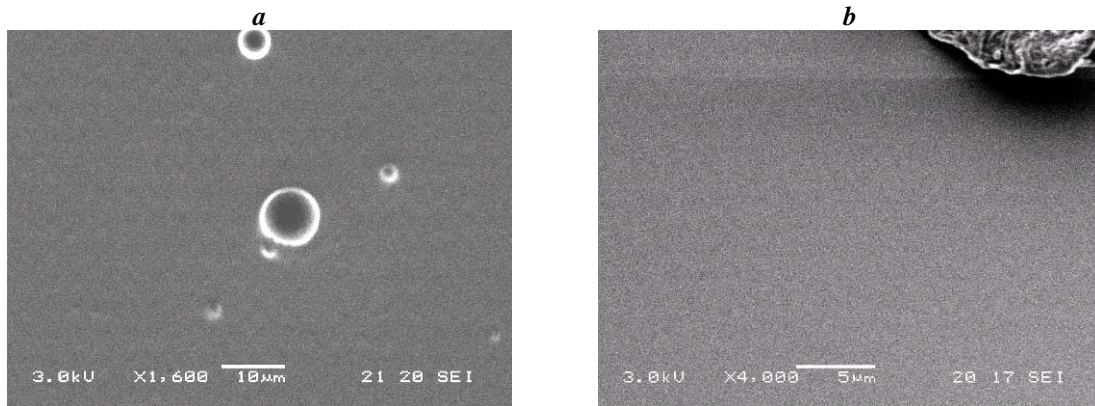


Figure 5.10. SEM images of a PDMS slab that was treated for 5 minutes in an oxygen plasma

It can be seen again that no cracking has occurred. The left SEM image shows some spots in the PDMS. These are expected to be the air bubbles that came into being during the spinning step of the processing procedure. If deep enough these could form pinholes that cause a fluidic connection between the two sides of the PDMS slab. The air bubbles are expected to be spherical. The diameter of the largest air bubble is $10\mu\text{m}$, which also is the maximum of the depth of the hole. The PDMS has a thickness of $20\mu\text{m}$ and therefore the air bubbles in the image cannot be pinholes. But the spots can also be other irregularities in the PDMS, like pinholes.

When pinholes were present, there should be fluorescent species at the upper surface of the PDMS. This was tested by placing a drop of water on the PDMS channel where dextran FITC remains were visible, after measuring the light intensity, caused by the

fluorescence, with a PMT. After five minutes waiting the drop of water was removed with tissue paper. The light intensity decreased with 4.3%. This small effect can be caused by the fact that pinholes are present, but can also be caused by phenomena like photobleaching (see paragraph 2.4). Further research on this phenomenon can be done by putting the PDMS slabs with the remains under a confocal microscope and investigate whether the fluorescence is at the top or the bottom of the PDMS slab.

Conclusion

After experiments with fluorescent species in the microchannels, which are fabricated following the procedures explained in chapter 3, a part of the fluorescent species remains in the channel or PDMS. This is most likely caused by adsorption and absorption of the fluorescent species in the PDMS. The result is that channels can be used for only one experiment. Important is this effect is negligible during short lasting experiments of less than 30 minutes, because it only appeared after several hours of pervaporation.

5.3 Conductivity gradient focusing by pervaporation

In paragraph 5.1 it was proven that a pervaporation flow can be created in the microchannels. This paragraph deals with the set of experiments that was carried out to investigate whether it is possible to do conductivity gradient focusing in the conductivity gradient caused by the salt and buffer concentration profile that results from the pervaporation.

5.3.1 Experiments

The solutions that were injected in the reservoirs for the first conductivity gradient focusing experiments were the same as the solutions of the pervaporation experiment, namely a TB buffer of 0.01 M, a 25 mM KCL background analyte and 10^{-7} M fluorophore dextran FITC 500,000 conjugate (hereafter called dextran FITC) or 10^{-5} fluorescein. The channels had the same properties as the previous used channels. The experiments were done 9 times. The experiments described in this section had the most stable results of the conductivity gradient focusing by pervaporation experiments.

Experiments with dextran FITC

First the reservoirs were filled with the dextran FITC solution. After 15 minutes a voltage of 10V was applied along the channel. Then the voltage was increased from 10V to 150V in steps of approximately 20V. This experiment was repeated for different channel arrays. Figure 5.11 shows the fluorescence in the upper 30 channels of a microchannel array at $V = 0V, 50V, 80V$ and $100V$. The current was $1.56\mu A$ at 50V and $2.36\mu A$ at 100V. The images were taken 1 minute after the moment that the voltage was applied.

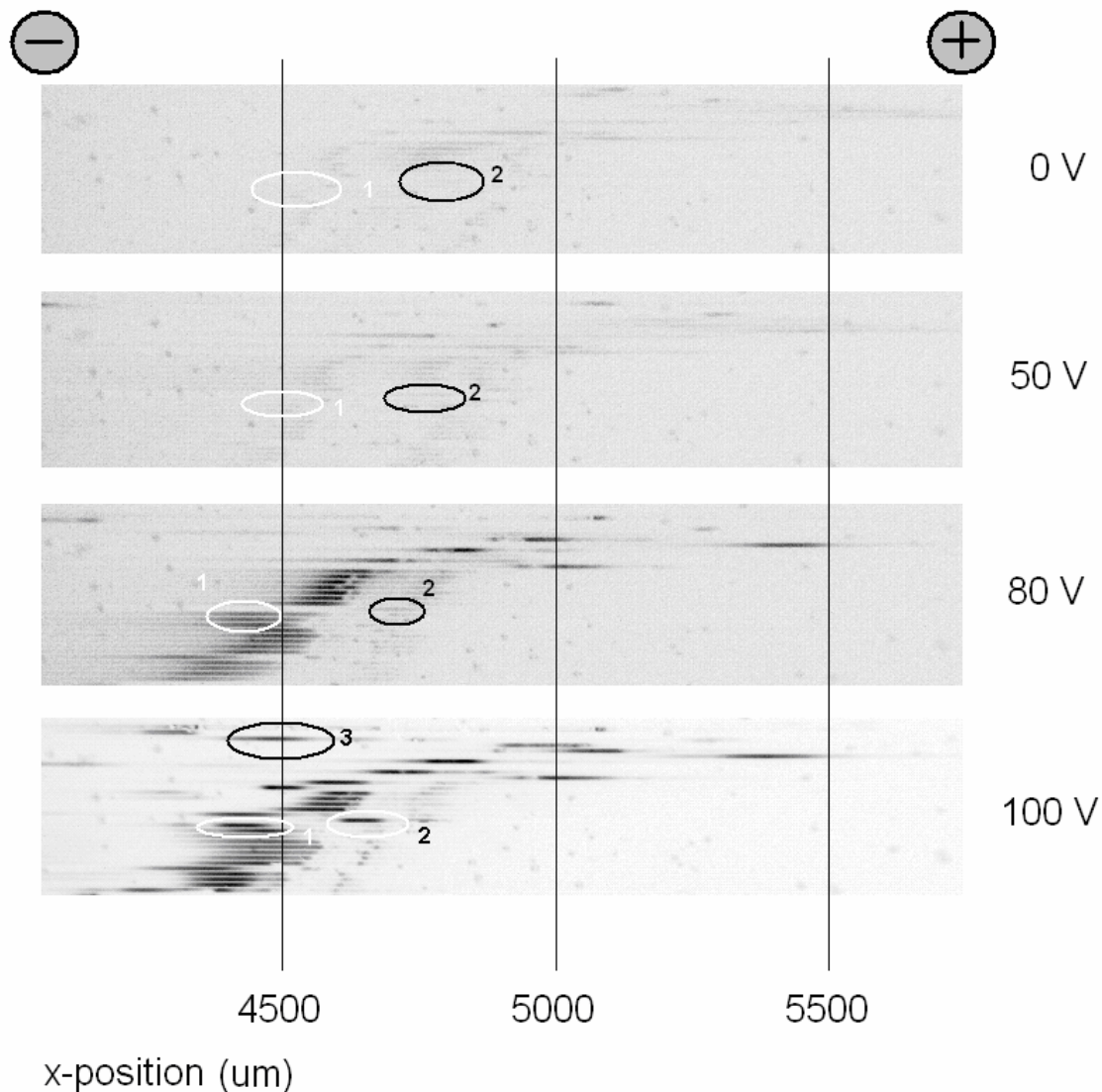


Figure 5.11. Inverted fluorescence images of parallel channels which were photographed during pervaporation while a voltage of 0, 50, 80 or 100 V was applied along the channel. The fluorescent species is dextran FITC. The time between the voltage switches was about 1 minute. The anode (+) and the cathode (-) are depicted in the upper side of the image.

It can be seen that when increasing voltage and time, the accumulation of fluorescence increases; the concentration peaks become higher and less wide. The voltage step from 50V and 80V resulted in a relatively big change. This can be seen in figure 5.12, where the corrected intensity of one peak is plotted in time. The correction is done by dividing the measured maximal intensity of the peak by the measured background signal.

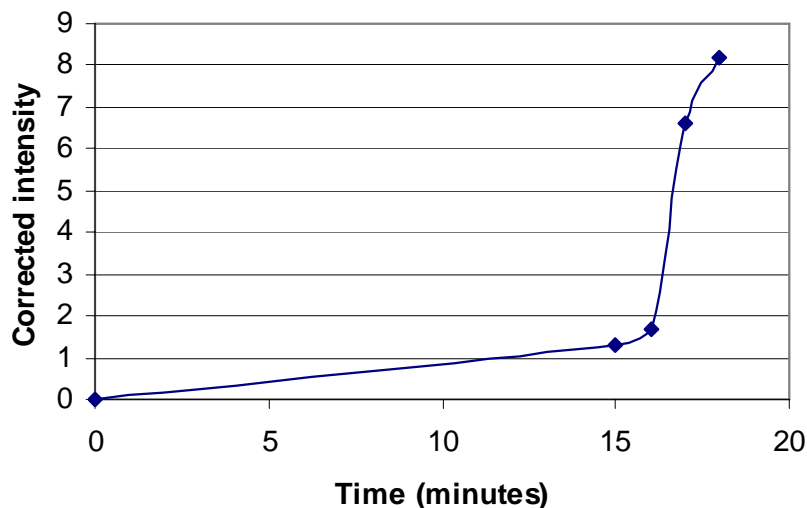


Figure 5.12. Corrected intensities of one peak of figure 5.11, the experiment during pervaporation while a voltage of 50 (at 16 minutes), 80 (at 17 minutes) or 100 V (at 18 minutes) was applied along the channel. The fluorescent species is dextran FITC. The time between the voltage switches was about 1 minute.

The concentration peaks are different for different channels. Some peaks change in x-position, but most peaks stay at one position. Peak 1 travels maximally 100 μm and peak 2 200 μm . Peak 3 suddenly appears at 100V; it came from the left side of the image and travelled minimally 500 μm . The peak width of peak 2 in the image was monitored. This is depicted in figure 5.13.

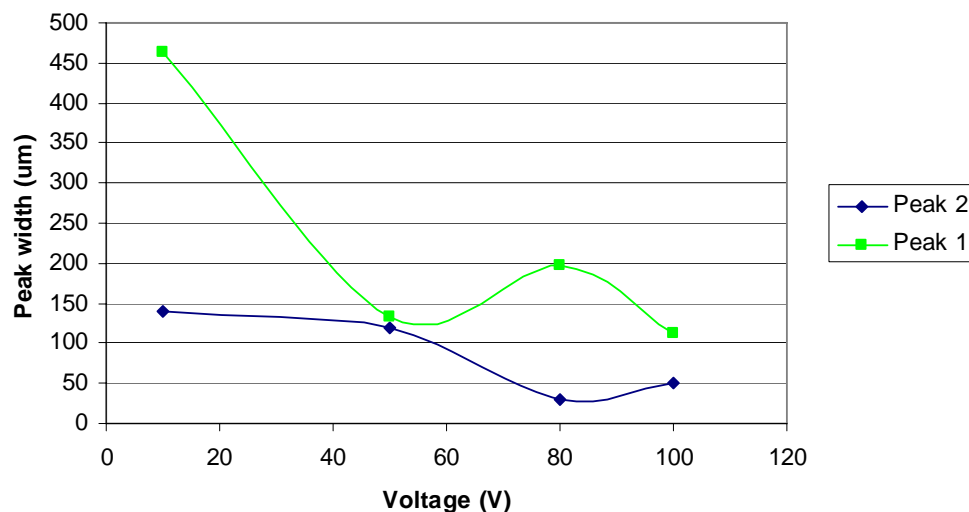


Figure 5.13. Peak widths at 0.5h of the peaks of figure 5.11, the experiment during pervaporation while a voltage of 10, 50, 80 or 100 V was applied along the channel. The fluorescent species is dextran FITC. The time between the voltage switches was about 1 minute. For 10 and 50V the measurement was not accurate.

The peak widths in these plots could not be determined accurately for 10 and 50 V, because of the background noise. The plots only give an indication of the trend that the peak width decreases when the voltage becomes higher, but this relation is instable.

The minimal concentration factor that was estimated in the previous experiment was 25.

The measured current during the experiments is plotted as function of the applied voltage in figure 5.14

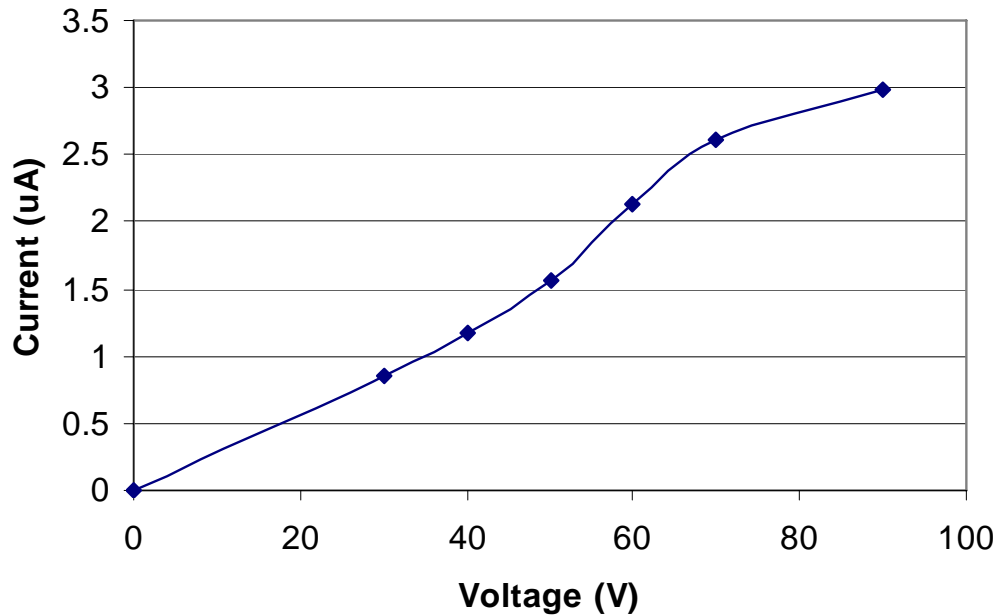


Figure 5.14. V-I diagram pervaporation

It can be seen that the relation between current and voltage is not completely linear, but a slope of about $30\text{V } \mu\text{m}^{-1}$ can be extracted from this V-I diagram.

In this experiment at voltages above about 100V a clear movement of the peaks was observed. Figure 5.15 shows the images of the upper 15 channels of the same array, taken at 0, 40, 60 and 80 seconds after 150V was applied. The current was $3.95 \mu\text{A}$.

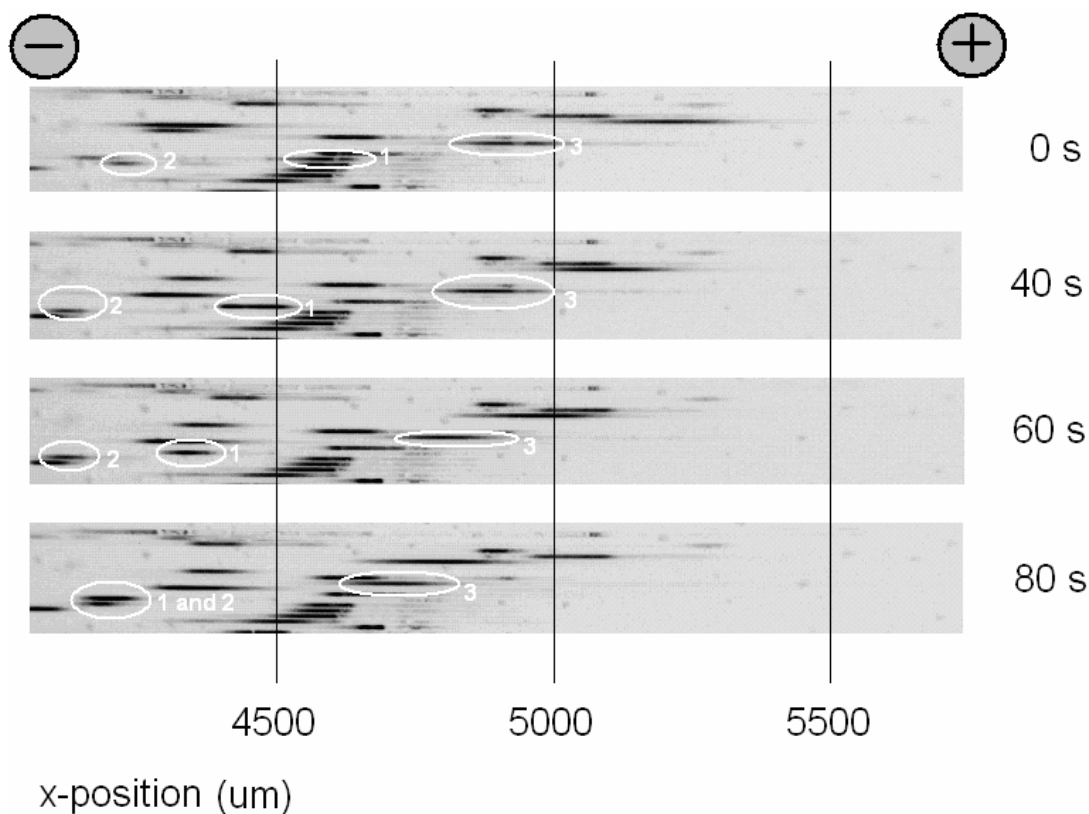


Figure 5.15. Inverted fluorescence images of the same parallel channels as in figure 5.11, photographed at 0, 40, 60 and 80 seconds after the 150V was applied during pervaporation. The fluorescent species is dextran FITC. The anode (+) and the cathode (-) are depicted in the upper side of the image.

In this image three peaks are marked. Peak 1 moves in one direction with an average velocity of about $5 \mu\text{m s}^{-1}$ over $400 \mu\text{m}$; from the centre of the image towards the left corner and becomes narrower in time. Peak 2 moves with an absolute average velocity of about $2 \mu\text{m s}^{-1}$ over $80 \mu\text{m}$, but not in one direction. It becomes larger in time. Peak 3 moves in the same direction as peak 1 with an average velocity of about $3 \mu\text{m s}^{-1}$ over $240 \mu\text{m}$. Other peaks do not move or change in width. A part of these peaks could be flushed away with EOF afterwards, and a part could not. Figure 5.16 shows the peak width at $0.5h$ of the peaks.

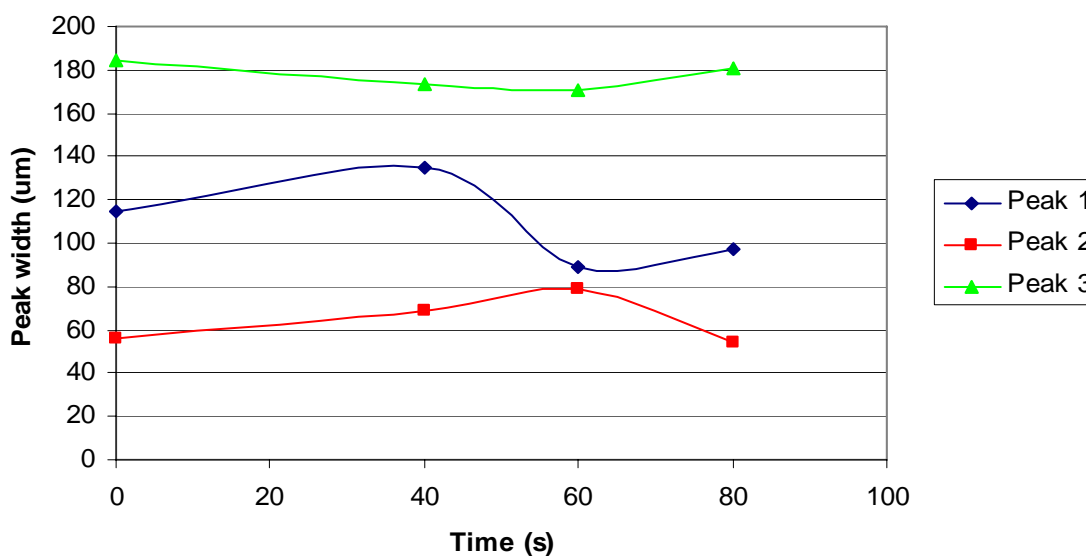


Figure 5.16. Peak widths at 0.5h of the peaks of figure 5.14, the experiment during pervaporation while a voltage of 150 V was applied along the channel. The fluorescent species is dextran FITC. The anode (+) and the cathode (-) are depicted in the upper side of the image.

It can be seen that the peak width of peak 1 fluctuates between 90 µm and 135 µm. Peak 2 fluctuates between 54 µm and 79 µm and peak 3 between 171 µm and 184 µm. This means that peak 1 and 2 changed about 33% in peak width at 0.5h and peak 3 about 7%.

Experiments with fluorescein

The last experiment was repeated, but now with channels filled with a fluorescein solution and a voltage of 170V. The current was not measured during this experiment. Figure 5.17 shows a part of the lower 15 channels of the channel array at 0, 40, 60 and 80 seconds after the voltage was applied.

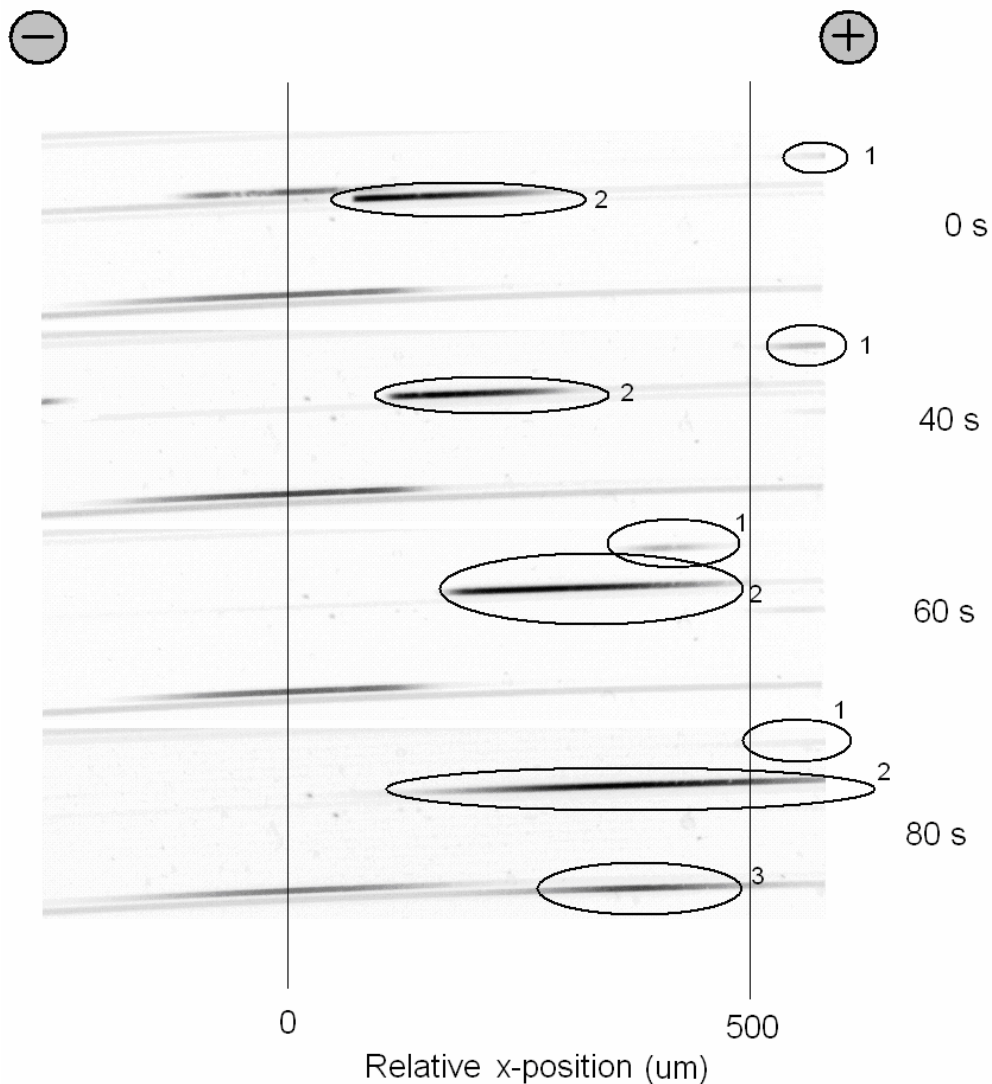


Figure 5.17. Inverted fluorescence images of the lower parallel channels which were photographed at 0, 40, 60 and 80 seconds after the 170V was applied, during pervaporation. The fluorescent species is fluorescein. The anode (+) and the cathode (-) are depicted in the upper side of the image.

In this image also three peaks are marked. Peak 1 moves in two directions over $100\ \mu\text{m}$ with a fluctuating velocity between about $0.25\ \mu\text{ms}^{-1}$ and $1\ \mu\text{ms}^{-1}$. Peak 2 widens and moves from the centre of the image to the right corner with an average velocity of $2.5\ \mu\text{ms}^{-1}$ over $200\ \mu\text{m}$. Peak 3 suddenly appears in the last image, it came from the right side. Other peaks do not move or change in width.

Figure 5.18 shows a part of the upper 15 channels of the same channel array, also at 0, 40, 60 and 80 seconds after the voltage was applied.

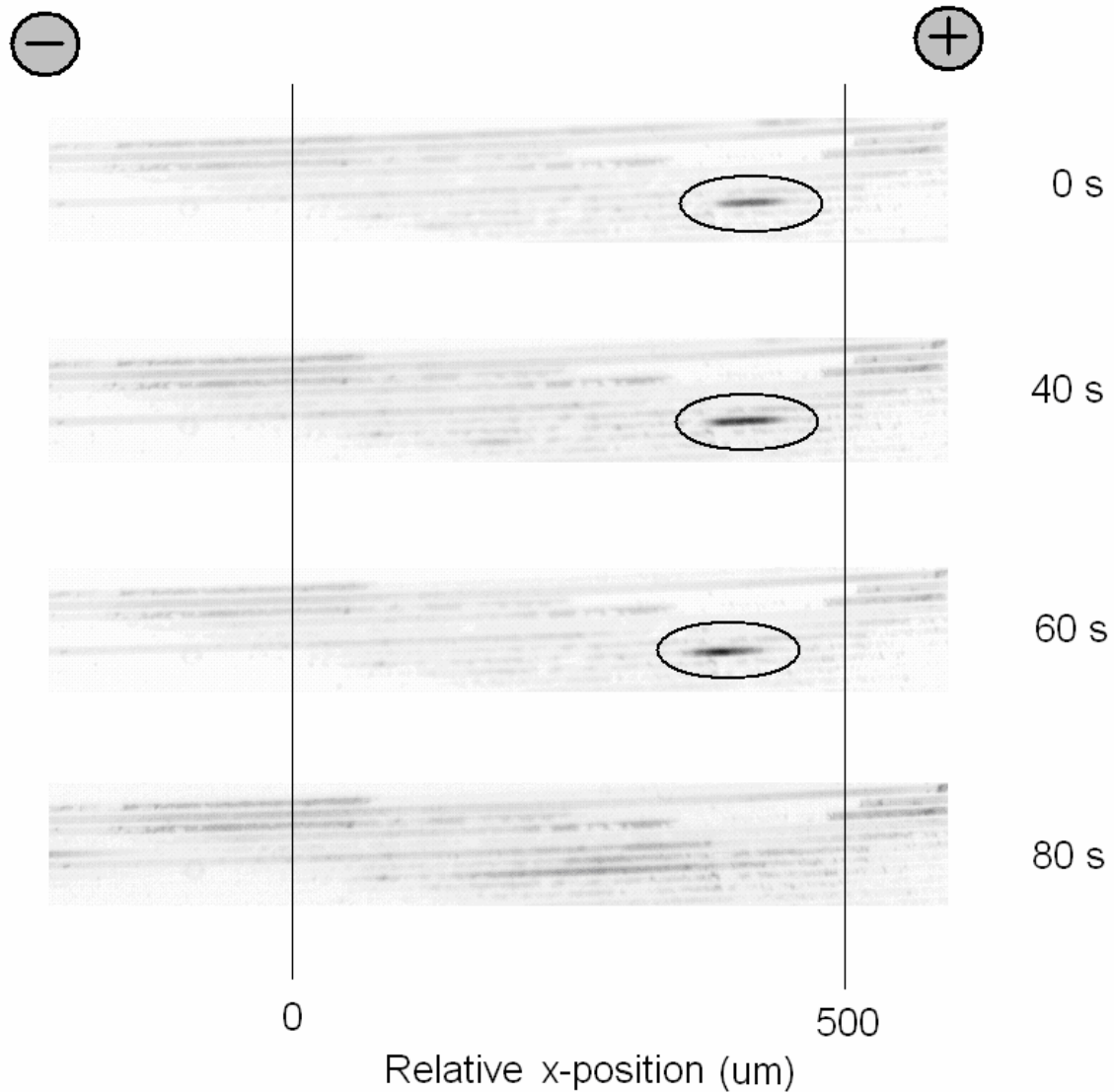


Figure 5.18. Inverted fluorescence images of the upper 15 channels as in figure 5.17 photographed at 0, 40, 60 and 80 seconds after the 170V was applied during pervaporation. The fluorescent species is fluorescein. The anode (+) and the cathode (-) are depicted in the upper side of the image.

Here one peak can be noticed clearly. It moves in time with about $1\mu\text{ms}^{-1}$ over $60\mu\text{m}$ and its width changes in time. At 80 seconds it suddenly disappears. Figure 5.19 shows the peak widths at $0.5h$ of peak 2 in figure 5.17 (lower part of the channel) and the peak in figure 5.18 (higher part of the channel)

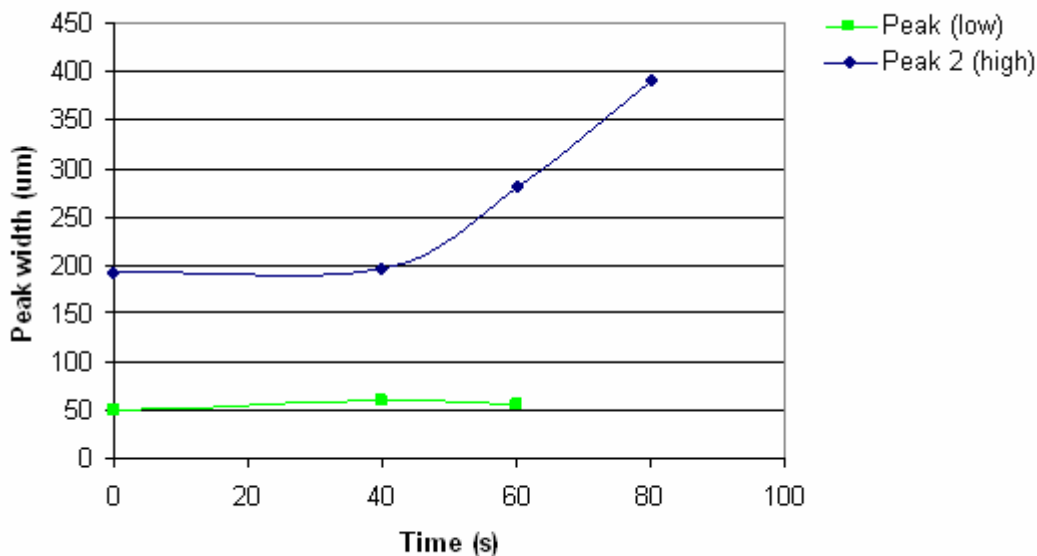


Figure 5.19. Peak width of peak 2 at 0.5h of the peaks of figure 5.17 and the peak of figure 5.18, the experiment during pervaporation while a voltage of 170 V was applied along the channel. The fluorescent species is fluorescein.

It can be seen that the peak width at 0.5h of the higher peak is stable (15% change in width) and the peak width of the lower peak increases in time (55%).

The minimal concentration factor that was estimated in this experiment was 40.

5.3.2 Discussion

Origin of the flows and fluxes

When applying a voltage along the channels, the concentration peaks became higher and narrower than the peaks caused only by pervaporation. This means that with the addition of the voltage other species fluxes than the pervaporation and diffusion induced fluxes are introduced. Because an electrical current was measured through the channels, the channels were conductive allowing electroosmotic and electrophoretic flow. Therefore the added fluxes can be due to electroosmotic flow, induced by the bulk liquid and an electrophoretic flux, induced by migration of charged species. Electroosmotic flow and electrophoretic flux are described in paragraph 2.1.

According to Ren *et al.*, the electroosmotic mobility of aqueous solutions with pH 7.0 in hybrid PDMS (40%) / glass channels (60%) is about $4 \cdot 10^{-8} \text{ m}^2 \text{ V}^{-1} \text{ s}^{-1}$ [43]. Because the channels that are used for these experiments are made of PDMS (45%) and glass (55%), and therefore have approximately the same PDMS/glass contribution, this (maybe somewhat) value for the electroosmotic mobility can approximately be used. With equation 2.23 it can be calculated that the estimated electroosmotic velocity of the bulk is $6 \cdot 10^{-4} \text{ ms}^{-1}$ in case of an applied voltage of 150V and a channel length of 1 cm.

The diffusion coefficient of dextran FITC 500,000 conjugate is $0.31 \cdot 10^{-10} \text{ m}^2 \text{ s}^{-1}$. With equation 2.26 it can be calculated that its electrophoretic mobility is $-6.94 \cdot 10^{-8} \text{ m}^2 \text{ V}^{-1} \text{ s}^{-1}$ and the electrophoretic mobility of fluorescein is $-3.92 \cdot 10^{-8} \text{ m}^2 \text{ V}^{-1} \text{ s}^{-1}$. These are in the same order of magnitude as the electroosmotic mobility.

In the fluorescent channel images, the anode (+) is always on the right side and the cathode (-) on the left side. This means that the electroosmotic flow is directed from the left to the right of the channel, and the electrophoretic flow from the right to the left side in case of negatively charged ions. Because the pervaporation induced velocity is estimated to be about $8.64 \cdot 10^{-6} \text{ m s}^{-1}$, and therefore is a factor 111 smaller than the electroosmotic velocity, this flux is negligible. This means that the flows that are involved in the focusing of species are only the electroosmotic flow and the electrophoretic flow.

Accumulation of species

During the voltage sweep experiment it could be seen that, besides accumulation that was already caused by pervaporation, no further accumulation takes place in the channel. At 80 V and higher accumulation could be observed. This can be explained by figure 2.12. At the start (0V), the electroosmotic and electrophoretic velocity is zero. When the voltage increases the velocities also increase, resulting in accumulation of species at a zero-crossing or deceleration point. It can not be explained by figure 2.12 why the peak intensities do not increase linear with the voltage.

The width of the concentration peaks decrease when the applied voltage becomes higher. This can also be explained by the fact that when the voltage increases, the total species flux at positions where no zero-crossing or deceleration position exist increases. More species will move towards the zero-crossings or deceleration position.

Peak instability

The peaks in the voltage sweep experiment and the constant voltage experiments fluctuated in width and x-position in the channels both for dextran FITC and fluorescein. This is the result from instable behaviour. This can not be caused by joule heating or pH changes, as calculated in chapter 2. The instabilities can be explained by figure 2.12:

Electroosmotic flow depends on the zeta potential of the channel walls and is sensitive for concentration changes; the electroosmotic velocity decreases when the concentration of species in the channel increases. Because charged species concentration plugs move through the channels and ion concentrations are injected in the channel during the experiments, the concentration changes constantly. It can be derived from figure 2.12 that when the electroosmotic velocity increases, the total velocity also increases or decreases and the velocity profile shifts up or down, resulting in a shift or a vanishing of the zero-crossing or deceleration position (and position of the peak). When the electroosmotic flow becomes too high, there will also be no zero-crossing anymore and the plug will flow towards the left of the channel. When the electroosmotic velocity becomes too low,

the electrophoretic velocity has more influence on the system and causes the plug to flow to the right of the channel.

5.3.3 Conclusion

It could be seen that concentration peaks came into being when certain voltages were applied on the channels where a concentration gradient was created by pervaporation induced flux. This means that conductivity gradient focusing by pervaporation induced fluxes was accomplished. However, the behaviour of the dissolved species, and therefore also the concentration peaks, inside the channels was instable.

5.4 Conductivity gradient focusing by osmosis

Paragraph 2.1 of the theory chapter describes that osmosis should also induce fluxes in the microchannel, just like pervaporation. This paragraph deals with the set of experiments that was carried out to investigate whether it is possible to do conductivity gradient focusing in the conductivity gradient caused by the salt and buffer concentration profile that results from osmosis. The concentration profile caused by osmosis cannot be observed by the camera, because of low concentrations. Therefore no analysis of the flow induced by osmosis can be done.

5.4.1 Experiments

To create an osmosis induced flow instead of a pervaporation induced flow, a drop of 1M KCL solution was placed above the channel arrays. Several experiments with different fluorophores were done. The experiments described in this section had the most stable results of the conductivity gradient focusing by osmosis experiments.

Experiments with dextran FITC

The solution that was injected in the reservoirs for the first experiment consisted of a TB buffer of 0.01 M, a 1M KCL background analyte and 10^{-7} M fluorophore dextran FITC 500,000 conjugate. An array of 50 parallel microchannels, with $d = 20 \mu\text{m}$, $w = 8 \mu\text{m}$, $h = 1 \mu\text{m}$ and $L_e = 5 \text{ mm}$, was used for the experiment.

10 minutes after the solution was injected, a drop of water was placed on the PDMS roof. This resulted in that the experiment started with a high species concentration in the middle of the channel, due to pervaporation. After 15 minutes after the placement of the water drop a voltage of 50V was applied along the channel. The current was 12.4 μA . Before the voltage was applied, no fluorescence could be seen in the microscope. At the moment that the voltage was applied, fluorescent peaks travelled from the cathode towards the anode leaving a track of fluorescent species. The peaks disappeared in the middle of the channel.

After 10 minutes a voltage of 80V was applied. The current was 15.5 μA . Figure 5.20 shows images that were taken at 0, 60, 120 and 180 seconds after the moment that the voltage of 80V was applied.

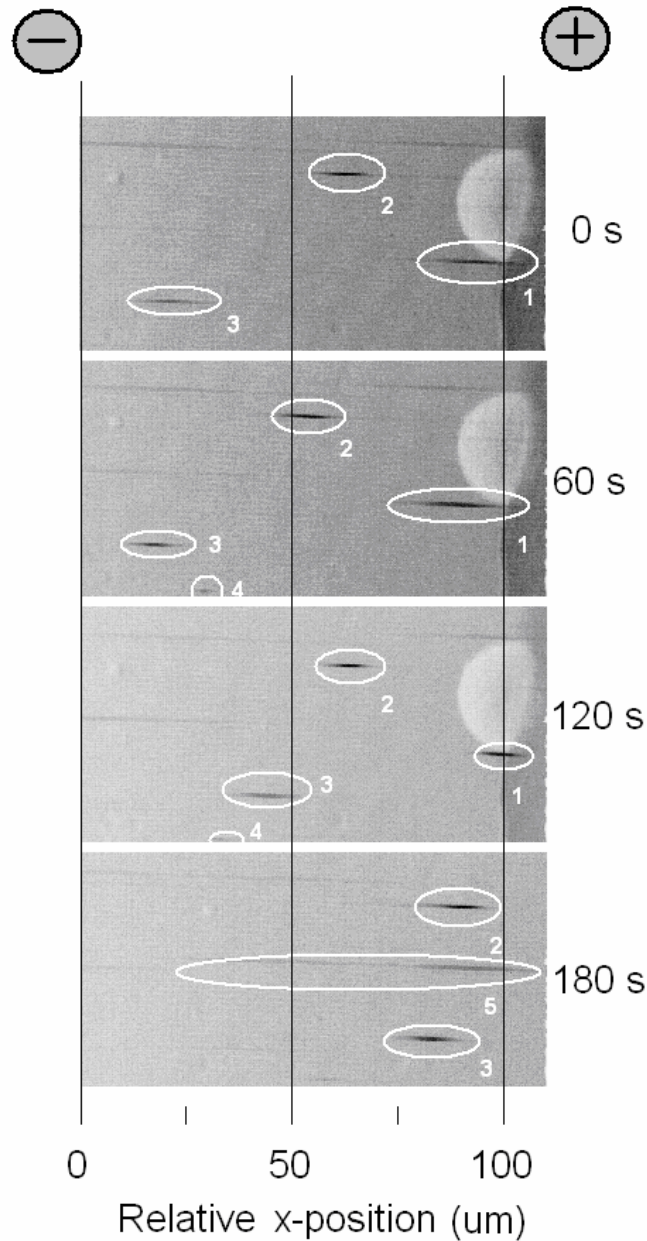


Figure 5.20. Inverted fluorescence images of parallel channels, taken at 0, 60, 120 and 180 seconds after the 80V was applied after osmosis. The fluorescent species is dextran FITC 500k conjugate. The anode (+) and the cathode (-) are depicted in the upper side of the image.

In this image four peaks are marked. All peaks move in two directions and change in width. Peak 3 has the biggest average velocity of about $30 \mu\text{m s}^{-1}$. Peak 2 has a velocity of maximally $10 \mu\text{m s}^{-1}$ and peak 1 $0.2 \mu\text{m s}^{-1}$. Figure 5.21 shows the widths of the peaks at $0.5h$ for peak 1, 2 and 3.

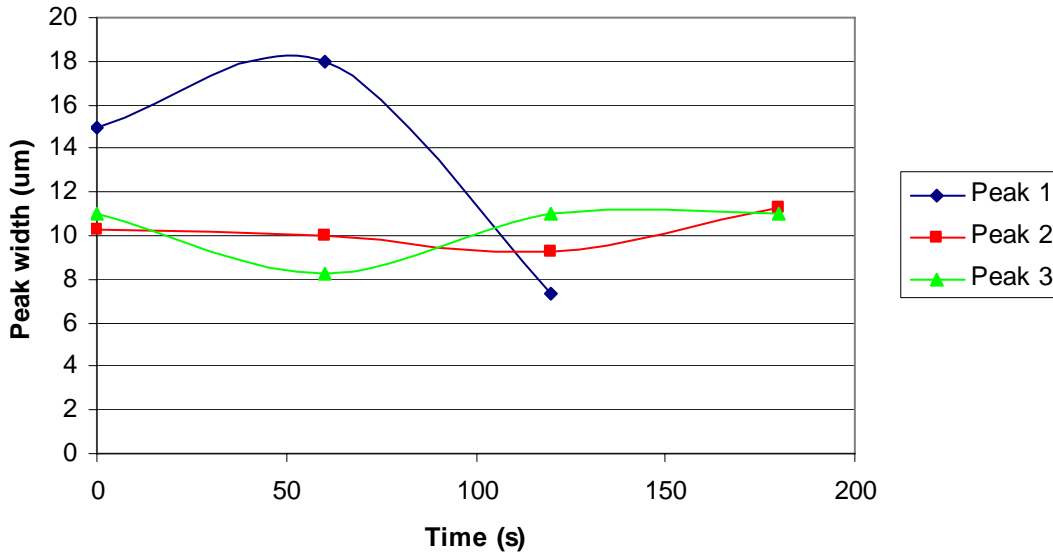


Figure 5.21. Peak width of the peaks of figure 5.20 at 0.5h, the experiment during osmosis while a voltage of 80 V was applied along the channel. The fluorescent species is dextran FITC.

It can be seen that the peaks are much smaller than the peaks from figure 5.16 in the pervaporation experiment with dextran FITC. Peak 1 changed 60% in width, peak 2 18% and peak 3 24%. The minimal concentration factor that was estimated in this experiment was 4.7.

The measured current during the experiment is plotted as function of the applied voltage in figure 5.22. Also the V-I diagram of figure 5.14 from the CGF by pervaporation experiment was plotted in this figure.

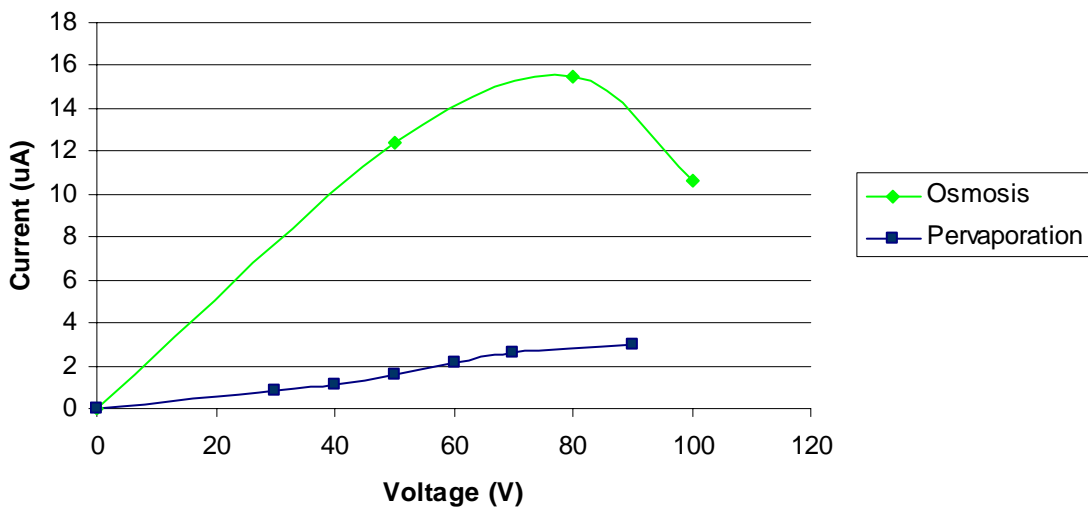


Figure 5.22. V-I diagram of the CGF by osmosis and pervaporation experiments

It can be seen that the current of the osmosis experiments increases faster than the current of the pervaporation experiments. This is due to the fact that the solution in the reservoirs during osmosis experiments contained more ions, and therefore conducts more current (see equation 2.28).

Experiments with fluorescein

The solution that was injected in the reservoirs for the first experiment consisted of a TB buffer of 0.5 M, a 1M KCL background analyte and 10^{-3} M fluorescein and 10^{-3} M rhodamine B. The last one is not visible for the L5 filter and can be neglected. This was also experimentally determined by measuring the light intensity from a drop of rhodamine B.

An array of 50 parallel microchannels, with $d = 20 \mu\text{m}$, $w = 8 \mu\text{m}$, $h = 1 \mu\text{m}$ and $L_e = 5 \text{ mm}$, was used for the experiment. The experiment was repeated 7 times. The results described below were collected from the experiment with the most stable result.

In this experiment a water drop was placed on the channel roof before injecting the solution in the reservoirs. Then a voltage of 30V was applied for 1 minute, and then a voltage of 50V was applied. The measured current was $14.8 \mu\text{A}$. Figure 5.23 shows the images that were taken at 50V after 2 minutes and 0, 40, 80 and 120 seconds.

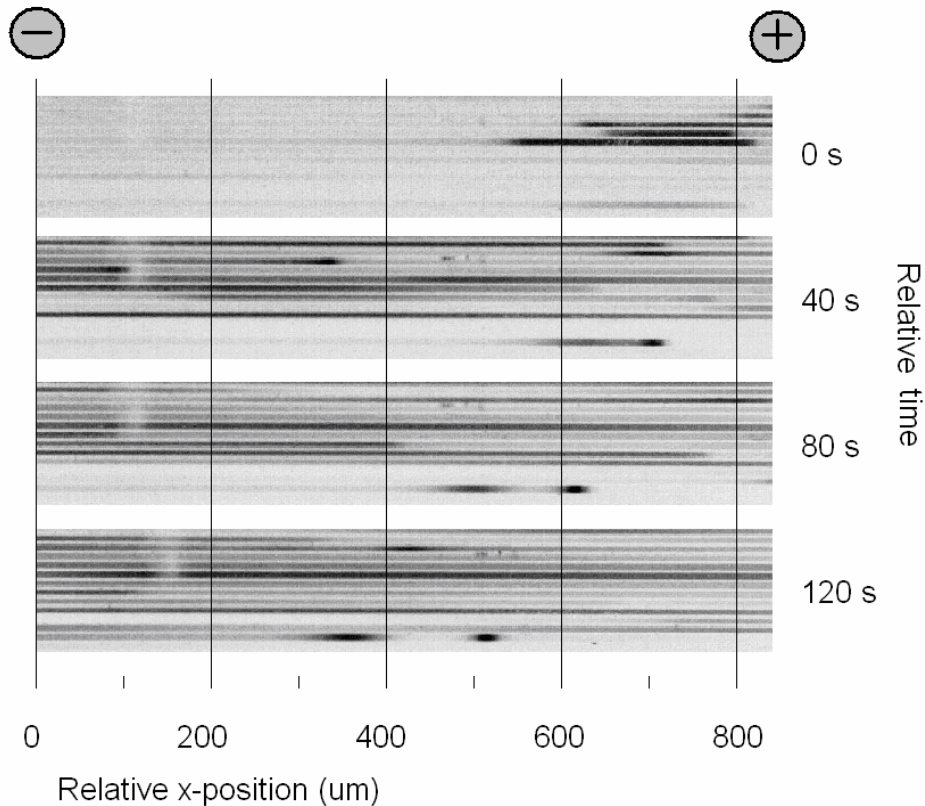


Figure 5.23. Inverted fluorescence images of parallel channels, photographed at 0, 40, 80 and 120 seconds after the 50V was applied during osmosis. The fluorescent species are fluorescein and rhodamine B. The anode (+) and the cathode (-) are depicted in the upper side of the image.

Two phases could be determined during the experiment: the switch-on phase and the steady state phase. In the switch-on phase, which is depicted in the previous figure, it could be seen that the peaks came from the anode (right side of the image) and travelled towards the cathode with a velocity of $39.7 \mu\text{m s}^{-1}$. Most of the peaks left a trace of fluorescent species behind. When they reached the middle of the channel, they were spread out. Below in the image two separate peaks can be seen in one channel. They move slower than the other peaks, namely about $1.7 \mu\text{ms}^{-1}$. After 120 seconds they moved together in two directions over maximal $200 \mu\text{m}$ (steady state). One minute later the peaks spread out and also move to the left side of the image.

Figure 5.24 shows the normalized intensity profiles of the channel with the separated peaks at 0, 40, 80 and 120 seconds.

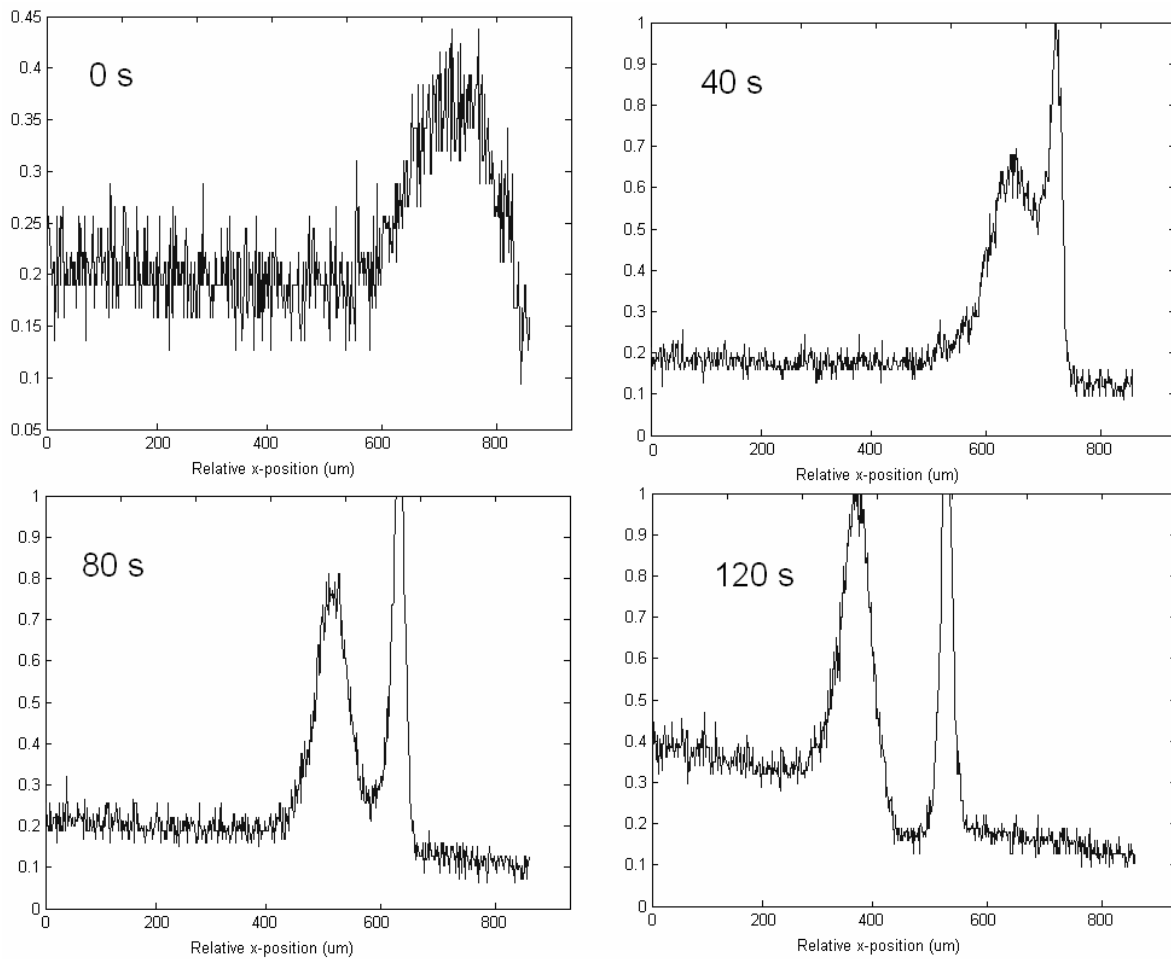


Figure 5.24 Intensity profile of the channel with the separated peaks at 0, 40, 80 and 120 seconds during the osmosis experiment with fluorescein and rhodamine B.

The left (peak 1) and the right peak (peak 2) are one peak at 0 seconds and split during the experiment. The peak widths of the peaks are given in figure 5.25.

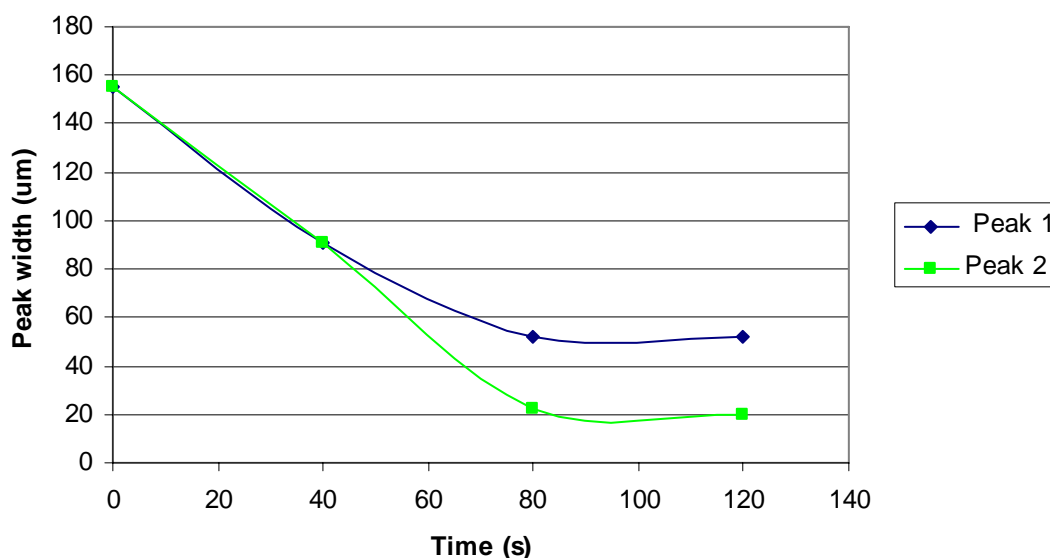


Figure 5.25 Peak widths of the separated peaks at 0, 40, 80 and 120 seconds during the osmosis experiment with fluorescein and rhodamine B.

The peak width of peak 1 decreased with 67% and peak 2 with 87%. The minimal concentration factor that was estimated in this experiment was 7.7.

5.4.2 Discussion

Also with the osmosis induced conductivity gradient focusing experiments the concentration peaks became higher and narrower than the peaks only caused by osmosis, when a voltage was applied. This means that osmosis induced conductivity gradient focusing was accomplished.

Origin of the flows and fluxes

Just like described in section 5.3.2 the flows that are involved in the focusing of species are only the electroosmotic flow and the electrophoretic flux. The osmotic flow velocity is expected to be even smaller than the pervaporation flow velocity, because the pressure difference over the membrane is lower. Following the same calculations as done in section 5.3.2, the electroosmotic velocity is expected to be $1.2 \cdot 10^{-4} \text{ m s}^{-1}$ and the electrophoretic velocity in the same order of magnitude.

Accumulation of species

The starting situation in different CGF-by-osmosis experiments was different. The CGF by osmosis experiment with dextran FITC started in the steady state phase, because the channels contained concentration peaks caused by pervaporation before the experiment started. How accumulation of species happened during this experiment was explained in chapter 2 with figure 2.13. In the other experiments just demineralised water (no dissolved species) was present in the channel. The behaviour in these experiments has to be split in two phases: the switch-on phase and the steady state phase.

In the switch-on phase the concentration of species in the middle of the channel is zero. Peaks travelled from the anode towards the middle of the channel, and disappeared. Also once a double peak that stayed in the right side of the channel was observed. It is not completely understood what the explanation of these switch-on phenomena is, but an attempt is made here below:

The starting situation is that the ionic concentration in the channels is much lower than in the reservoirs. A plug with the reservoir species concentration travels from the anode towards the cathode by electroosmotic flow. This is supported by the fact that the measured flow velocities of the plugs are approximately the electroosmotic velocity as calculated above. This causes the electric field to decrease in the channel at the position of the plug and the track behind it and causes the electric field to increase in the rest of the channel. Species from the cathode travel with the electrophoretic velocity and will be strongly decelerated when they meet the interface with the more concentrated solution (plug front). This results in accumulation of species at the front of the plug. This accumulation travels with the plug speed towards the cathode and were observed as peaks during the experiment. When the plug front reaches the channel centre, the concentration peak vanishes. This can be due to the fact that osmosis induced flows spread out the sample. Behaviour as described above can also be seen in field-amplified sample stacking (FASS) [59].

The channel with the double peak shows other, more steady state-like, behaviour. A peak travelled from the anode towards the cathode and split at a certain position at the right side from the channel centre. Around this position the peaks move slowly in two directions and vanish after a few minutes. Here the balance between electroosmotic and electrophoretic induced flux is more equal. Maybe the steady state phase has reached earlier in this channel than in the other channels. Because rhodamine B is invisible due to the L5 filter and only fluorescein could be seen, these two peaks can not be caused by separation of two different species. It can also not be caused by self-quenching (which happens with fluorescein concentrations of 10^{-3} M or higher) for both peaks do not have the same height. The fact that two peaks were observed can maybe be explained by the fact that the total flux in the channel was disturbed by switch-on phenomena resulting in a high electrophoretic flux at the left of the channel, which causes the second zero-crossing, where normally no accumulation of species take place, also to be an deceleration point (see section 2.1.6). Now two accumulation positions are present in the channel.

When the minimal concentration factor for the CGF by osmosis and CGF by pervaporation are compared, it was calculated that the minimal concentration factors of the CGF by pervaporation experiments are more than 5 times higher than the minimal concentration factors of the CGF by osmosis experiments. This is most likely caused by the 3 times higher voltage that was applied with pervaporation. No conclusions can be drawn from these figures, because these are *minimal* concentration factors and accurate measurements.

The peaks in the CGF by osmosis experiments are smaller than the peaks in the CGF by pervaporation experiments, despite of the lower voltage that was applied. This can be due to the fact that the pervaporation experiments are maybe executed with a too high voltage (see section 2.1.6), which causes the accumulation points not to be zero-crossings where species are supplied from both sides, but accumulation positions where the total flux decreases causing the species to accumulate more slowly. Wider peaks can be expected here.

Peak instability

Instable behaviour of the peaks was also noticed in these experiments, just like noticed in the CGF by pervaporation experiments. The causes of instability will be the same as described for the pervaporation experiments.

When the 'steady state' dextran FITC experiments of both CGF methods are compared, it can generally be noticed that the peaks of the osmosis experiments have a larger velocity, despite of the lower voltage that was applied with osmosis. This can be due to higher concentration changes during the osmosis experiment causing the electroosmotic flow to be more instable.

The average change in peak width per second is higher for the pervaporation experiments. This can also be due to the higher voltage that was applied during the pervaporation experiments causing the peaks not to be zero-crossings, but other accumulation positions as described above.

5.4.3 Conclusion

It could be seen that concentration peaks came into being when certain voltages were applied on the channels where a concentration gradient was created by osmosis induced flux. This means that conductivity gradient focusing by osmosis induced fluxes was accomplished. However, the behaviour of the dissolved species, and therefore also the concentration peaks, inside the channels was instable. Compared to CGF by pervaporation experiments, CGF by osmosis is less stable; peaks travel with higher velocities through the channels. The peaks however are smaller for the osmosis experiments. The minimal concentration factor of the CGF by pervaporation experiments was higher than the minimal concentration factor of the CGF by osmosis experiments.

5.5 Separation

The previous two paragraphs show that it is possible to concentrate charged species by conductivity gradient focusing with pervaporation and osmosis. The next step is to separate two different species. Because the osmosis experiments were expected to be more stable than pervaporation experiments, the separation experiments were carried out with osmotic flow. Actually the osmosis experiments appeared not to be more stable than

the pervaporation experiments. The obtained peak width was smaller for osmosis experiments and that can be advantageous in these experiments.

5.5.1 Experiments

Experiments with a solution of fluorescein and rhodamine 6G were done. The solution that was injected first in the reservoirs consisted of a TB buffer of 0.5 M, a 1M KCL background analyte and 10^{-3} M fluorescein and 10^{-3} M rhodamine 6G. The second solution had equal components, but the fluorescein and rhodamine 6G concentration was 10^{-5} M.

A drop of water was placed upon the channel before injecting the first solution in the reservoirs. After 15 minutes a voltage of 30V (5.9 μ A) was applied along the channel. Figure 5.26 shows images of the channels at 0, 10, 20, 30 and 40 seconds after the 30V was applied. It shows respectively the upper and lower channels of the channel array.

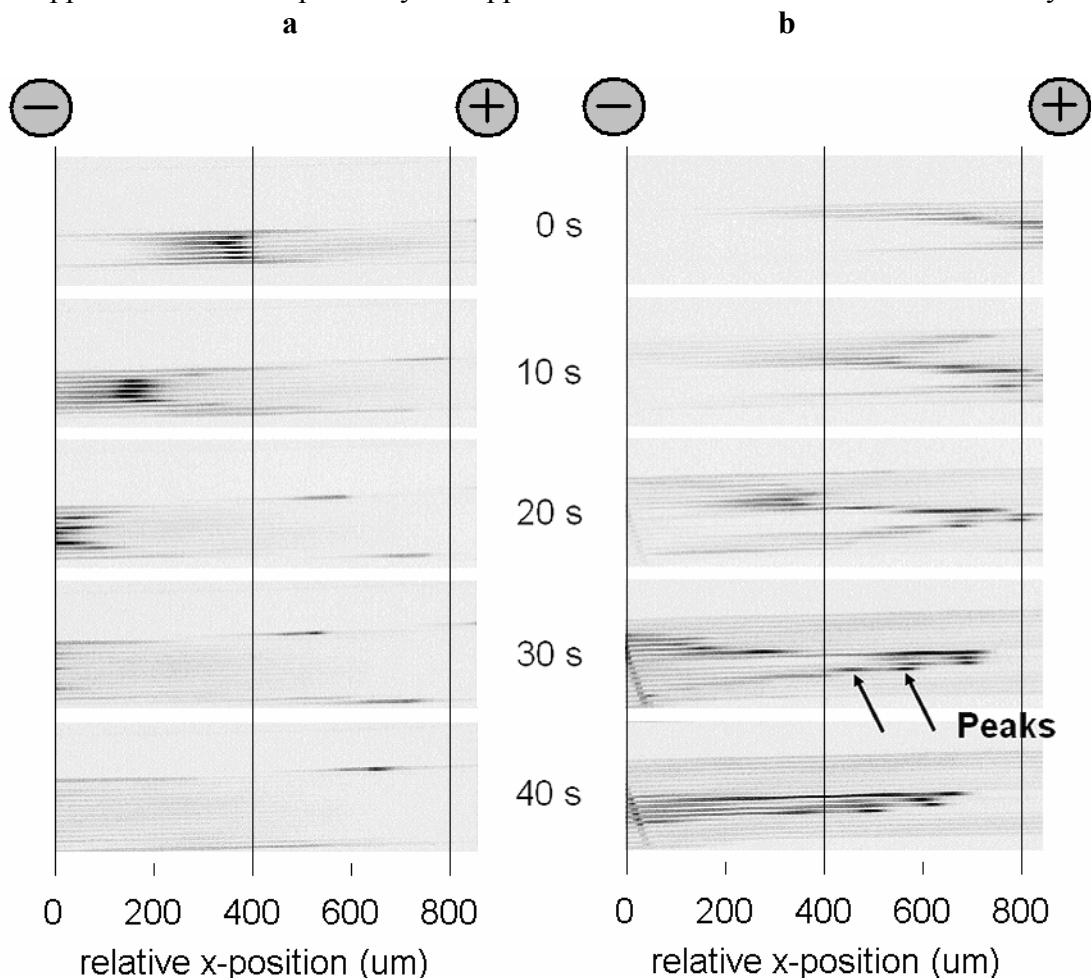


Figure 5.26. Inverted fluorescence images of the upper (a) and lower (b) parallel channels, photographed at 0, 10, 20, 30 and 40 seconds after the 30V was applied. The fluorescent species are fluorescein and rhodamine 6G. The anodes (+) and the cathodes (-) are depicted in the upper side of the image.

It can be seen that the peaks travel from the right (anode) to the left (cathode) side of the image. The flow velocity of these peaks is about $20 \mu\text{m/s}$. The peaks disappeared in the middle of the channel. Figure 5.27 shows the intensity profile of the marked peaks in figure 5.26.

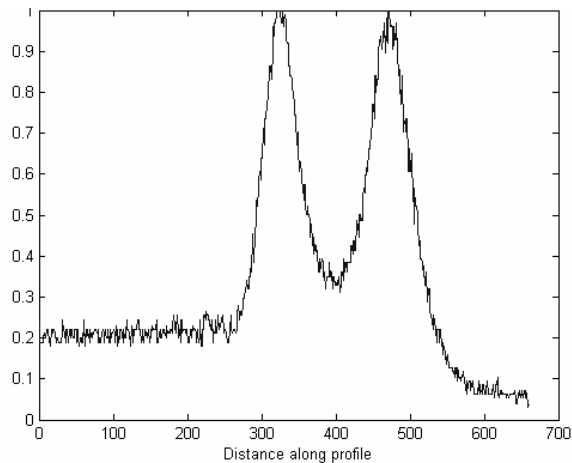


Figure 5.27. Intensity profile of the channel with the separated peaks at 30 seconds during the separation experiment with fluorescein and rhodamine 6G.

Two separate peaks can be noticed. When a voltage of 200 volt was applied in some channels an oscillating phenomenon was observed. Figure 5.28 shows that two peaks are present in one channel. They both came from the right side of the channel.

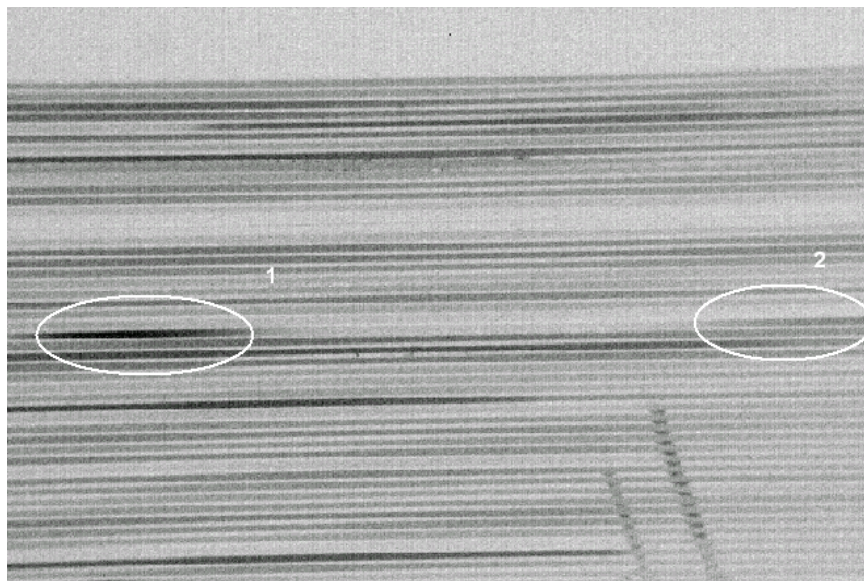


Figure 5.28. Two following peaks in one channel during the separation experiment with fluorescein and rhodamine 6G.

The frequency of the peak appearance was about 0.5 Hz.

The experiment was repeated 4 times with the same solution with a fluorescein and rhodamine 6G concentration of 10^{-5} M. One of these experiments also showed a separated peak traveling through the channel in the same way. The oscillating phenomenon was not observed.

5.5.2 Discussion

Double peaks were observed in several channels. These can not be caused by self-quenching for the reason that in the second experiment the fluorescein and rhodamine 6G concentration was 10^{-5} M, which is expected to be concentrated about 10 times according to the previous paragraph. Also higher concentration peaks, which should also self-quench, can be noticed at 20 seconds. The explanation given in section 5.4.2 for the double peaks can also be applied here. Because two different fluorophores with opposite charge are used in these experiments, the double peaks can also be separations of these different species, as described in section 2.1.6.

The oscillating phenomenon can not be explained and should be investigated further.

5.5.3 Conclusion

When doing experiments with fluorescein and rhodamine 6G double peaks are observed several channels. It can not be proven that these peaks are caused by the separation of the species.

Chapter 6 - Conclusions

This report concerns the investigation of whether the water permeability of a semi permeable membrane can be used to create a conductivity gradient of dissolved species inside a microchannel by pervaporation or osmosis and whether subsequently pervaporation- or osmosis-induced conductivity gradient focusing is possible in microchannels. To investigate this, microfluidic devices were designed and fabricated.

Microfluidic devices

Successful fabrication of microchannels was possible when narrow channel arrays were used. The microchannels became hydrophilic when they were treated with oxygen plasma.

Conductivity gradient focusing

A pervaporation driven flux of dextran FITC or fluorescein was created in a glass microchannel with a PDMS roof. A minimal concentration factor of 28.6 was observed. The flow velocity that was reached was at least $5.4 \cdot 10^{-6} \text{ m s}^{-1}$. The separate concentration profiles along the channel arrays were positioned at almost the same position in the centre of the channel. The pervaporation flux was very large, causing dissolved species to crystallize or to become gel-like.

Successful conductivity gradient focusing (CGF) experiments were done in microchannels with pervaporation and osmosis driven fluxes. The peaks were instable: they changed in height and width and moved along the channel. The experiments with CGF by pervaporation were more stable, because the peaks moved less along the channel. The width of the peaks concentrated with the CGF by osmosis experiments was lower. A minimal concentration factor of 40 was observed with CGF by pervaporation.

Indications were found for separation of different species with CGF by osmosis. However, this could not be proven.

Chapter 7 - Recommendations

Good results were obtained with channel arrays with a channel width of minimal 8 μm . Smaller structures caused problems with hydrophobicity. Improvement would be possible by using channels or channel arrays that are placed on the wafer with at least 1 cm spacing, in order to have enough space to glue the reservoirs and place water drops for osmosis experiments.

The controllability of the pervaporation induced fluxes should be better. The pervaporation induced flux needs to be fast during experiments and should be reduced when experiments have elapsed in order to prevent crystallization and gel forming of species in the channels. This can for example be done by placing another microfluidic channel on an existing channel.

When designing and fabricating improved devices it is very important to read chapter 3 of this report. Many problems with PDMS are described and even solved here. This can save lots of time.

New experiments should be done with a camera with a fixed gain in order to do quantitative measurements.

New experiments can be done in order to investigate the proven phenomena in more detail or to explore the possibilities of these phenomena:

- The effect of electroosmotic flow suppression on the stability of the experiments should be investigated by doing the same experiments with EOF suppressor.
- The separation experiment with fluorescein and rhodamine 6G should be repeated while using a filter block that can make a distinguish between the fluorophores. This is necessary to prove separation.
- Separation experiments with a solution of dextran FITC 500,000 conjugate and dextran FITC 4,000 conjugate, which have different electrophoretic mobilities and diffusion coefficients, can be done.

Phenomena deserving more study

Fluorescent species were absorbed and adsorbed in or at the PDMS during long lasting experiments. This means that PDMS can act like a membrane for small species which deserves more study. Also the possibility of electrophoresis of species through PDMS deserves more study.

During an osmosis experiment an oscillating phenomena in some channels was observed and deserves more study.

References

- [1] D. Ross and L.E.Locascio, '*Microfluidic temperature gradient focusing*', Anal. Chem. 74 (2002) 2556-2564
- [2] E.Vrouwe, proefschrift '*Quantitative microchip capillary electrophoresis for inorganic ion analysis at the point of care*', 2005
- [3] C.F.Ivory, '*A brief review of alternative electrofocusing techniques*', Sep. Sci. and Techn. 35 (2000) 1777-1793
- [4] J.C.T.Eijkel and A.van den Berg, '*Water in micro- and nanofluidics systems described using the water potential*', Lab on a Chip 5 (2005) 1202-1209
- [5] J.C.T.Eijkel, J.G.Bomer and A.van den Berg, '*Osmosis and pervaporation in polyimide submicron microfluidic channel structures*', Appl. Phys. Let. 87 (2005) 114103
- [6] G.C.Randall and P.S.Doyle, '*Permeation-driven flow in poly(dimethylsiloxane) microfluidic devices*', PNAS 102 (2005) 10813-10818
- [7] J.Leng, B.Lonetti and P.Tabeling, '*Microevaporators for Kinetic Exploration of Phase diagrams*', Phys. Rev. Let. 96 (2006) 084503
- [8] E.Verneuil, A.Buguin and P.Silberzan, '*Permeation-induced flows: Consequences fo silicone-based microfluidics*', Europhysics Let. 68 (2004) 412-418
- [9] J.G.Wijmans and R.W.Baker, '*Solution-diffusion model: a review*', J. Membrane Sci. 107 (1995) 1-21
- [10] E.Favre, P.Schaetzel, Q.T.Ngyugen, R.Clément and J.Néel, '*Sorption, diffusion and vapor permeation of various penetrants through dense poly (dimethylsiloxane) membranes: a transport analysis*', J.Mem.Sci. 92 (1994) 169-184
- [11] X.Ren, M.Bachman, C.Sims, G.P.Li and N.Allbritton, '*Electroosmotic properties of microfluidic channels composed of poly(dimethylsiloxane)*' J. of Chrom. B 762 issue 2 (2001) 117-125
- [12] C.S.Effenhauser, A.Manz and H.M.Widmer, '*Glass chips for high-speed capillary electrophoresis separations with submicrometer plate heighths*', Anal. Chem. 65 (1993) 2637-2642

- [13] A.J.Bard, L.R.Faulkner, *Electrochemical Methods, Fundamentals and Applications*, John Wiley & Sons, 1980, ISBN 0-471-05542-5
- [14] Personal communication with Jan Eijkel, March 2007
- [15] Y.Wang and D.L.Taylor, *Methods in cell biology – Volume 29 Fluorescence microscopy of living cells in culture, part A*, Academic Press, 1989, ISBN 0-12-564129-X
- [16] S.Staal, Afstudeerverslag '*Counterflow electrofocusing*', 2004
- [17] L.Song, E.J.Hennink, I.T.Young and H.J.Tanke,' *Photobleaching Kinetics of Fluorescein in Quantitative Fluorescence Microscopy*', *Bioph. J.* (1995) 68, 2588-2600
- [18] Invitrogen, <http://probes.invitrogen.com/handbook/sections/0001.html>, March 2007
- [19] J.L.Robeson and R.D.Tilton,'*Effect of Concentration Quenching on Fluorescence Recovery after Photobleaching Measurements*', *Biophys. J.* 68 (1995) 2145-2155
- [20] S.Hamann, J.F.Kiilgaard, T.Litman, F.J.Alvarez-Leefmans, B.R.Winther and T.Zeuthen,' *Measurement of Cell Volume Changes by Fluorescence Self-Quenching*', *J.Fluorescence* 12 (2002) 139 - 145
- [21] M.W.Toepke and D.J.Beebe,'*PDMS absorption of small molecules and consequences in microfluidic applications*', *Lab Chip* 6 (2006) 1484-1486
- [22] J.Goulpeau, D.Trouchet, A.Ajdari and P.Tabeling,'*Experimental study and modeling of polydimethylsiloxane peristaltic micropumps*', *J. Apl. Phys.* 98 (2005) 044914
- [23] Willmad LabGlass, <http://www.wilmad-labglass.com/pdf/Borosilicate%20Glass%20Properties.pdf>, March 2007
- [24] D.A.Walker,'*A fluorescence technique for measurement of concentration in mixing liquids*', *J. Phys. E: Sci. Instrum.* 20 (1987) 217-224
- [25] Wikipedia, <http://www.wikipedia.org>, March 2007
- [26] C.R. Moylan, M.E. Best, and M. Ree, '*Solubility of Water in Polyimides: Quartz Crystal Microbalance Measurements*', *J. Polym. Sci.: Polym. Phys.* 29 (1991) 87
- [27] Thinfilm, http://www.thinfilm.com/docs/atp_poly_bridge_rules.pdf, March 2007

- [28] *'Lab instructions – Microfluidics – Microstructure technology II'*, Uppsala Universitet, viewed on August 29 2006
- [29] J.C.McDonald, D.C.Duffy, J.R.Anderson, D.T.Chiu, H.Wu, O.J.A.Schueller and G.M.Whitesides, *'Fabrication of Microfluidic systems in poly(dimethylsiloxane)'*, *Electrophoresis* 21 (2000) 27-40
- [30] G.G.Bausch, J.L.Stasser, J.S.Tonge and M.J.Owen, *'Behavior of Plasma-Treated Elastomeric Polydimethylsiloxane Coatings in Aqueous Environment'*, *Plasma and Polymers* 3 (1998) 23-34
- [31] E.Delamarche, D.Juncker and H.Schmid, *'Microfluidics for Processing Surfaces and Miniaturizing Biological Assays'*, *Adv. Mat.* 17 (2005) 2911-2933
- [32] T.Uragami, *'Concentration of aqueous ethanol solutions by porous poly(dimethylsiloxane) membranes during temperature difference controlling evaporation'*, *Desalination* 193 (2006) 335–343
- [33] Y.Tamai, H.Tanaka, K.Nakanishi, *'Molecular Simulation of Permeation of Small Penetrants through Membranes. 2. Solubilities'*, *Macromolecules* 28 (1995) 2544-2554
- [34] M.E.Rezac, T.John and T.H.Pfromm, *'Effect of Copolymer Composition on the Solubility and Diffusivity of Water and Methanol in a Series of Polyether Amides'*, *J.Appl.Pol.Sci.* 65 (1997) 1983-1993
- [35] D.Armani, C.Liu and N.Aluru, *'Re-configurable fluid circuits by PDMS elastomer micromachining'*, 12th Int. Conf. on MEMS 99 (1998) 222-227
- [36] N.R.Tas, P.Mela, T.Kramer, J.W.Berenschot and A. van den Berg, *'Capillarity induced negative pressure of water plugs in nanochannels'*, *Nano Lett.* 3 (2003) 1537.
- [37] S.Herber, proefschrift *'Development of a hydrogel-based carbon dioxide sensor'* (2005)
- [38] P.W.Atkins, *Physical Chemistry*, 5th edition (1994) Oxford University Press
- [39] D.C.Duffy, J.C. McDonald, O.J.A.Schueller and G.M.Whitesides, *'Rapid Prototyping of Microfluidic Systems in Poly(dimethylsiloxane)'*, *Anal. Chem.* 70 (1998) 4974 – 4984
- [40] O.J.A.Schueller, D.C.Duffy, J.A.Rogers, S.T.Brittain and G.M.Whitesides, *'Reconfigurable diffraction gratings based on elastomeric microfluidic devices'*, *Sens. And Act.* 78 (1998) 149-159

- [41] B.Kim, E.T.K.Peterson and I.Papautsky, '*Long-Term Stability of Plasma Oxidized PDMS Surfaces*', Proc. 26th Ann. Int. Conf. IEEE EMBS (2004) 5013 – 5016
- [42] J.L.Fritz, M.J.Owen, '*Hydrophilic Recovery of Plasma-Treated Polydimethylsiloxane*', J.Adhesion 54 (1995) 33-45
- [43] X.Ren, M.Bachman, C.Sims, G.P.Li and N.Allbritton, '*Electroosmotic properties of microfluidic channels composed of poly(dimethylsiloxane)*' J. of Chrom. B 762 issue 2 (2001) 117-125
- [44] S.K.Sia and G.M.Whitesides, '*Microfluidic devices fabricated in poly(dimethylsiloxane) for biological studies*', Electrophoresis 24 (2003) 3563-3576
- [45] J.M.K.Ng, I.Gitlin, A.D.Stroock and G.M.Whitesides, '*Components for integrated poly(dimethylsiloxane) microfluidic systems*', Electrophoresis 23 (2002) 3461-3473
- [46] J.A.Vickers, M.M.Caulum and C.S.Henry, '*Generation of Hydrophilic Poly(dimethylsiloxane) for High-Performance Microchip Electrophoresis*', Anal. Chem. 78 (2006) 7446 - 7452
- [47] E.S.Choi, S.S.Yang, '*Improvement of Electroosmotic Flow Characteristic in Poly(dimethylsiloxane) channels via a Long Life Chemical Surface Modification*', 7th Int. Conf. Min. Chem. Bio. An. Syst. (2003)
- [48] H.Makamba, Y.Hsieh, W.Sung and S. Chen, '*Stable Permanently Hydrophilic Protein-Resistant Thin-Film Coatings on Poly(dimethylsiloxane) Substrates by Electrostatic Self-Assembly and Chemical Cross-Linking*', Anal.Chem. 77 (2005) 3971-3978
- [49] S.Hu, X.Ren, M.Bachman, C.E.Sims, G.P.Li and N.L.Allbritton, '*Surface-Directed, Graft Polymerization within Microfluidic Channels*', Anal. Chem. 76 (2004) 1865-1870
- [50] Keithley, <http://www.keithley.com>, March 2007
- [51] Leica, <http://www.leica-microsystems.com>, March 2007
- [52] Olympus, <http://www.olympus-europa.com>, March 2007
- [53] Sigma-Aldrich, <http://www.sigmaaldrich.com>, March 2007
- [54] J. W. McBain; C. R. Dawson, '*The Diffusion of Potassium Chloride in Aqueous Solution*', Proc. Royal Soc. London series A, Math. Phys. Sci. 148 (1935) 32-39

- [55] S.A.Rani, B.Pitts and P.S.Steward, '*Rapid Diffusion of Fluorescent Tracers into Staphylococcus epidermidis Biofilms Visualized by Time Lapse Microscopy*', Antimic. Ag. and Chem. Ther. 49 (2005) 728-732
- [56] Oregon Medical Laser Center, <http://omlc.ogi.edu/spectra/PhotochemCAD/html/fluorescein-dibase.html>, March 2007
- [57] J.R.Lawrence, G.M.Wolfaardt, D.R.Korber, '*Determination of Diffusion Coefficients in Biofilms by Confocal Laser Microscopy*', Appl. And env. Microbiol. 60 (1994) 1166-1173
- [58] J.M.Watson and M.G.Baron, '*The behaviour of water in poly(dimethylsiloxane)*', J. Membrane Sci. 110 (1996) 47-57
- [59] Stanford Microfluidics Laboratory, <http://microfluidics.stanford.edu/stack.htm>, March 2007

Appendices

Appendix A. Process flow pervaporation channel glass wafer

Method A

	Material	100 mm pyrex wafers	
1	Cleaning	5 minutes oxygen plasma: Tepla 500W	
2	Lithography	Photoresist: 20 sec 4000 rpm 908/12 photoresist spinning 1 minute 95 °C Expose 5 minutes maskaligner ElectroVision; mask: ELEKTRODE 2 min 95 °C 30s + 15s develop in OPD-dev I and II 5 minutes 95 °C	
3	DRIE	Deep Reactive Ion Etching in AdixenDE Program: SiO ₂ Time: 3 minutes	
4	Remove photoresist	40 mTorr 60W 20 sccm O ₂ 5 min	

Method B

	Material	100 mm pyrex wafers	
1	Cleaning	5 minutes oxygen plasma: Tepla 500W 50% O ₂	
2	Sputtering	DC-sputtergunsystem "Sputterke" Initial pressure <1E-6 mbar Ar-sputter pressure 1,5E-3 mbar (13 sccm Ar); power 200 W, 50 sec Cr Ar-sputter pressure 3E-3 mbar (25 sccm Ar); power 200 W, 4 min 30 sec Au Result: 10 nm Cr / 200 nm Au	
3	Lithography	Photoresist: 20 sec 4000 rpm 908/12 photoresist spinning 1 minute 95 °C Expose 5 minutes maskaligner	

		ElectroVision; mask: ELEKTRODE 2 min 95 °C 30s + 15s develop in OPD-dev I and II 5 minutes 120 °C	
	IBE	Anisotropic etching of the Cr/Au layer. 20 min 500V/30 mA beam under 20°	
	Remove photoresist	40 mTorr 60W 20 sccm O ₂ 5 min	
	Etching of Pyrex	BHF etching (solution of HF and NH ₄ F) 52 min 18°C, no agitation	
	Etching of Cr/Au	In gold-etch until the chromiumlayer appears In chromium-etch until the wafer is transparent	

Appendix B. Process flow PDMS

1	Dummy wafer	3M CG3720 foil on silicon wafer with tape	
2	PDMS preparation	1:10 base:curing agent Sylgard 184 10 minutes blend in shaker Degas in vacuum chamber	
3	PDMS spinning	Aceton on dummy wafer at 2000 rpm Teflon 3M EGC1700 at 2000 rpm PDMS 20s at 4000 rpm	
4	PDMS curing	60°C for 60 minutes Cut the foil from the dummy wafer	
5	Surface modification	5 minutes plasma cleaning in 400 mTorr in Harrick plasma cleaner/sterilizer at RF level 'Hi', also for the glass wafer	
6	PDMS assembly	Roll the foil on the glass wafer Cut loose the PDMS from the foil at the edges Pull the foil from the glass/PDMS wafer	
7	Interface	Cut holes in the PDMS at channel ends Glue reservoirs at the holes	
8	Storage	Fill the channel with water immediately after assembly for hydrophilicity	